ELECTROWETTING OF IONIC LIQUIDS AND DEVELOPMENT OF AN ELECTROWETTING BASED TUNABLE RC FILTER AND ITS USES AS AN ANALYTICAL DETECTOR

by

YASITH SAMEERA NANAYAKKARA

Presented to the Faculty of the Graduate School of
The University of Texas at Arlington in Partial Fulfillment
of the Requirements
for the Degree of

DOCTOR OF PHILOSOPHY

THE UNIVERSITY OF TEXAS AT ARLINGTON

December 2010

To my beloved wife, loving parents, and grand parents.

ACKNOWLEDGEMENTS

I would like to thank my supervising professor, Daniel W. Armstrong, for his constant support, encouragement, and guidance throughout my doctoral studies. I am indebted to him for teaching me not only research, but also several life lessons. I am grateful to Dr Hyejin Moon for her support and allowing me to use her laboratory for my research. I also thank professor Richard B. Timmons and professor Krishnan Rajeshwar for serving on my committee. I am indebted to professor Rasika Dias and professor Gamini Rajapakse for letting me know about UT-Arlington Chemistry program and assisting me with the admissions process.

It is a pleasure to thank Barbara and my colleagues from both Dr. Armstrong's group and Dr. Moon's group for their support and friendship. I owe my deepest gratitude to the Department of Chemistry and Biochemistry at UT Arlington for financial aid and all department staff members for their kind assistance.

I was lucky to have my primary, secondary, and tertiary education in Sri Lanka from St. Anthony's College-Kandy and University of Peradeniya, at both of which I received free education. It is an honor for me to thank all the Sri Lankan citizens for funding the Sri Lankan Free Education System with their tax money.

Most importantly, this work would not have been possible without the love, care and support of my wife, parents, siblings and my grand parents. They have been with me through both the difficult and happy moments of my life.

November 8, 2010

ABSTRACT

ELECTROWETTING OF IONIC LIQUIDS AND DEVELOPMENT OF AN ELECTROWETTING BASED TUNABLE RC FILTER AND ITS USES AS AN ANALYTICAL DETECTOR

YASITH SAMEERA NANAYAKKARA, Ph.D.

The University of Texas at Arlington, 2010

Supervising Professor: Daniel W. Armstrong

Wettability control of a liquid drop by an external electric field or "electrowetting" recently was the subject of special interest among researchers due to its utility for a variety of applications. Some of these include "electrowetting on dielectric (EWOD)" based digital microfluidic lab-on-a-chip devices, EWOD lenses and EWOD displays. In these EWOD based devices, water or aqueous electrolytes are used as the liquid medium. However, the use of water or aqueous electrolytes has several limitations and may reduce the efficiency as well as accuracy of these devices. Low thermal stability, evaporation, fouling and fixed physiochemical properties are a few of the drawbacks of water and aqueous electrolytes. To overcome these limitations the alternative use of ionic liquids (ILs) in EWOD based devices are suggested in this dissertation.

ILs are a special class of non-molecular liquids, which do not evaporate. High thermal stability and tunable physiochemical properties are few of the other unique properties of ILs. In order to use in EWOD based devices, the electrowetting prop-

erties of 19 different ILs were examined under DC voltage conditions. All tested ILs showed electrowetting of various magnitudes on an amorphous flouropolymer layer. The effects of IL structure, functionality, and charge density on the electrowetting properties were studied. Compared to water and aqueous electrolytes, ILs showed enhanced stability at higher voltages.

With the obtained clear knowledge of electrowetting behavior of ILs under DC voltage conditions, electrowetting behavior of ILs under AC voltage conditions were examined. Nine different ILs at 3 different AC frequencies (60 Hz, 1 kHz, 10 kHz) were investigated experimentally. The electrowetting properties of ILs were found to be directly related to the frequency of the AC voltage. These relationships were further analyzed and explained theoretically. The electrowetting properties of ILs under AC voltages were compared to that under DC voltages. All tested ILs showed greater apparent contact angle changes with AC voltage conditions than with DC voltage conditions. The effect of structure and charge density also were examined. Electrowetting reversibility of ILs under AC voltage conditions was studied. The physical properties of ILs and their electrowetting properties under both DC and AC voltage conditions were tabulated in order to use as references for the engineering of task-specific electrowetting agents (ILs) for future EWOD based applications. Further, the study showed that in AC voltage conditions, an EWOD experimental setup acts as a liquid RC filter.

Also the study revealed that, the cut-off frequency (f_C) of this type of RC filter is a function of conductivity, dielectric constant, surface tension and double layer thickness of the liquid as well as the applied voltage. That relationship was used to develop a tunable RC filter and an analytical detector. Industrial biocides with different solvents were used to test the performance of this detector. Low limits of

detections were achieved for the tested biocides and the detector seems to be broadly applicable and have very low fabrication costs.

TABLE OF CONTENTS

LIST OF FIGURES

LIST OF TABLES

CHAPTER 1

INTRODUCTION

1.1 Electrowetting

Electrowetting is the decrease of apparent contact angle of a liquid drop upon application of an external electric field across the solid/liquid interface.[1] This phenomenon is observed on both bare conductive surfaces as well as dielectric coated conductive surfaces. When the external electric field is removed from the system, the apparent contact angle tends to approach its original value, if the electrowetting is performed on a smooth dielectric surface like Teflon.[2] Figure 1.1 shows the simplest experiment setup for electrowetting on dielectric (EWOD). Figure 1.1.a describes the state of the droplet before applying the external voltage (zero external voltage). In this figure, θ_0 is the apparent contact angle at zero external voltage; while γ, γ_{SV} and γ_{SL} are the interfacial tensions associated with the liquid/vapor, solid/vapor and solid/liquid interfaces. Figure 1.1.b shows the state of the droplet after applying the external voltage, where θ is the apparent contact angle at any given external voltage.

The apparent contact angle of a liquid drop can be changed back and forth (easily controlled) by changing the external electric field. The relationship between external electric field across the dielectric layer (V) and the apparent contact angle (θ) can be described by the Young-Lippmann equation,[1]

$$cos\theta = cos\theta_0 + \frac{c}{2\gamma}V^2 = cos\theta_0 + \frac{\epsilon\epsilon_0}{2\gamma t}V^2 \tag{1.1}$$

Where c is the specific capacitance, ϵ is the relative permittivity of the dielectric layer (dielectric constant), ϵ_0 is the permittivity of a vacuum, γ is the surface tension

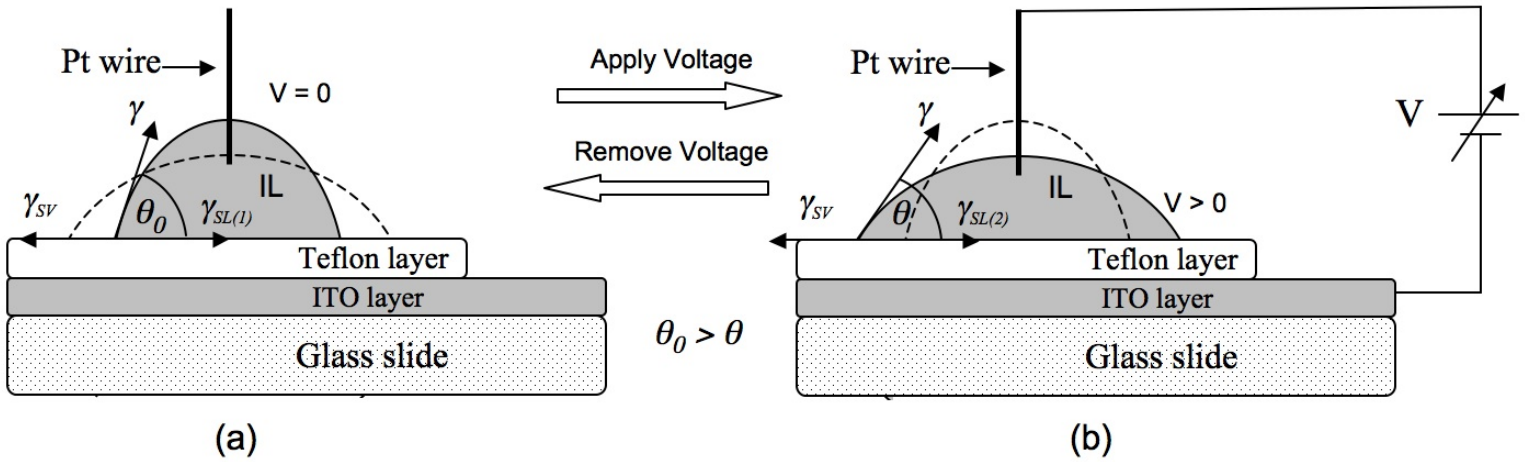

Figure 1.1: Simple electrowetting on dielectric (EWOD) experiment setup

Here θ_0 is the contact angle at zero external voltage and θ is the contact angle at any given voltage. γ, γ_{SV} and γ_{SL} are the interfacial tensions associated with the liquid/vapor, solid/vapor and solid/liquid interfaces.

of the liquid, t is the thickness of the dielectric layer, θ is the contact angle at the designated voltage across a dielectric layer, and θ_0 is the contact angle at zero voltage. Typically, θ tends to decrease when V increases. At some point (saturation point) the contact angle does not continue to change in a regular factor with increasing voltage. The voltage and corresponding contact angle where this occurs is referred to as the saturation voltage and saturation angle, respectively.

Control of the apparent contact angle of a liquid drop by external electric field is useful in many ways and has many applications.[1,3] In next section, some of its applications are described in brief.

1.2 Electrowetting Applications

In general, electrowetting experiments can be designed in two ways in order to be used in applications. In the first design method (see Figure 1.2.a) a droplet is stationed in one position and only the shape (contact angle) of the drop changes with the external electric field (stationary drop method). In the second method (see Figure 1.2.b), the electrowetting effect along with dielectroporetic forces, is used to move (actuate) a droplet from one position to another position (drop actuation method). Both methods are used in variety of applications (see Figure 1.3) as described in the following paragraphs.

1.2.1 Electrowetting Applications with the Stationary Drop Method

Electrowetting has been used successfully to develop variable fluid focal lenses for cell phones and digital cameras.[4] Since there are no mechanically moving parts in electrowetting lenses, they can be fabricated in micro-scale. Also the power consumption of these EWOD lenses are much lower than that of traditional lens systems. Varioptic produces EWOD lenses commercially for digital cameras and cell phones.[5]

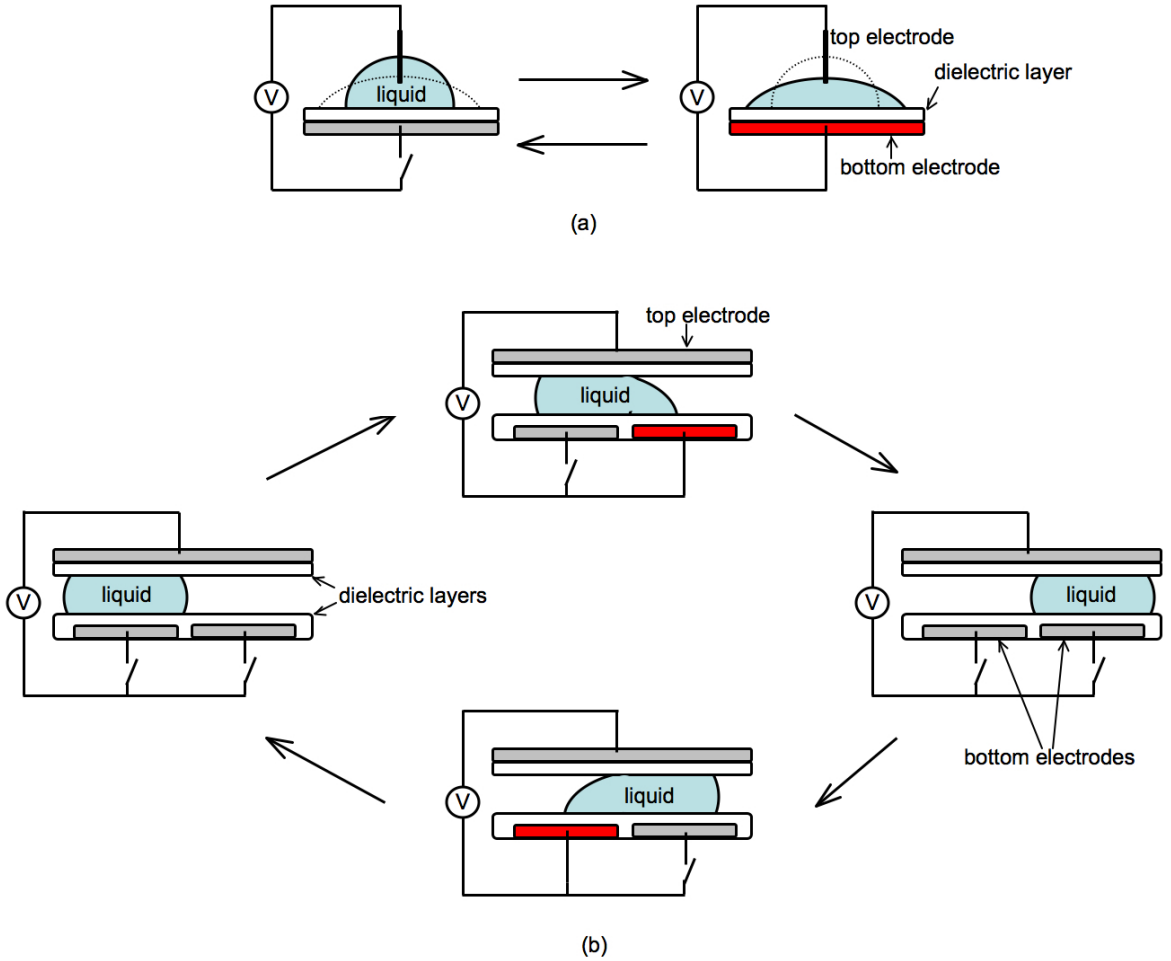

Figure 1.2: Two basic types of EWOD based device designs: a) stationary drop method, b) drop actuation method

In stationary drop method, a drop is stationed in one position, only the shape of the drop changes when the electrode is activated or deactivated. In drop actuation method, a drop is actuated by activating and deactivating the adjacent electrodes, an array of these type of electrodes are used in EWOD microfluidic devices.

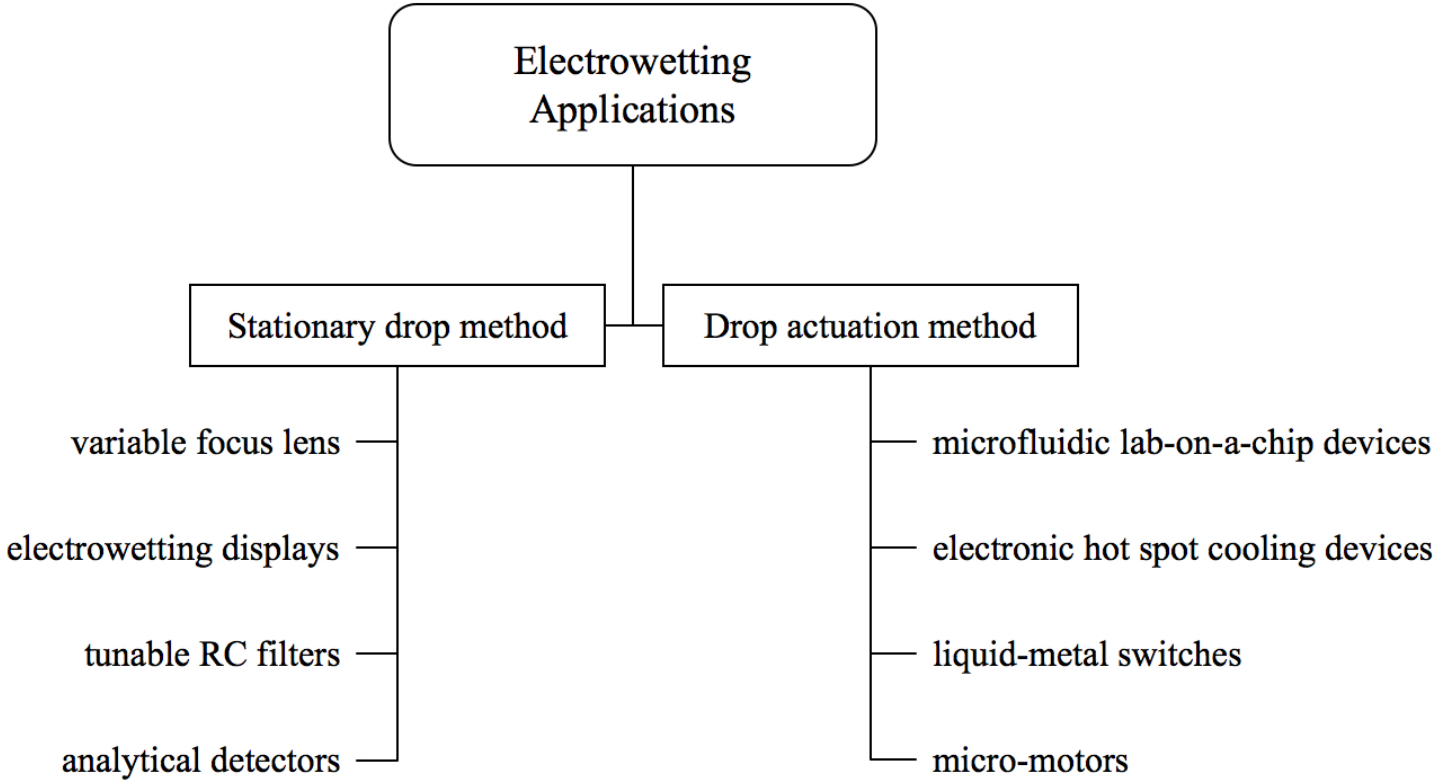

Figure 1.3: An overview of electrowetting applications

Another important application of the static drop method is "electrowetting displays".[6] Electrowetting displays are considered as competitive alternatives to liquid crystal displays. Electrowetting displays are used as displays in cellphones, digital cameras, portable video players and e-papers. Liquavista fabricates a variety of commercial electrowetting displays.[7] Apart from these two well-known applications, we recently developed a tunable RC filter using a stationary drop electrowetting method.[8] Then we modified that RC filter as an analytical detector to identify a variety of compounds including industrial biocides.[9] The development of the tunable RC filter and its uses are discussed in Chapter 4 of this dissertation. In Chapter 5, the development of the analytical detector and its uses are discussed.

1.2.2 Electrowetting Applications with Drop Actuation

Since electrowetting forces (some times along with dielectrophoretic forces) can effectively be used to actuate a droplet from one position to another, electrowetting has been used to develop a variety of microfluidic lab-on-a-chip devices.[10] EWOD based lab-on-a-chip devices are versatile compared to traditional lab-on-a-chip devices due to several advantages such as; a) low power consumption, b) no pumps or mechanically moving parts, c) independent control of droplets, d) flexible and programmable droplet paths and e) scalability of the platform to multiplexed assays. EWOD based lab-on-a-chip devices are used in biological sample preparation and several analysis processes[11–16] as well as liquid-liquid extraction devices.[17,18] In addition to lab-on-a-chip devices, EWOD based drop actuation method is used in micro heat transfer devices,[19] micromotors[20] and EWOD switches[21]

Water or aqueous electrolyte droplets are most widely used in EWOD based devices. However, the use of water or aqueous electrolytes in EWOD based devices

creates many problems. The following section describes the limitations of using water and aqueous electrolytes in EWOD based devices.

1.3 Limitations of Using Water and Aqueous Electrolytes in EWOD Based Devices

The major problem associated with water and aqueous electrolytes is their evaporation. This limits the device operation time and accuracy of the results produced by the device. As an example, if 1 M solution of compound A is used in a EWOD based microfluidic device, after 10 minutes the concentration of solution A would be more than 1 M due to solvent evaporation. Hence in the case of long time-period operations, the accuracy of the results produced by the device is questionable. One common resolution for this problem is to surround the droplet with silicone oil, however that can contaminate the droplet and could produce poor results. In addition, fouling can occur via precipitation of salts from aqueous electrolytes.[22] Another drawback of water and aqueous electrolytes is their low thermal stability, this limits the operating temperature of EWOD based devices and as a consequence, most EWOD based devices are operable only at ambient conditions. Some EWOD devices need to have controlled physical properties of their operating liquid drops.[10] As an example some EWOD based microfluidic devices need to have a liquid which is capable of selectively extract some proteins. Also in micro heat transfer devices, liquids should have higher thermal conductivities along with low evaporation. However, controlling the physical properties of a traditional liquids (i.e., water or aqueous electrolytes) to suit the application is a difficult task.

To overcome above mentioned limitations of water and aqueous electrolytes, the alternative use of ionic liquids (ILs) is suggested. A brief introduction to ILs and their advantages over traditional liquids are discussed in the following section.

1.4 Ionic Liquids

Ionic Liquids (ILs) are a special class of liquids which do not evaporate with time. ILs are typically composed of organic ions. They are liquid under 100°C. ILs that have melting point lower than ambient temperature are called room temperature ionic Liquids (RTILs). Typically, ILs are composed of unsymmetrically substituted nitrogen or phosphorous containing cations (e.g., imidazolium, pyrrolidinium, pyridinium, phosphonium) with inorganic (e.g., Cl^-, PF_6^-, BF_4^-) or sometimes organic anions.[23] Some typical IL cations and anions are shown in Figure 1.4. Synthesis of ILs were first reported by Wilkes et al. in 1982. They were based on 1-alkyl-3-methylimidazolium cations.[24] Since then, scientists around the world have produced thousands of different ILs. The interest in research involving ILs grew due to their unique properties such as negligible vapor pressure, high thermal stability and physiochemical properties that can be tuned depending on the application.

ILs are used in variety of scientific and technical areas.[23,25,26] Figure 1.5 gives an overview of the applications of ILs in chemistry. lLs can be used in liquid-liquid extractions due to their alcohol like polarities and salt like composition.[27,28] ILs are used as gas chromatography (GC) stationary phases since they have low volatility, variable viscosities, excellent thermal stability, and variable polarities.[29] In liquid chromatography(LC) ILs are used as stationary phases[30] as well as mobile phase additives.[31] In capillary electrophoresis (CE) ILs are used to modify capillary walls,[32] as non-aqueous electrolytes[33] and as modifiers in micellar CE.[34] In MALDI mass-sepectroscopy (MS), ILs are used as matrices.[35,36] In ESI-MS ILs are used as pairing reagents to detect anions in the positive mode.[37–39] In addition ILs are used in various aspects of electrochemistry,[40] including electrochemical sensors.[41] Applications of ILs in electrowetting is discussed in the next section.

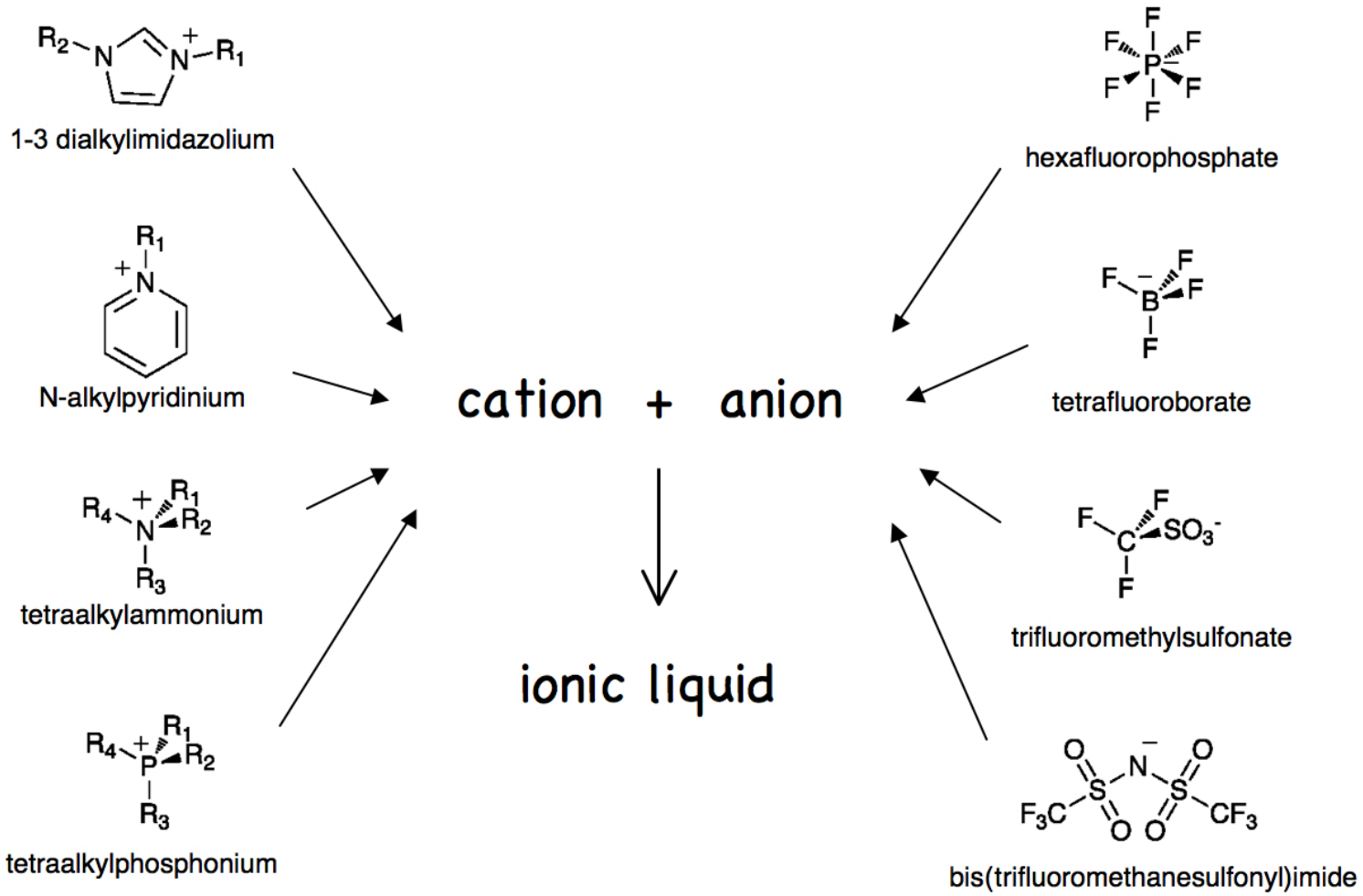

Figure 1.4: Common cations and anions of ionic liquids. R_1, R_2, R_3, and R_4 are alkyl groups and can be the same or different

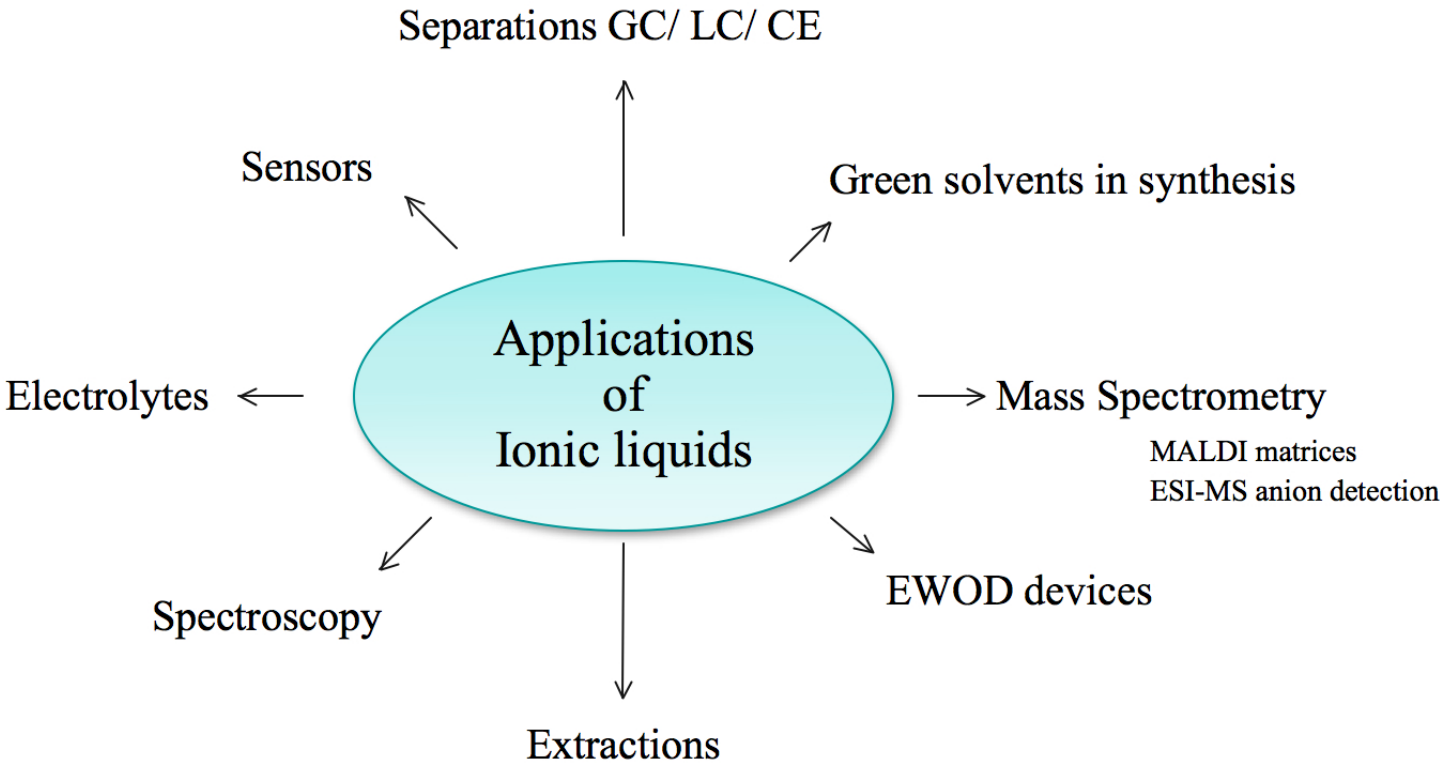

Figure 1.5: An overview of applications of ionic liquids

1.5 Ionic Liquids in Electrowetting

The use of ILs in an EWOD based microfluidic device was first reported by Chatterjee, et al. in 2006.[42] In that work it was shown that two ILs, $[bmim][BF_4]$ and $[bmim][PF_6]$ can successfully move on an EWOD based chip. Later in that year Millefiorini et. al. studied the electrowetting properties of three ionic liquids on amorphous fluoropolymer layer under DC electrc field.[43] In the same year Dubois et al. used ILs as solvents to perform chemical reactions in an EWOD based chip.[44] Again in the same year, Ricks-Laskoski et al studied electrowetting behavior of an IL polymer.[45] In 2008, we reported a comprehensive study of ILs under DC electric fields.[46] In that study 19 different ILs, including mono, di, and tricationic plus mono and di-anionic ILs were used to study the effect of IL structure, functionality and charge density on electrowetting behavior. In addition, the stability of ILs under higher voltages and the effect of water on the electrowetting by ILs were examined. Those studies are discussed in detail in Chapter 2. In the same year, 2008, Halka and Freyland studied electrowetting of 2 ILs under high vacuum conditions on different dielectric substrates.[47] In 2009, we reported on the electrowetting behavior of linear-tricationic ILs,[48] used an IL in EWOD based micro heat transfer device[19] and in EWOD based liquid-liquid micro extraction devices.[18] In the same year Restolho et al studied contact angle saturation and irreversibility of ILs when they undergo electrowetting.[49]

In early 2010, we reported an extensive study on the electrowetting of ILs under AC electric fields.[2] In that study, the AC frequency dependence on the electrowetting of 9 different ILs (including mono-, di-, and tricationic) was studied. The objectives were to explain the theoretical relationships between all relevant factors and to compare the electrowetting of ILs using AC vs. DC voltage fields systematically. Also, the effect of IL structure and charge density was examined for AC conditions. Fur-

ther, electrowetting reversibility and the effect of water content on electrowetting was evaluated. Those studies are discussed in detail in Chapter 3. In the same year we demonstrated the synthesis of ILs on EWOD based microfluidic chip.[50] In mid-2010, we invented a liquid IL based tunable RC filter using electrowetting.[8] Details about the development of the tunable RC filter are presented in Chapter 4 of this dissertation. In the same year, 2010, Paneru et al. reported electowetting behavior of an IL in a solid/liquid/liquid system.[51,52] Shortly after that Zhang et al tested several ILs with same kind of system with both AC and DC electric fields.[53]

Typically electrowetting properties under AC electric fields differ those from under DC electric fields. These differences can easily be understood by examining RC filter effect. The next section will outline the RC filter effect in electrowetting.

1.6 RC Filter Effect in Electrowetting

1.6.1 RC Filter

A resistor-capacitor (RC) filter is an electronic circuit which consist of resistors and capacitors. RC filters are used to discriminate unwanted frequency elements from a specific signal. RC filters can broadly be categorized into two types: low-pass RC filters and high-pass RC filters. Figure 1.6.a and 1.6.b show schematics of simple first order, low-pass and high-pass RC filter respectively.

When a signal is proceeded through a low-pass RC filter, it passes low frequencies, but attenuates the frequencies which are higher than a certain frequency called the *cut -off frequency* (f_C). Conversely, a high-pass RC filter passes high frequencies, but attenuates the lower frequencies with respect to f_C. The f_C of a simple first order RC filter can be calculated with the following equation,[54]

$$f_C = \frac{1}{2\pi RC} \tag{1.2}$$

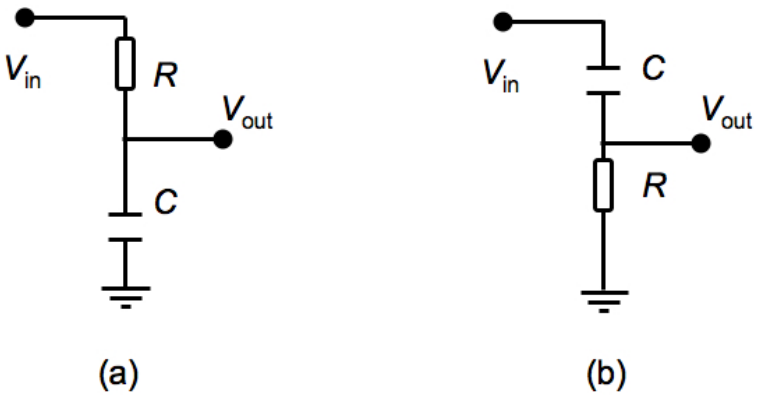

Figure 1.6: Schematic Diagrams of First Order, Simple a) Low-Pass RC Filter, b) High-Pass RC Filter

Here R is the resistance value in ohms (Ω) and C is the capacitance value in Farads (F). However for complex RC filters (i.e., RC filters which have more than one resistor or capacitor), the f_C calculation equation is much complicated than equation 1.2. For such filters, (as well as for simple RC filters) experimental determination of f_C is possible. Typically a *gain* ($=20 * log[V_{out}/V_{in}]$) versus *frequency* plot is used to experimentally determine the f_C of a certain filter.[54] Figure 1.7 shows the *gain* versus *frequency* plot of a hypothetical RC filter. Using that plot, f_C is determined from the intersection of the curve and the -3 dB line.

1.6.2 RC Filter Circuit Model in an Electrowetting Experiment

Generally, when an electrowetting test is performed for a specific liquid under an AC electric field, the obtained results differ from the same test performed under a DC electric field. Scientists suggest this may be due to the "*RC filter type*" effect in an electrowetting experimental setup.[2,55–59] This means that the liquid drop can act as a capacitor (C_{liquid}) and resistor (R_{liquid}) connected in parallel, in addition to the dielectric layer of the experiment setup which can act as a capacitor ($C_{dielectric}$) (See, Figure 1.8.a and 1.8.b). Since there is no place to monitor the output voltage

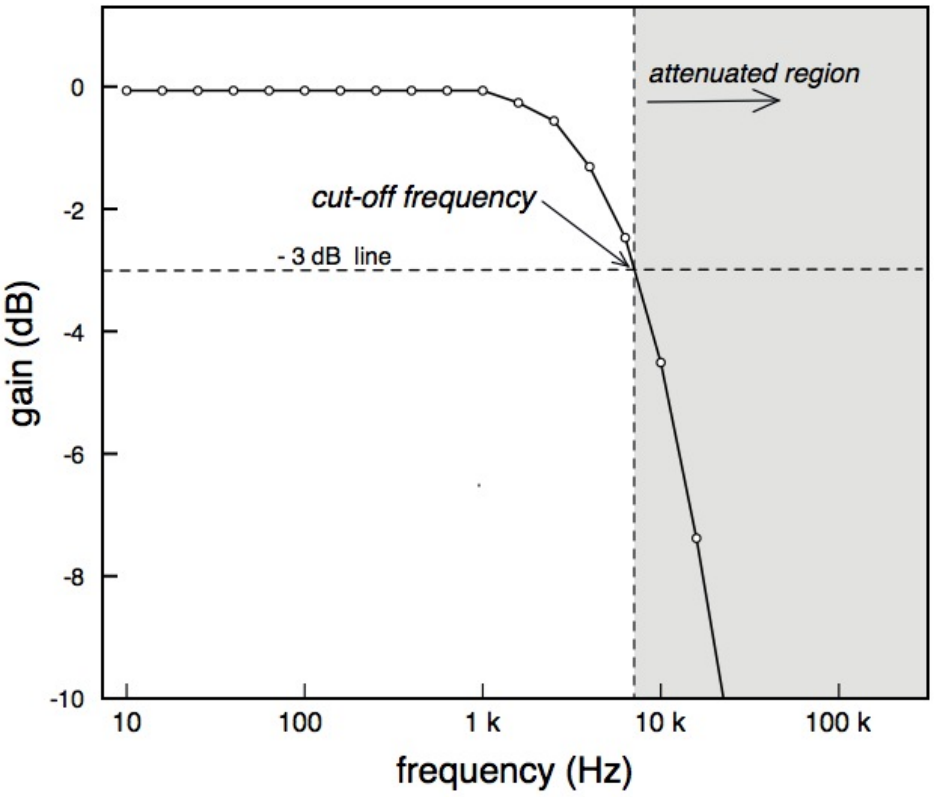

Figure 1.7: A Typical Gain Versus Frequency Plot

Cut-off frequency value (f_C) is determined from the intersection of the curve and the $-3\ dB$ line. Note that the frequency axis is in logarithmic scale. The frequency range in the x-axis may vary depending on the filter.

with the experiment setup shown in Figure 1.8.a, the f_C value cannot be determined from a conventional electrowetting setup. Therefore the direct relationship between f_C and other factors (such as applied voltage and physiochemical properties of the liquid) cannot be established. However if an extra resistor is added to the system as shown in Figure 1.8.c one can easily measure f_C. Note that, f_C for the system shown in Figure 1.8.a and f_C for the system shown in Figure 1.8.c should be numerically different. However, since the R value is a constant, one can easily explore how physiochemical properties of the liquid and the applied voltage affect f_C. In Chapter

4, an investigation of the relationship between applied voltage and f_C, which leads to a development of a tunable RC filter, is discussed. In chapter 5, we outline an investigation into the relationship between the physiochemical properties of liquids and the corresponding f_C's which leads to the development of an analytical detector.

1.7 Summary

Electrowetting on dielectric is used in variety of applications. In general water or aqueous electrolytes are used as the liquid medium in these applications. However use of water or aqueous electrolytes in EWOD based applications have several disadvantages. Therefore the alternative use of ionic liquids is suggested in this dissertation. ILs are a special class of liquids that do not have appreciable vapor pressure, but do have several unique physicochemical properties that traditional liquids lack. Electrowetting properties of ILs seem to be unique and tunable. Using these unique properties, an IL is successfully used to develop an EWOD based tunable RC filer. Further studies proved EWOD based RC filters can be used as powerful analytical detectors.

1.8 Organization of Dissertation

Chapter 2 of this dissertation will describe the electrowetting behavior of ILs under DC electric field. The effect of IL structure, functional groups and charge density on electrowetting under DC fields will be discussed in detail. In addition, the stability of ILs in higher DC fields and the effect of the water content of ILs will also be discussed in this chapter.

In contrast, Chapter 3 will examine the electrowetting behavior of ILs under AC electric fields: Differences in electrowetting under AC vs. DC electric fields

will be discussed in detail. Also, the effect of AC frequency on electrowetting will be explained theoretically and experimentally along with the effect of structure and charge density of the ILs. Finally, the reversibility of electrowetting and effect of water content will be discussed.

Chapter 4 will describe about the development of an EWOD based tunable RC filter using an IL as the liquid drop. Also possible future applications of this RC filter will be discussed.

Chapter 5 will report the development of an analytical detector using a RC filter. Proof of principle of this analytical detector will be presented using industrial biocides. In addition, future directions and advantages over existing detectors will be discussed. Finally a general summary will be presented in chapter 6.

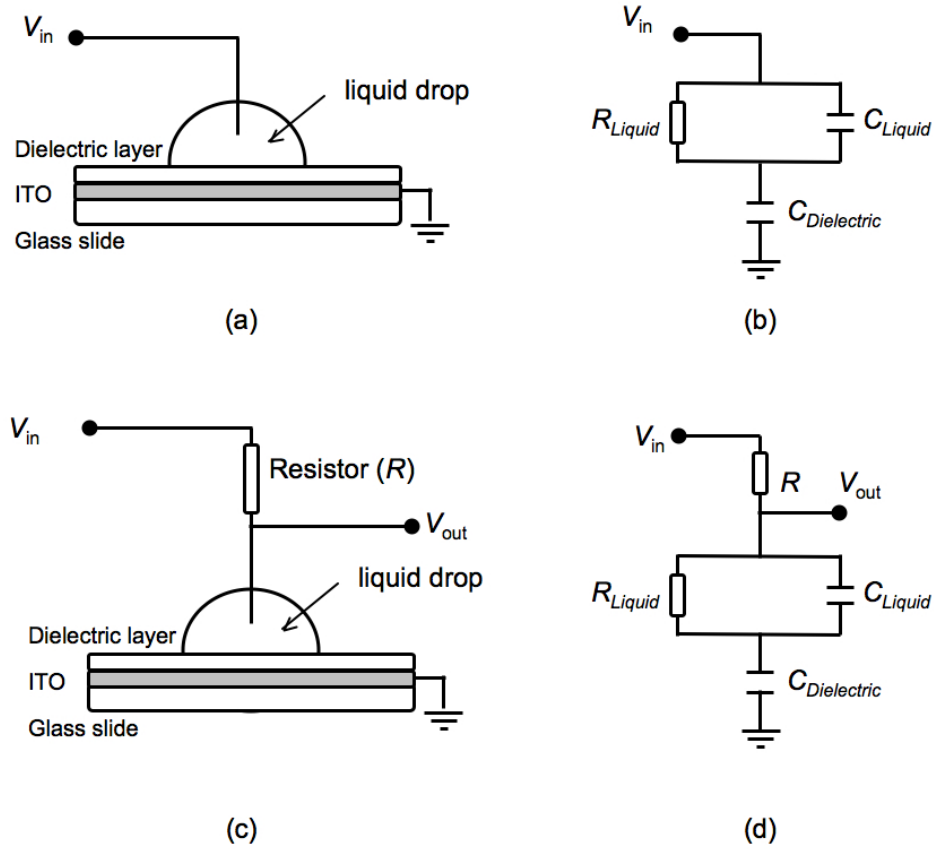

Figure 1.8: Electrowetting setups and equivalent circuit models a) a conventional electrowetting setup, b) equivalent circuit model for the conventional electrowetting setup, c) an extra resistor is added to the conventional electrowetting setup in order to measure f_C, d) equivalent circuit model for the modified electrowetting setup. Note that imperfect dielectric layers could cause leakage current across the dielectric layer; in that case the extra resistor value ($R_{dielectric}$) should be added in parallel to $C_{dielectric}$

CHAPTER 2

A FUNDAMENTAL STUDY ON ELECTROWETTING BY TRADITIONAL AND MULTIFUNCTIONAL IONIC LIQUIDS

Water or aqueous electrolytes are the dominant components in electrowetting on dielectric (EWOD)-based microfluidic devices. Low thermal stability, evaporation, and a propensity to facilitate corrosion of the metal parts of integrated circuits or electronics are drawbacks of aqueous solutions. The alternative use of ionic liquids (ILs) as electrowetting agents in EWOD-based applications or devices could overcome these limitations. Efficient EWOD devices could be developed using task-specific ILs. In this regard, a fundamental study on the electrowetting properties of ILs is essential. Therefore electrowetting properties of 19 different ionic liquids, including mono-, di-, and tricationic, plus mono- and dianionic ILs were examined. All tested ILs showed electrowetting of various magnitudes on an amorphous flouropolymer layer. The effects of IL structure, functionality, and charge density on the electrowetting properties were studied. The enhanced stability of ILs in electrowetting on dielectric at higher voltages was studied in comparison with water. Deviations from classical electrowetting theory were confirmed. The physical properties of ILs and their electrowetting properties were tabulated. These data can be used as references to engineer task-specific electrowetting agents (ILs) for future electrowetting-based applications.

2.1 Introduction

Electrowetting is the decrease in contact angle achieved by applying an external voltage across a solid/liquid interface. The control of wettability by using external

electric fields has opened new opportunities in microfluidics. The motion of small volumes of liquid segments can be controlled by programmed electric fields. Recently, interest in electrowetting on dielectric (EWOD) has increased substantially compared to interest in simple electrowetting. In EWOD, when the voltage is removed, a droplet returns to its original shape, while a droplet stays at its wetting shape in simple electrowetting.[60] Reversibility is critical for wettability control to be useful in microfluidic applications. EWOD has been successfully applied to develop digital (digitized droplet based) microfluidics.[61,62] Digital EWOD microfluidic devices have provided successful laboratory-on-a-chip platforms for various biological sample preparation and analysis processes.[11–16] Besides bioanalytical applications, electrowetting has also been found to be very useful in many other applications such as fluid lens systems,[4] electrowetting displays,[6] programmable optical filters,[63] paint drying,[63] micromotors,[20] electronic microreactors,[44] and to control fluids in multichannel structures.[64]

Traditionally, water or aqueous electrolyte solutions are used in most EWOD experiments and applications. Although water has useful solvent properties, its low thermal stability, evaporation, and propensity to facilitate corrosion of the metal parts of integrated circuits or electronics still can cause problems in various applications. Another drawback in most microfludic devices is fouling, which occurs in many ways.[22] For example, in microfludic devices, fouling can occur via precipitation of salts from aqueous electrolytes due to evaporation and from degasification of the electrowetting solvents. Clearly the use of aqueous electrolytes as electrowetting agents in a variety of devices can have significant limitations. Unfortunately, few substances have been proposed or successfully tested as viable substitutes for water.[15] In this regard, we believe that ionic liquids (ILs) may have advantages over water and other aqueous electrolytes. For example, they are liquid over a wider range of

temperatures,[65,66] they have negligible or very low vapor pressures, most ILs have high thermal stability,[66] most ILs are nonflammable,[67] and they have "tunable" solvent properties that can be selected and optimized for specific tasks.[68] Consequently, ILs may be ideal replacements for, or complementary to, traditional aqueous electrolytes in many electrowetting applications. Specifically, fouling can be effectively controlled in electrowetting-based microfluidic devices by using ILs due to their nonvolatility and favorable solvent properties for diverse compounds. A previously published communication about electrowetting of ILs[43] demonstrated electrowetting of ILs on an amorphous fluoropolymer surface, but their experiment was limited to three simple and less stable ILs. Dubois et al. reported the use of IL droplets as electronic microreactor on an open digital microfluidic chip.[44] Also, Chatterjee et al. demonstrated the successful use of two ILs in digital microfluidic devices.[42] However, a systematic study of the effect of IL structure on their electrowetting behaviors has not been done to our knowledge. With the emergence of new types of ILs, including dicationic,[66,69] tricationic,[70,71] and even dianionic[72] types, the electrowetting properties are expected to be more diverse and potentially can be tailored for variety of EWOD applications. In this study, the electrowetting behaviors of 19 different ILs, including mono-, di-, and tricationic, plus mono- and dianionic ILs were examined. The effects of structure, functionality, and charge density on the electrowetting properties were examined. The relevant physical properties of these ILs were determined. Finally, some ILs are suggested as potential replacements for traditional electrowetting solvents for specific applications. By examining physical properties and electrowetting properties of a broad range of ILs one can identify suitable agents for particular applications.

2.1.1 Theoretical Background.

An equation that relates the contact angle (θ) of a liquid drop on a dielectric surface to the external applied voltage (V) can be derived from a combination of Young's equation and Lippmann's equation (eq 2.1).[1]

$$cos\theta = cos\theta_0 + \frac{c}{2\gamma}V^2 = cos\theta_0 + \frac{\epsilon\epsilon_0}{2\gamma t}V^2 \tag{2.1}$$

Where c is the capacitance per unit area (specific capacitance), ϵ is the relative permittivity of the dielectric layer (dielectric constant), ϵ_0 is the permittivity of a vacuum, γ is the surface tension of the liquid, t is the thickness of the dielectric layer, θ is the contact angle at the designated voltage across a dielectric layer, and θ_0 is the contact angle at zero voltage. At some point (saturation point) the contact angle does not continue to change in a regular factor with increasing voltage. The voltage and corresponding contact angle where this occurs is referred to as the saturation voltage and saturation angle, respectively. According to equation 2.1, a plot of contact angle versus applied voltage should be a parabola as shown in Figure 2.1.

Five quantities can be extracted from such plots and used to characterize the eletrowetting of different solvents (Figure 2.1). They are as follows: θ_0 is the contact angle at zero voltage, $\Delta\theta_L$ is the change in contact angle at negative voltages, and $\Delta\theta_R$ is the analogous contact angle change at positive voltages. V_L is the saturation voltage in the negative voltage realm, and V_R is the analogous saturation voltage in the positive voltage realm. In this work, we demonstrate that a wide variety of ionic liquids follow typical electrowetting behaviors and that this behavior can vary with the nature of the IL. Although we focused on the electrowetting properties of ILs, with a view toward their use in EWOD based microfluidic devices, it should be noted that droplets can be moved or actuated by various other forces along with electrowetting forces.[56–58,73] The physics of these forces are still being investigated

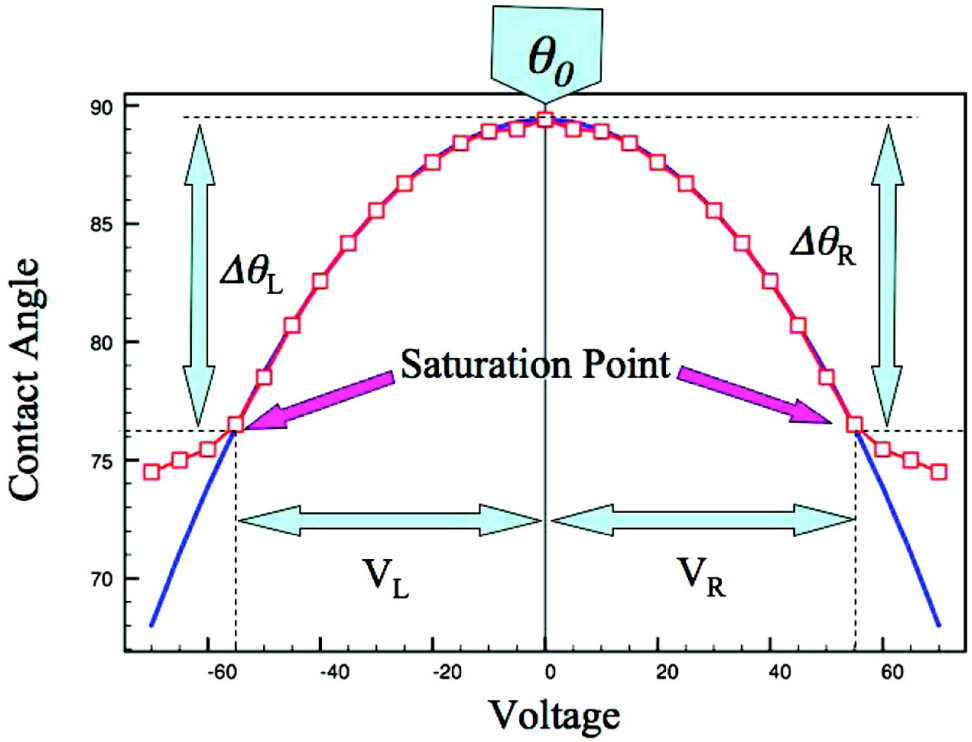

Figure 2.1: Characteristic parameters that can be measured from an electrowetting curve

for common liquids such as water. Thus, the study and understanding of even more complex and diverse solvents such as ionic liquids are likely to be important future endeavors.

2.2 Experimental Section

The structures of the studied ionic liquids are shown in Figure 2.2. and some of their physical properties are listed in Table 2.1. IL17 and IL18 were provided from CYTEC (www.cytec.com, West Paterson, NJ). All of the other ILs were synthesized in our laboratory as reported previously.[66,69,71,72]

The experimental setup for the electrowetting determinations is shown in Figure 2.3. The electrowetting experiments were performed somewhat differently from those

reported by Millefiorini et al.[43] First, indium tin oxide (ITO, 30-nm thickness) pre-coated unpolished float glass slides (www.delta-technologies.com, Still- water, MN) were dip-coated with an amorphous fluoropolymer layer (Teflon). The Teflon solution was prepared by dissolving 4% (w/v) of Teflon AF1600 (www2.dupont.com, Wilmington, DE) in Fluoroinert FC 75 solvent (www.fishersci.com, Barrington, IL). The dipping speed was set to 750 $\mu m/s$ in a custom-made dip coater. Once 3/4 of the slide was dipped in the solution, dipping was stopped for 5 s, and then the slide was raised at the same speed. The coated slides were then heat treated for 6 min at 112 °C, 5 min at 165 °C and 15 min at 328 °C in an oven.Teflon- coated glass slides were then allowed to cool to room temperature, washed thoroughly with acetone and deionized water, and air- dried. The resulted Teflon thickness was $260 \pm 10nm$. The thickness was measured using a Tencor Alphastep 200 Profilometer. The electrowetting experiment was conducted using a contact angle goniometer CAM 101 system (Figure 2.3a; www. ksvltd.com, Monroe, CT).

Typically, a drop of ionic liquid was placed on top of the Teflon layer using a capillary tube. The volume of the drop was calculated by using CAM 200 software (www.ksvltd.com, Monroe, CT); the drop volume was between 3 and 8 μL for all experiments. The voltage was applied in 5 V increments starting from 0 to +70 V, using a Keithley 2400 SourceMeter (www.keithley.com, Cleveland, OH). The positive probe was attached to the Pt wire (36 gauge), and negative probe was attached to the ITO layer (Figure 2.3b). Afterward, a fresh drop of IL was placed at a different position on the surface and the above procedure was repeated for 0 to -70 V. Only for IL19 the experiment was conducted from 0 to +200 V and from 0 to -160 V. After each experiment with one IL, the platinum wire was thoroughly washed with acetone and DI water, respectively, and air-dried. At each voltage increment, a picture was taken and contact angles were measured using CAM 200 software. Finally, the contact

angle versus voltage curves were plotted. For some selected ILs, the above procedure was repeated applying voltage from 0 to +100 V in 5 V increments, from 100 to 150 V in 10 V increments, from 150 to 500 V in 50 V increments, and from 500 to 1000 V in 100 V increments, followed by the same procedure for negative voltages. However, when applying higher voltages, some ILs tended to decompose or to burn; at that point applying voltage was stopped. The purpose of applying higher voltages is to determine the stability of ILs upon higher voltages. The effect of water on electrowetting of ILs was studied by using both a water-miscible (i.e., IL1) and a water-immiscible IL (IL4). A series of IL1 + water solutions (w/w) were prepared, and the θ_0 values were measured for each solution. Then electrowetting experiments were conducted for solutions of 5, 10, and 20% (w/ w) water containing IL1. Exactly 0.5 mL of the water-immiscible IL4 was mixed with 5 mL of water, shaken for 2 min, and then allowed to settle. After 1 h, two layers were clearly observed. Water layer was decanted, and the electrowetting experiment was conducted for the IL4 layer. All experiments were conducted in ambient atmosphere at 23 ± 1°C unless otherwise noted. In regard to their safety, all the tested ILs are nonflammable; however, IL3 may produce HF upon decomposition.

2.3 Results and Discussion

Table 2.1 summarizes some physical properties of the studied ILs, and Table 2.2 summarizes the five electrowetting parameters obtained for 19 different ILs.

2.3.1 Anion Effects

Ionic liquids IL1-IL4 have the same cation, $BMIM^+$. The size of the anion and the delocalization of its charge increases from IL1 to IL4. The reported diameters of the anions are IL1 = 3.62 $\mathring{A}$, IL2 = 3.90 $\mathring{A}$, IL3 = 5.10 $\mathring{A}$, and IL4 = 7.57 $\mathring{A}$.[74]

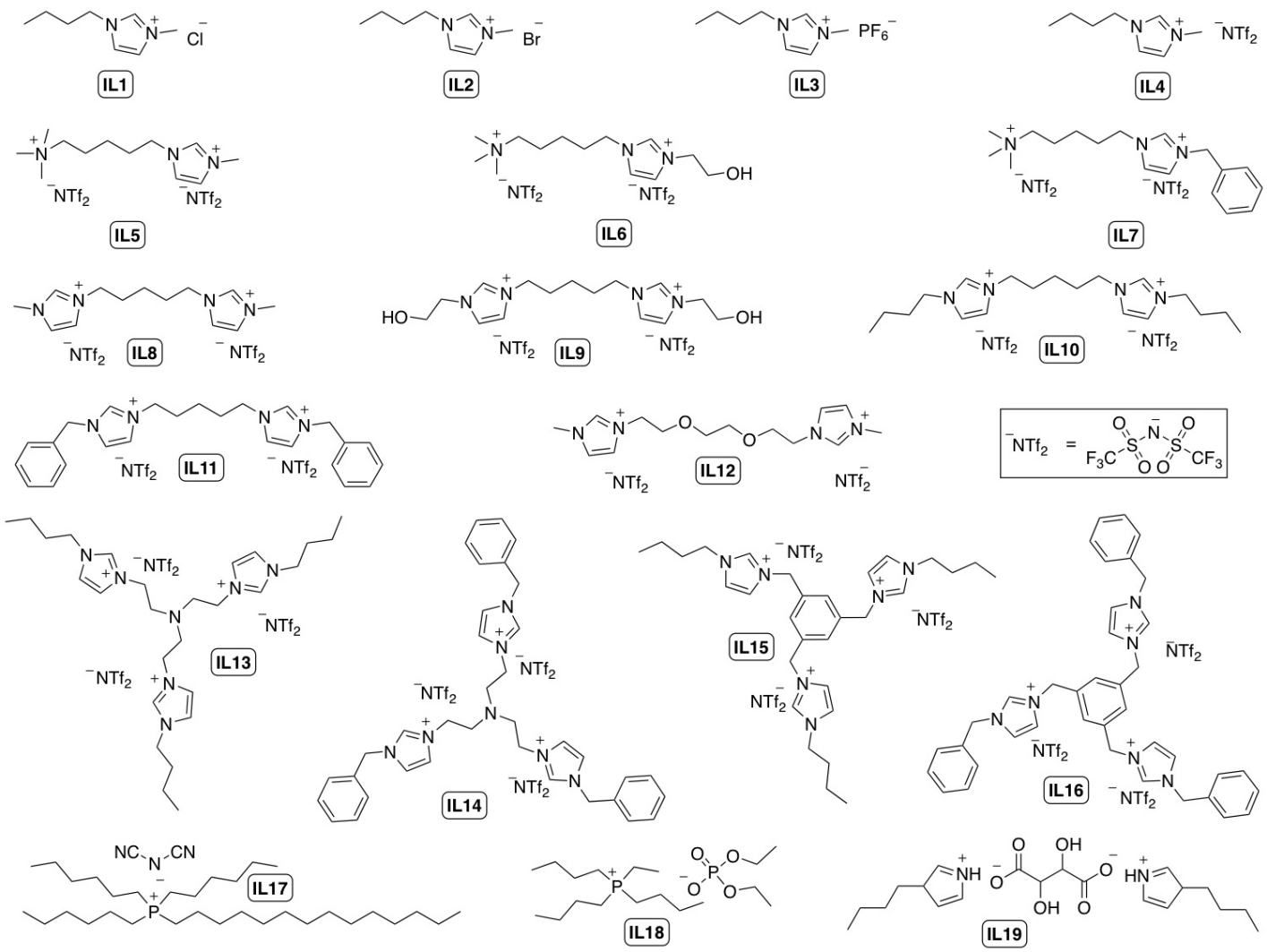

Figure 2.2: Structures and numbering system for the ILs tested.

Table 2.1: Physical Properties of the Studied ILs[a]

ionic liquid	MW (g/mol)	melting point (^{o}C)	density ρ (g/cm3)	refractive index	viscosity at 30 ^{o}C (cSt)	approximate thermal stability (^{o}C)	surface tension (dyne/cm)	work of adhesion (dyne/cm)	miscibility with water
IL1	174.7	65	1.10	1.523	1701	145	60.7	53.3	M
IL2	219.1	70	1.30	1.538	804		54.3	47.7	M
IL3	284.2	-8	1.36	1.411	170		44.8	45.6	I
IL4	419.4	-4	1.43	1.427	36	185	32.8	41.3	I
IL5	771.7	-51.5	1.54	1.431	357	302			I
IL6	801.2	-54.2	1.54	1.435	398	133			I
IL7	847.1	-36.2	1.50	1.458	1217	328			I
IL8	794.2	-61.0	1.57	1.441	251	365			I
IL9	854.2	-65.0	1.58	1.456	241	257			I
IL10	878.3	-62.0	1.44	1.433	355	376	41.5	51.8	I
IL11	960.9		1.08	1.511	6021				I
IL12	840.7		1.36	1.444	350		43.4	47.9	I
IL13	1311.2	-47.5	1.41	1.451	1580	308	43.2	52.9	I
IL14	1413.2	-6.7	1.51	1.493	25000$-$30000	348			I
IL15	1330.2	-24.6	1.53	1.467	2320	344			I
IL16	1432.2	-87.4	1.55	1.588	$20000 - 25000$	262	52.9	60.3	I
IL17	493.8	$> -76 < -22$	0.90	1.484	269	360	40.8	49.3	I
IL18	384.5	$> -76 < -22$	1.01	1.470	360.6	350	38.5	47.2	M
IL19	314.3		1.08	1.500	2104		55.3	52.4	M

[a]Structures and names of the ILs are shown in Figure 2.2. For measurement techniques and data sources see Ref [46].
WM =Water Miscibility, M= Miscibile, I= Imiscible

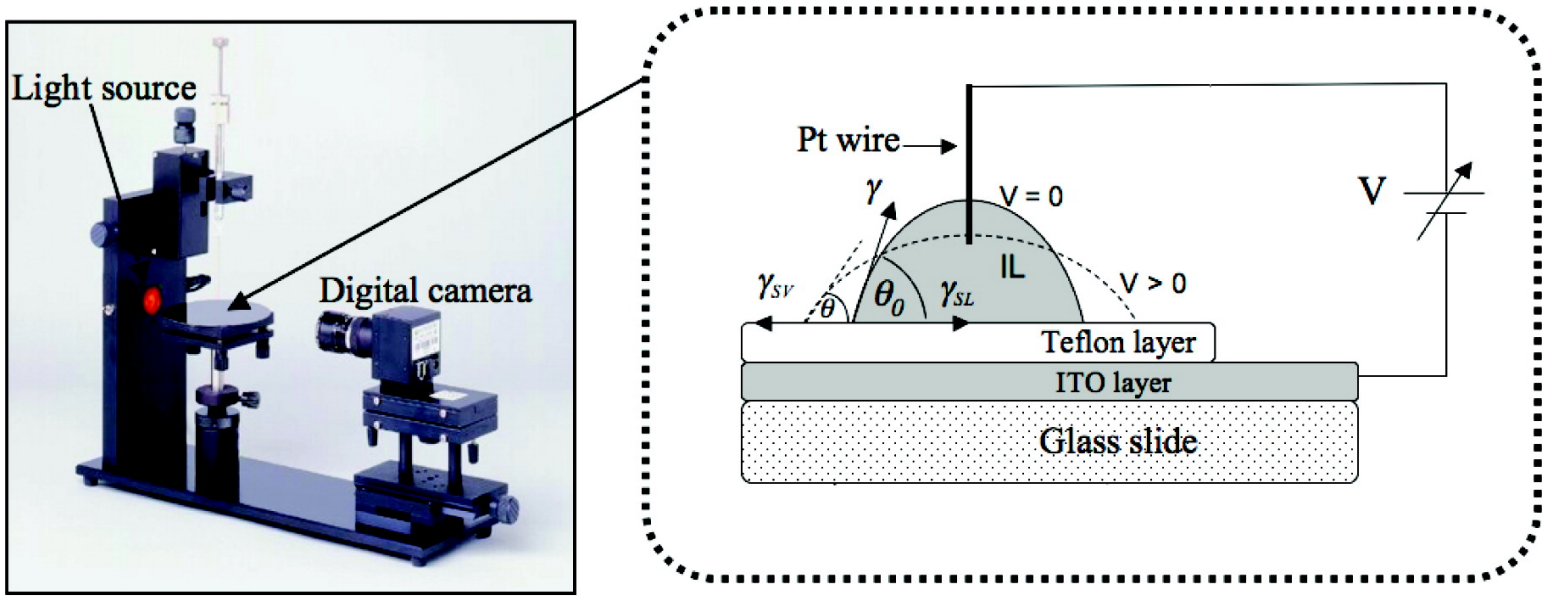

Figure 2.3: Electrowetting experimental setup: (a) CAM 101 system; (b) schematic diagram of glass slide and IL drop. Solid line of the drop represents the drop shape without any external voltage. Dashed line of the drop represents the drop shape with external voltage applied

2.3.1.1 Anion Effect on the θ_0 Value

Figure 2.4a shows the electrowetting curves of IL1-IL4. It is observed that an increase in the size of the anion and charge delocalization leads to a decrease in the θ_0 value. The θ_0 value obtained for IL1 is similar to that of IL2 even though the diameter of Cl^- is slightly smaller than that of Br^-. θ_0 is the contact angle at zero external voltage, which can be described by Young's equation (eq 2.2) as the equilibrium contact angle.[75]

$$\theta_0 = cos^{-1}[\frac{\gamma_{SV} - \gamma_{SL}}{\gamma}] \tag{2.2}$$

Here, γ, γ_{SV}, and γ_{SL} are the interfacial tensions associated with the liquid/vapor, solid/vapor, and solid/liquid interfaces, which are the only three parameters that govern the θ_0 value (Figure 2.3b). Increasing the size and charge delocalization leads to a decrease of the surface tension (γ); this is due to a combination of entropic contribution and enthalpic contributions. An increase in the size of anions will increase the entropy, which lowers the ordering of ions within the liquid and accordingly on the surface.[76] Delocalization of charge will decrease the ability to form hydrogen bonds. Both contributions ultimately reduce the surface tension of IL.[76] From IL1 to IL4, the size of the anion and charge delocalization increase; as a consequence, the surface tension of these ILs decreases in a logical fashion. According to equation 2.2 and considering the (γ_{SV} - γ_{SL}) values are approximately same for the four ILs, a decrease in γ will result decrease in the θ_0 value. Thus, it can be concluded that size of the anion and charge delocalization have a direct relationship with the θ_0 value.

2.3.1.2 Effect of the Anion on $\Delta\theta_L, \Delta\theta_R, V_L$, and V_R

In Figure 2.4b, the electrowetting plots of IL-IL4 were overlaid normal to the maximum θ_0 value. The negative branch of the curves was similar for all four ILs, while the positive branch shows some differences. It is clearly observed that $\Delta\theta_L$ and V_L values are comparable for all four ILs, whereas the $\Delta\theta_R$ and V_R values are all different. $\Delta\theta_R$ and V_R values tend to decrease IL2 > IL1 > IL3 > IL4, which also appears to be related to size and charge delocalization of the anion although IL2 seems to have a relatively high V_R.

2.3.1.3 Effect of the Anion on Curve Asymmetry

The liquid-solid interfacial free energy can be described by the work of adhesion between a liquid and a substrate (W_a). A stronger interaction between a liquid and a substrate will provide a higher work of adhesion value. The value of W_a is given by the Young-Dupré equation (eq. 2.3).[77]

$$W_a = \gamma(1 + cos\theta_0) \tag{2.3}$$

W_a values were calculated for the ILs for which surface tension values were available (Table 2.1). Teflon AF 1600 is a random copolymer of 4,5-difluoro-2,2-bis(trifluoromethyl)-1,3-dioxole (PDD) and tetrafluoroethylene.[75] The previous work of Quinn et al.[75] demonstrated that, as the PDD content increases, deviations from theory at positive voltages is significant due to the adsorption of hydroxide and halide ions to the Teflon layer. Although they reported a relatively small effect caused by halide anions, in our case, this effect appears to be more substantial. According to Table 2.1, W_a values decrease in the order of IL1 > IL2 > IL3 > IL4. The size of the anion increases in a similar order. It appears that smaller anions have stronger interactions with Teflon layer than larger anions. This can be clearly observed in

Figure 2.4c, where the contributions of Cl^-, Br^-, and PF_6^- to the asymmetry of the electrowetting curves are higher than those of NTf_2^-.

2.3.2 Effects of the Cationic Moieties

IL5-IL12 are dicationic ILs, which have same NTf_2^- anion. IL5-IL7 contain two different cationic moeties (unsymmetrical) while all other dications are symmetrical (i.e., the linked cationic moieties are the same). Figure 2.5 shows the electrowetting curves of IL5-IL12.

Table 2.2: Electrowetting Properties of Studied ILs.[a]

ionic liquid	θ_0	$\Delta\theta_L$	$\Delta\theta_R$	V_L	V_R
IL1	97	13	17	−60	50
IL2	97	15	27	−60	65
IL3	89	16	11	−60	35
IL4	75	10	7	−40	25
IL5	86	19	19	−50	55
IL6	88	15	14	−55	45
IL7	84	17	16	−50	40
IL8	83	14	11	−45	40
IL9	85	18	12	−55	35
IL10	76	17	14	−45	50
IL11	84	14	16	−50	40
IL12	84	14	16	−48	40
IL13	77	>25	>20	< −70	>70
IL14	88	15	18	−55	60
IL15	77	20	25	−55	60
IL16	82	>15	>14	< −70	>70
IL17	78	10	16	−30	40
IL18	77	7	13	−25	35
IL19	93	29	28	−160	190

[a]extracted from Figure 2.6, 2.4, 2.5 and 2.10

2.3.2.1 Cation Effect on the θ_0 Value

Among these ILs, IL10 has a considerably lower θ_0 value whereas the others have similar θ_0 values. According to eq 2.2, $(\gamma_{SV} - \gamma_{SL})$ and γ govern the θ_0 value. There is limited availability of IL surface tension data. However, there were sufficient amounts of IL10 and IL12 to determine their surface tensions and the values of the others can be predicted.[66,76] IL10 contains two butyl chains in its structure. Flexibility of these butyl chains can increase the molecular disorder or entropy of the system. This leads to an increase in the irregularity within the liquid and ultimately on the surface, consequently giving a lower surface tension value for IL10 than its related ILs.[76] According to eq 2.2, this relatively lower surface tension value translates directly into a lower θ_0 value for IL10. An analogous trend can be observed for the tricationic ionic liquids IL13-IL16. IL13, and IL15, with N-butyl substituents, have considerably lower θ_0 values than the benzyl-substituted analogues IL14 and IL16 (Table 2.2).

2.3.2.2 Cationic Effect on $\Delta\theta_L, \Delta\theta_R, V_L$, and V_R values

IL11 had considerably lower $\Delta\theta_L, \Delta\theta_R, V_L$, and V_R values than the other dicationic ILs, all of which had similar $\Delta\theta_L, \Delta\theta_R, V_L$, and V_R values (Table 2.2). IL11 contains two benzyl groups in its structure. Introduction of these two benzyl groups provides additional $\pi - \pi$ interactions for this ionic liquid, and these may lead to the lower values. It appears that effect of these benzyl groups can be found in the tricationic ionic liquids as well; $\Delta\theta_L, \Delta\theta_R$ values of IL14 and IL16 are much lower than those of IL13 and IL15 (Table 2.2).

2.3.2.3 Cationic Effect on Asymmetry of Electrowetting Curves

The asymmetry of the electrowetting curves for IL5-IL12 is generally less than that for IL1-IL4. IL5-IL12 are dicationic ILs, which have same NTf_2^- anion; hence, interactions with PDD in the Teflon layer are about same and lower than that for the anions of IL1-IL3, as was discussed previously. This leads to lower adsorption, ultimately resulting in lower asymmetry for all of the dicationic ILs that share same NTf_2^- anion. Analogous behavior is observed for tricationic ILs IL13-IL16.

2.3.3 Effect of the Number of Cationic Groups

Figure 2.6 shows the electrowetting curves of IL4, IL10, and IL13. These three ILs have a common anion (NTf_2^-) and the same butyl imidazolium cationic moiety. The difference between them is that IL4 is monocationic, IL10 is dicationic, and IL13 is tricationic. Regardless of the cationic charge, the θ_0 values of IL4, IL10, and IL13 are approximately same. This is due to their comparable surface tension values (Table 2.1). The $\Delta\theta_L, \Delta\theta_R, V_L$, and V_R values of this series of ILs decrease in the order of IL13 > IL10> IL4. Hence, it can be concluded that the number of charged cationic groups directly affects the $\Delta\theta_L, \Delta\theta_R, V_L$, and V_R values.

2.3.4 Other Relevant Observations

IL19 is the only dianionic IL studied. It has the largest $\Delta\theta_L, \Delta\theta_R, V_L$, and V_R values among all ILs studied (Table 2.2). IL17 and IL18 are phosphonium-based ILs. There does not seems to be significant differences in the electrowetting properties between phosphonium ILs and imidazolium ILs. It was observed that ILs were decomposed or burned, when experiments were conducted at much higher voltages. However, some ILs were stable even at 1000 V. Some of the ILs had different decom-

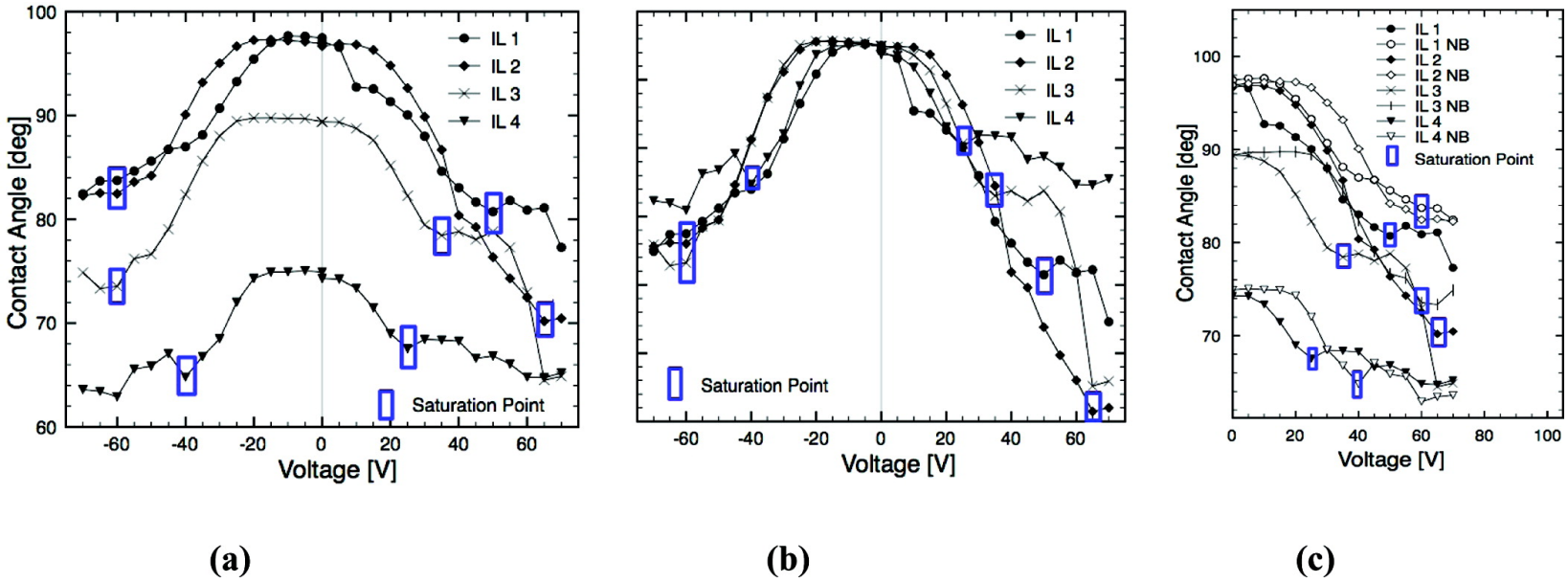

Figure 2.4: (a) Electrowetting curves of IL1-IL4. (b) Electrowetting curves of IL1-IL4 were overlaid normal to the maximum θ_0 value. (c) Folded curves showing the asymmetry in the electrowetting curves

position voltages at positive and negative voltages. Table 2.3 shows the maximum voltage values of selected ILs that can be obtained without any decomposition of the IL itself or breakdown of the Teflon layer. Comparison data for water were also tabulated in Table 2.3. Clearly, ionic liquids are stable at much higher voltages than water when they are used in electrowetting applications. Furthermore, it appears that the imidazaloim-based ILs (IL5-IL12) are more stable at high voltages than phosphonium-based ILs (IL17 and IL18).

Table 2.3: Stability of Selected ILs in Higher Voltages.

ionic liquid	Teflon layer thickness (nm)	maximum voltage at which liquid remains stable	
		positive (V)	negative (V)
IL5	260	350	>1000
IL6	260	>1000	>1000
IL8	260	>1000	>1000
IL9	260	>1000	800
IL11	260	150	>1000
IL12	260	>1000	900
IL13	260	200	200
IL17	260	200	150
IL18	260	90	500
water[a]	250	100[b]	
water[a]	550	120[b]	

[a]Data taken from ref [78]. [b]Reported as breakdown voltage with no voltage polarity indication.

2.3.5 Deviation from the Theoretical Curve

It is observed that, unlike water and other aqueous electrolytes, ILs show deviations from eq 2.1. A previous study by Millefiorini et al.[43] and Dubois et al.[44] also observed such deviations. According to equation 2.1, a plot of $2\gamma(cos\theta - cos\theta_0)$ versus V^2 should give the same c value (specific capacitance) for all ILs. However,

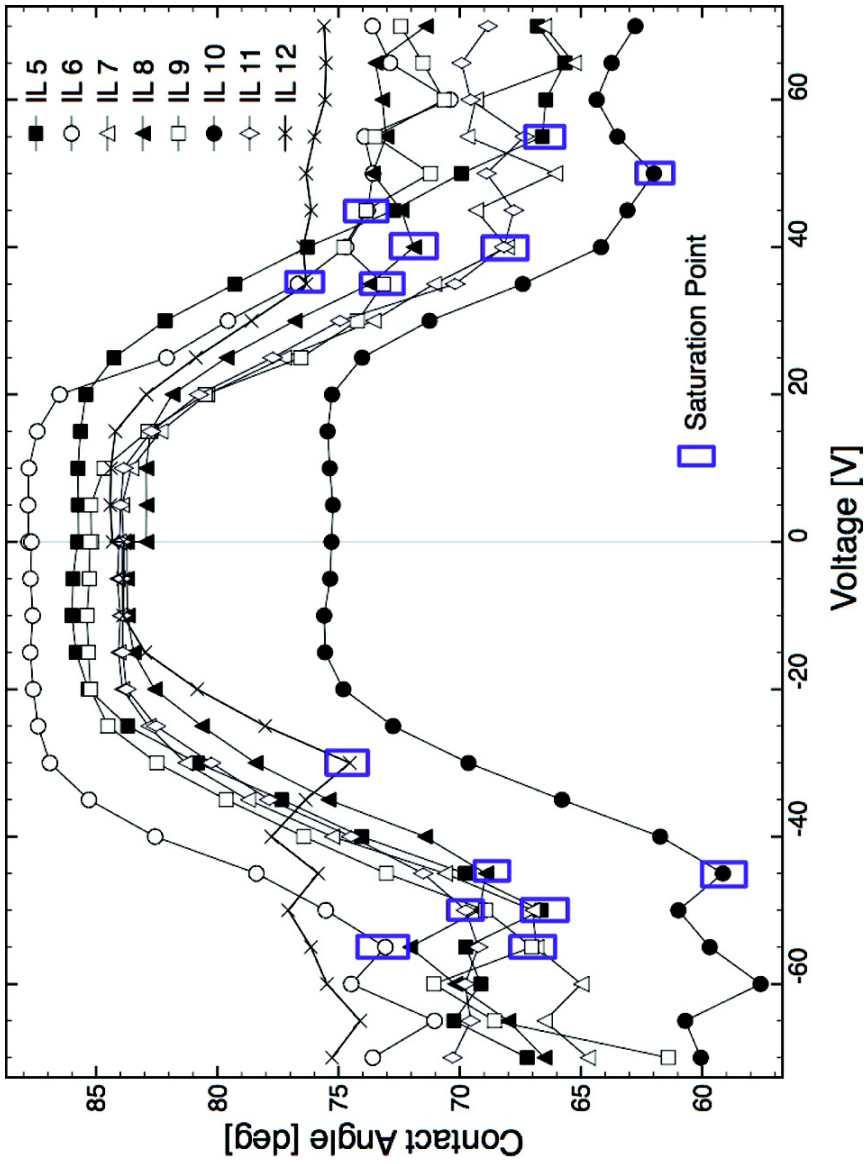

Figure 2.5: Electrowetting curves of dicationic ILs IL5-IL12.

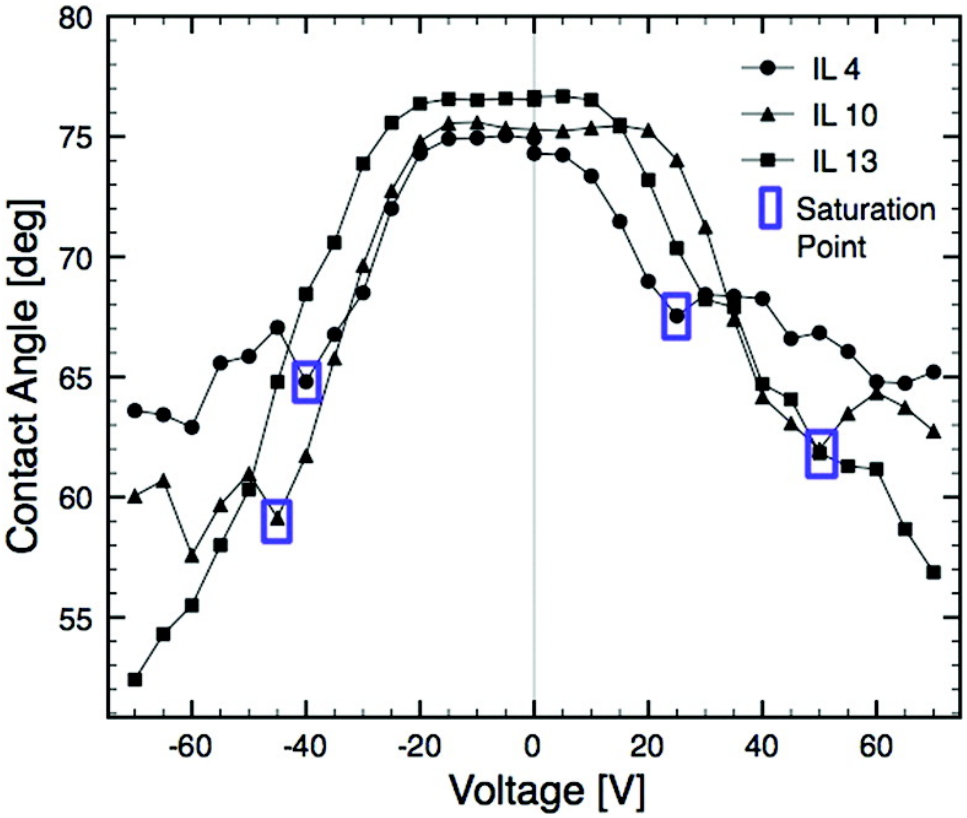

Figure 2.6: Electrowetting curves of IL4, IL10, and IL13.

the calculated c values for the ILs (Table 2.4) are different for each IL showing deviations from the theoretical c value. Note that the $2\gamma(cos\theta - cos\theta_0)$ versus V^2 were plotted separately for the positive and negative voltages. The individual c values were then extracted from the plots (see Figure 2.11-2.21). The theoretical c value in equation 2.1 can be calculated by $1/c = 1/c_d + 1/c_{H(aq)}$, where c_d is the capacitance of dielectric layer (Teflon) and $c_{H(aq)}$ is the capacitance of liquid double layer at the dielectric layer/aqueous electrolyte interface. However, due to the fact that $c_d \ll c_{H(aq)}$,[1] $c_{H(aq)}$ has less of an effect on the theoretical c value in equation 2.1. Therefore, the approximation $c \approx c_d$ is generally valid for water and other aqueous electrolytes [$c_d = \epsilon\epsilon_0/t$, ϵ, and t are dielectric constant (1.93) and thickness of the dielectric layer, respectively].[1] However, according to Table 2.4, the c values obtained

for ILs are all significantly lower than the theoretical c value. There may be several reasons for this. First, a finite leakage current across the dielectric layer (0-21 μA depending on the applied voltage value see Table 2.5) was observed during the EWOD measurement and it may be an evidence of some imperfections in thin ($260 \pm 10\ nm$) Teflon layer. The Teflon layer is not a perfect dielectric (capacitor) layer. Rather it can be modeled as a parallel connection of a resistor and a capacitor, which can cause smaller c. Similar deviations from electrowetting theory were reported elsewhere.[60,79] Moon et al. also pointed ion adsorption to the Teflon layer as a possible reason for the deviation.[60] Second, $c_{H(aq)}$ is calculated by modeling ions in aqueous electrolytes or water as charged spheres. However, Kornyshev[80] indicated that ILs should not be modeled as charged spheres due to the asymmetry of their structures. Hence, the capacitance of the liquid double layer at the dielectric layer/ionic liquid interface ($c_{H(IL)}$) may not be calculated in classical ways.[80] Therefore, the approximation $c \approx c_d$ in equation 2.1 may not be valid for ILs. Lastly, different functional groups and structural differences in ILs may influence $c_{H(IL)}$. Lazzari and co-workerscite[81] showed that ILs with the same anion and different cations, with approximately same size, have different capacitance responses due to different polarizabilities and differences in the structures of the two cations. Hence, again, the approximation $c \approx c_d$ is doubtful for ILs in equation 2.1.

Conversely, it was recently reported[82] that the double layer thickness of imidazolium based monocationic ILs at the Pt electrode have thickness values comparatively similar to those of aqueous electrolytes. In these calculations, the dielectric constants (ϵ) of imidazolium-based ILs were taken as 7.[82,83] Table 2.4 shows the calculated double layer thickness values at Teflon surface and a comparison to the values for the Pt surface.

Table 2.4: Comparison of c Values of ILs with the Theoretical c Value[a]

ionic liquid	c $(\mu F/m^2)$		$c_{H(IL)}$ at Teflon-IL interface $(\mu F/m^2)$[b]		t_{IL} at Teflon-IL interface (nm)[c]		$c_{H(IL)}$ at Pt electrode $(\mu F/m^2)$[82]	t_{IL} at Pt electrode (nm)[82]
	(+) V	(-) V	(+) V	(-) V	(+) V	(-) V		
$(c \simeq c_d)$[d]	66	66						
IL1	16	17	21	23	29×10^2	27×10^2		
IL2	12	9	15	10	42×10^2	59×10^2		
IL3	15	7	19	8	32×10^2	79×10^2	19×10^4	30
IL4	12	8	15	9	42×10^2	68×10^2	15×10^4	40
IL10	8	12	9	15	68×10^2	42×10^2		
IL12	10	16	12	21	53×10^2	29×10^2		
IL13	9	8	10	9	59×10^2	68×10^2		
IL16	5	6	5	7	115×10^2	94×10^2		
IL17	16	13	21	16				
IL18	12	16	15	21				
IL19	4	4	4	4				

c = specific capacitance, $c_{H(IL)} = c$ of double layer of IL, t_{IL} = double layer thickness of IL.
[a] c values are extracted only for the ILs for which surface tension data is available.
[b] calculated using the equation, $1/c = 1/c_d + 1/c_{H(IL)}$.
[c] calculated using the equation, $1/c_{H(IL)} = \epsilon\epsilon_0/t$, ($\epsilon = 7$ for imidazolium based ILs).[82]
[d] theoretical value.

Table 2.5: Leakage current across dielectric layer for selected ILs

Voltage (V)	Leakage Current (μA)				
	IL1 with 5% water (w/w)	IL1 with 10% water (w/w)	IL1 with 20%water (w/w)	IL4	water saturated IL4
70	10.5	16.2	12.0	19.0	9.0
65	5.1	13.3	10.6	21.0	10.0
60	0.6	11.2	7.3	18.0	8.0
55	0.8	4.5	4.6	12.0	4.0
50	0.5	4.0	4.9	11.2	6.0
45	0.2	3.9	2.4	8.0	7.2
40	0.2	3.8	1.8	5.7	6.6
35	0.3	2.3	1.1	4.7	6.3
30	0.3	1.5	0.6	2.7	5.9
25	0.2	1.0	0.2	1.7	5.5
20	0.1	1.2	0.1	0.8	5.4
15	0.1	1.2	0.1	0.5	5.1
10	0.1	0.5	0.0	0.2	0.0
5	0.0	0.1	0.0	0.1	0.0
0	0.0	0.0	0.0	0.0	0.0
0	0.0	0.0	0.0	0.0	0.0
-5	0.0	0.0	0.1	0.4	5.0
-10	0.0	0.0	0.1	0.6	0.1
-15	0.0	0.0	0.1	0.7	0.1
-20	0.0	0.0	0.2	0.7	0.1
-25	0.0	0.0	0.3	0.8	0.3
-30	0.0	0.1	0.5	0.8	0.6
-35	0.0	0.0	0.3	0.8	0.8
-40	0.0	0.1	0.1	0.9	1.1
-45	0.1	0.1	0.0	1.1	1.5
-50	0.2	0.1	0.1	1.2	2.0
-55	0.2	0.2	0.5	1.2	3.7
-60	0.6	0.7	0.5	1.7	5.0
-65	0.5	0.3	0.5	1.8	7.0
-70	0.5	0.3	1.5	2.0	7.0

2.3.6 Effect of Water

All ILs contain water to a certain extent as do all other liquids. Water and other solvents were removed using a rotary evaporator in the final synthesis step of the ILs as indicated in the Experimental Section. Approximately 0.5 mL of each IL was stored in a vacuum oven for 12-18 h with phosphorus pentoxide (P_2O_5) at room temperature before the test to minimize the water content. There are water-miscible ILs and water- immiscible ILs. The effect of water in the ILs on their electrowetting was studied using IL1 (a water miscible IL) and IL4 (a water- immiscible IL).

Figure 2.7 shows the θ_0 values of IL1 with different percentages of water. According to Figure 2.7, the higher the water percentage in IL1, the higher the θ_0 values obtained. Also, the surface tension values are proportional to the percentage of water in water-miscible ILs.[84] According to Figure 2.7, it can be concluded that a increase of water content will result an increase in the θ_0 value for water-miscible ILs. Figure 2.8 shows the electrowetting curves of IL1 and its diluted solutions. It can be observed that the positive branch of the curve for IL1 was not affected by water content of IL 1. However, the negative branch of the curve was affected by water content. According to Figure 2.8, it can be concluded that the higher the percentage of water, the higher the asymmetry of the obtained curves. IL4 is a water-immiscible IL. Figure 2.9 shows the electrowetting curves of IL4 and that of water-saturated IL4. It can be observed that both electrowetting curves are approximately same for the IL4 and water-saturated IL4. Therefore, it can be concluded that water has less or no effect on the electrowetting of water-immiscible ILs in this study. Also, absorption of water into the IL drops during the experiment can be considered to have a smaller or negligible effect.

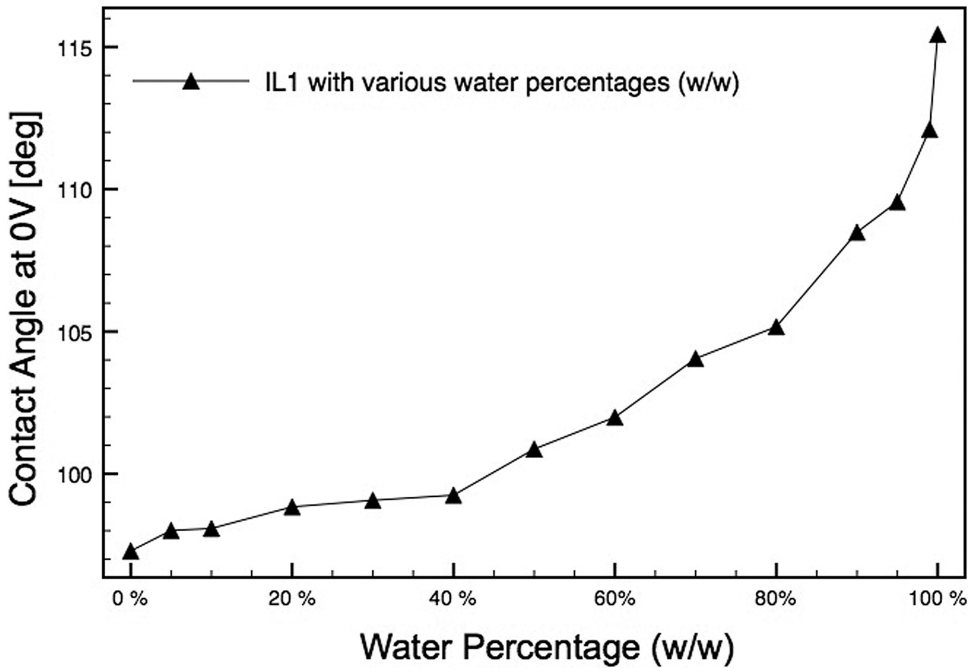

Figure 2.7: Contact angle at zero voltage vs water percentage in IL1

2.4 Conclusion

The successful electrowetting of nonpolar, dielectric surface by 19 different ILs was demonstrated. The electrowetting properties of these ILs depend on their ion size, number of functional groups, and overall structure. The electrowetting plots of ILs have larger deviation from equation 2.1; this may be due to leakage current, large size of ions, functional groups, and structure of ILs. ILs with 20° or more $\Delta\theta_L$ or $\Delta\theta_R$ values may be used in microfluidic devices. ILs with high $\Delta\theta_L$ and $\Delta\theta_R$ values plus low V_L and V_R values can be used in low-voltage electrowetting applications. Physical properties and electrowetting properties data of these ILs can be used as references to engineer task-specific electrowetting agents (ILs) for future electrowetting-based microflluidic applications. ILs are generally more resistant to decomposition at high voltages than water or aqueous solutions in electrowetting scenarios.

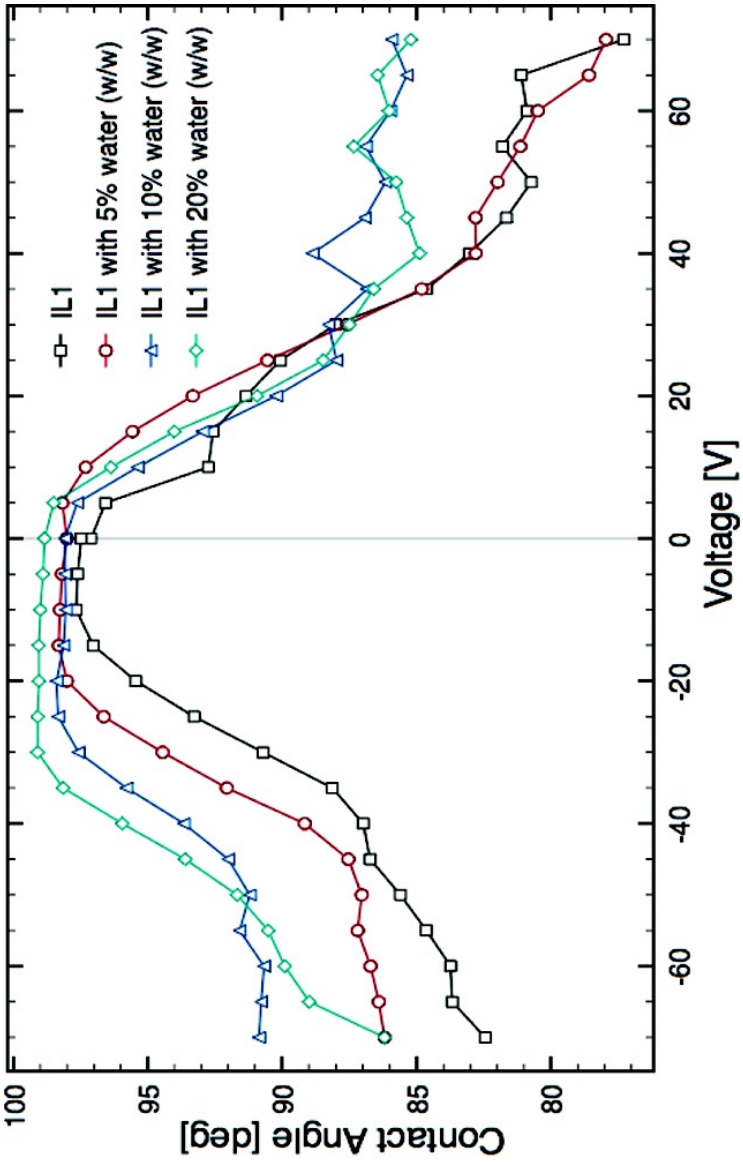

Figure 2.8: Electrowetting curves of IL1 and its diluted solutions

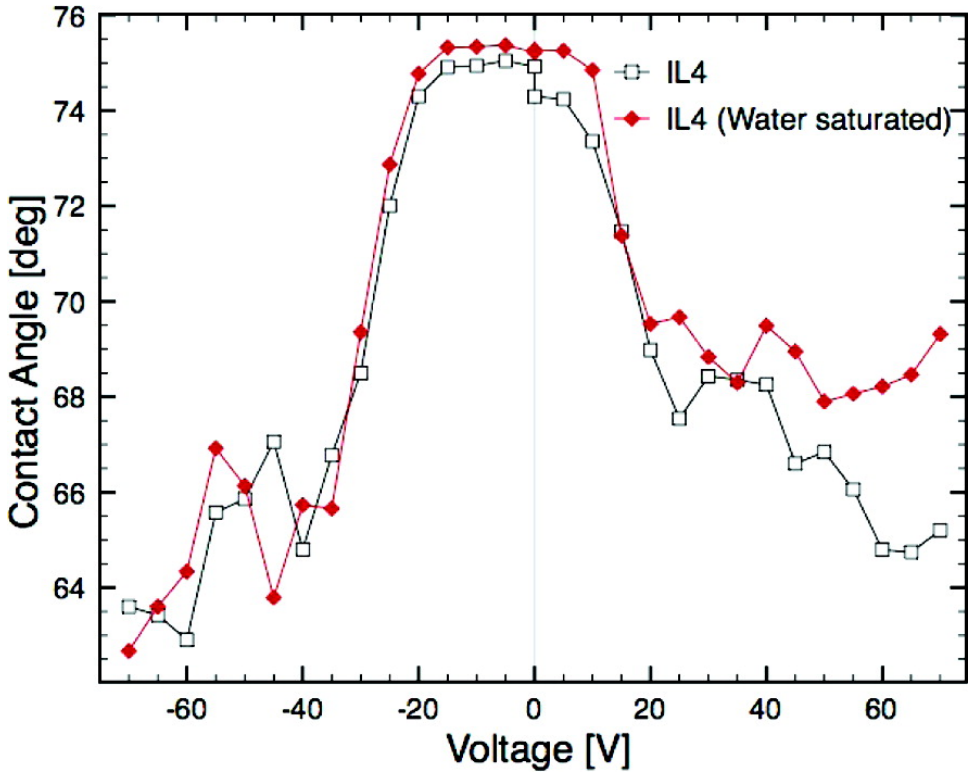

Figure 2.9: Electrowetting curves of IL4 and water saturated IL4

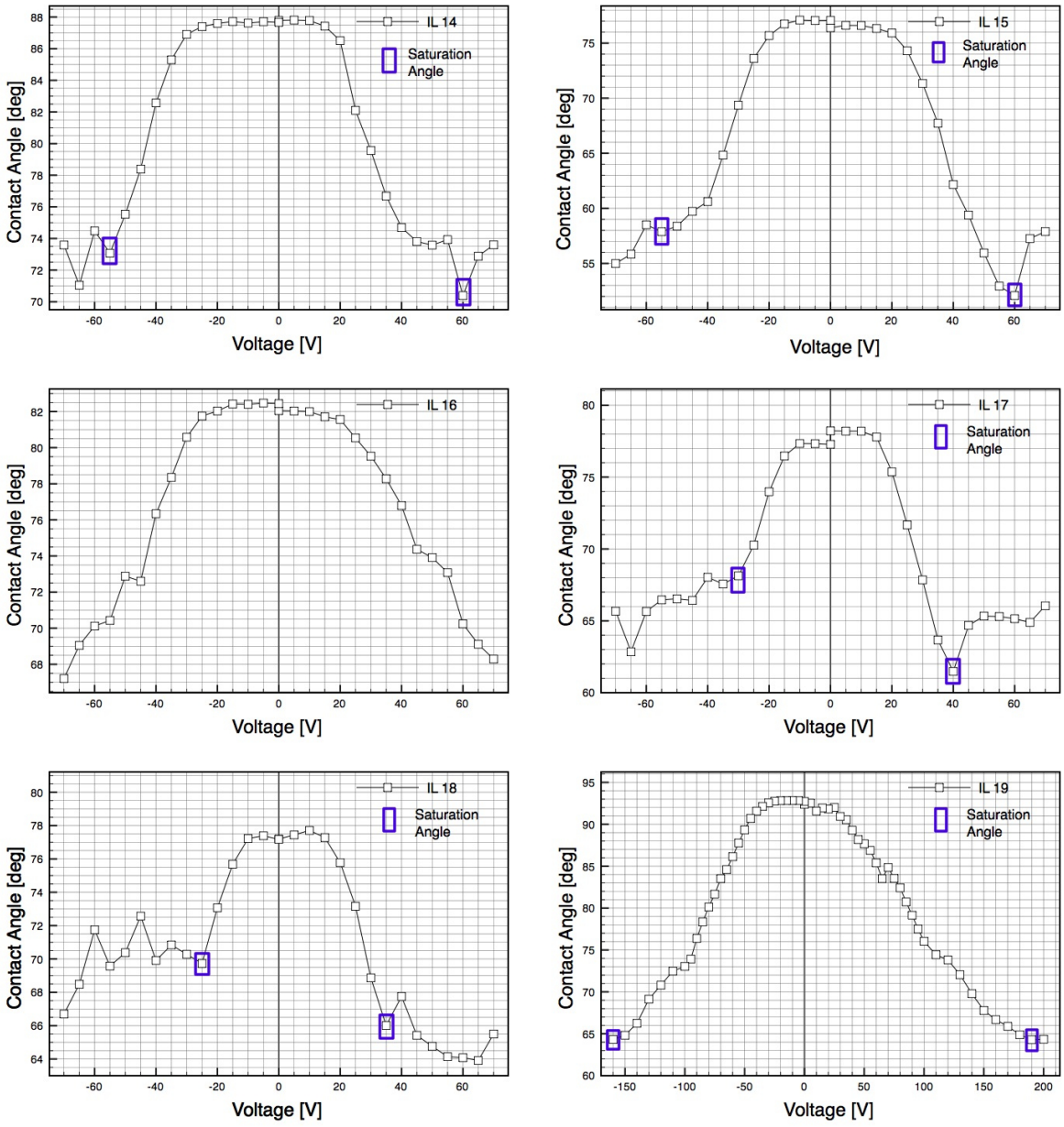

Figure 2.10: Electrowetting curves of IL14-IL19

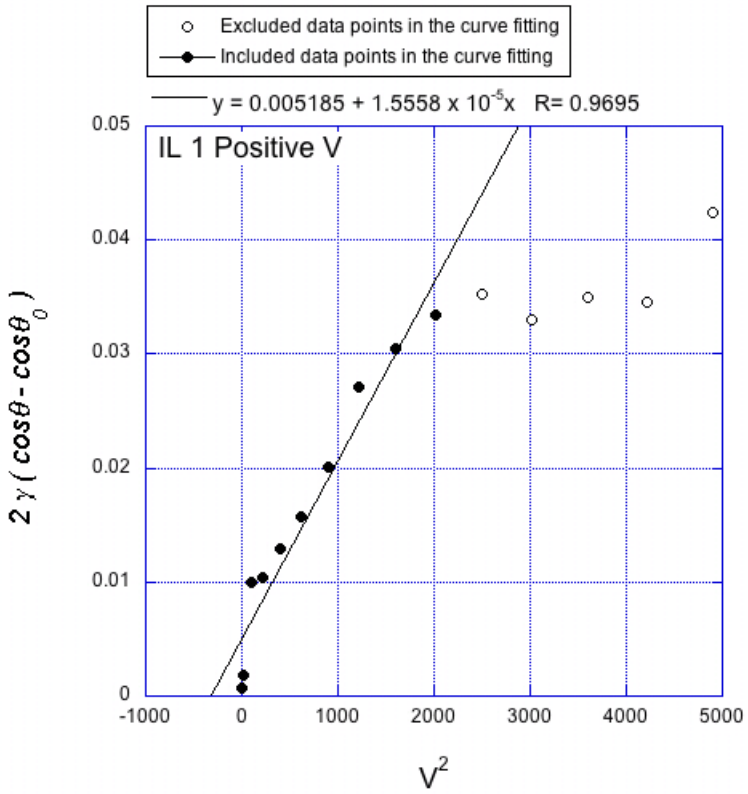

(a)

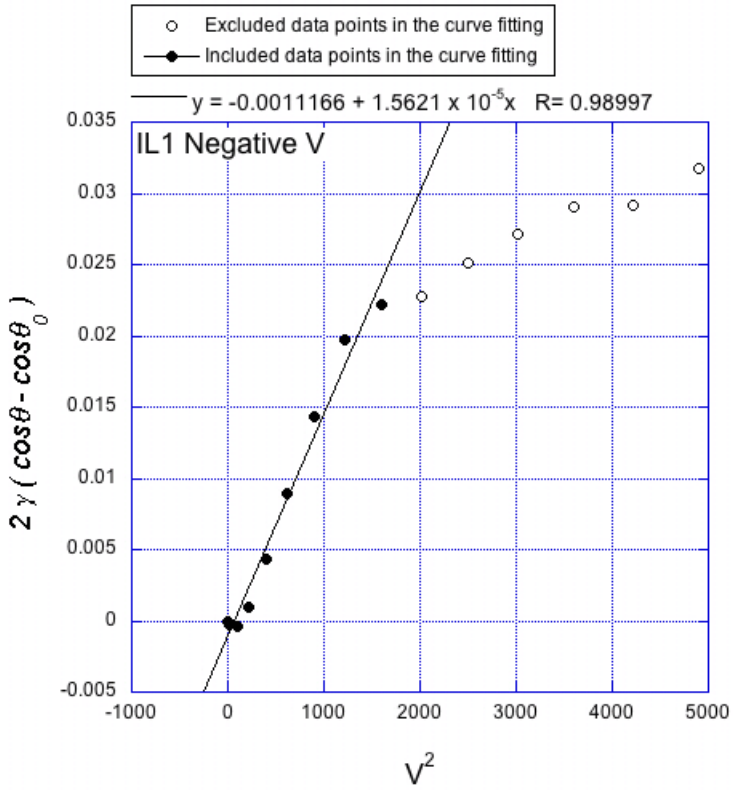

(b)

Figure 2.11: $2\gamma(cos\theta - cos\theta_0)$ vs. V^2 plots of IL 1: a) for positive voltages, b) for negative voltages

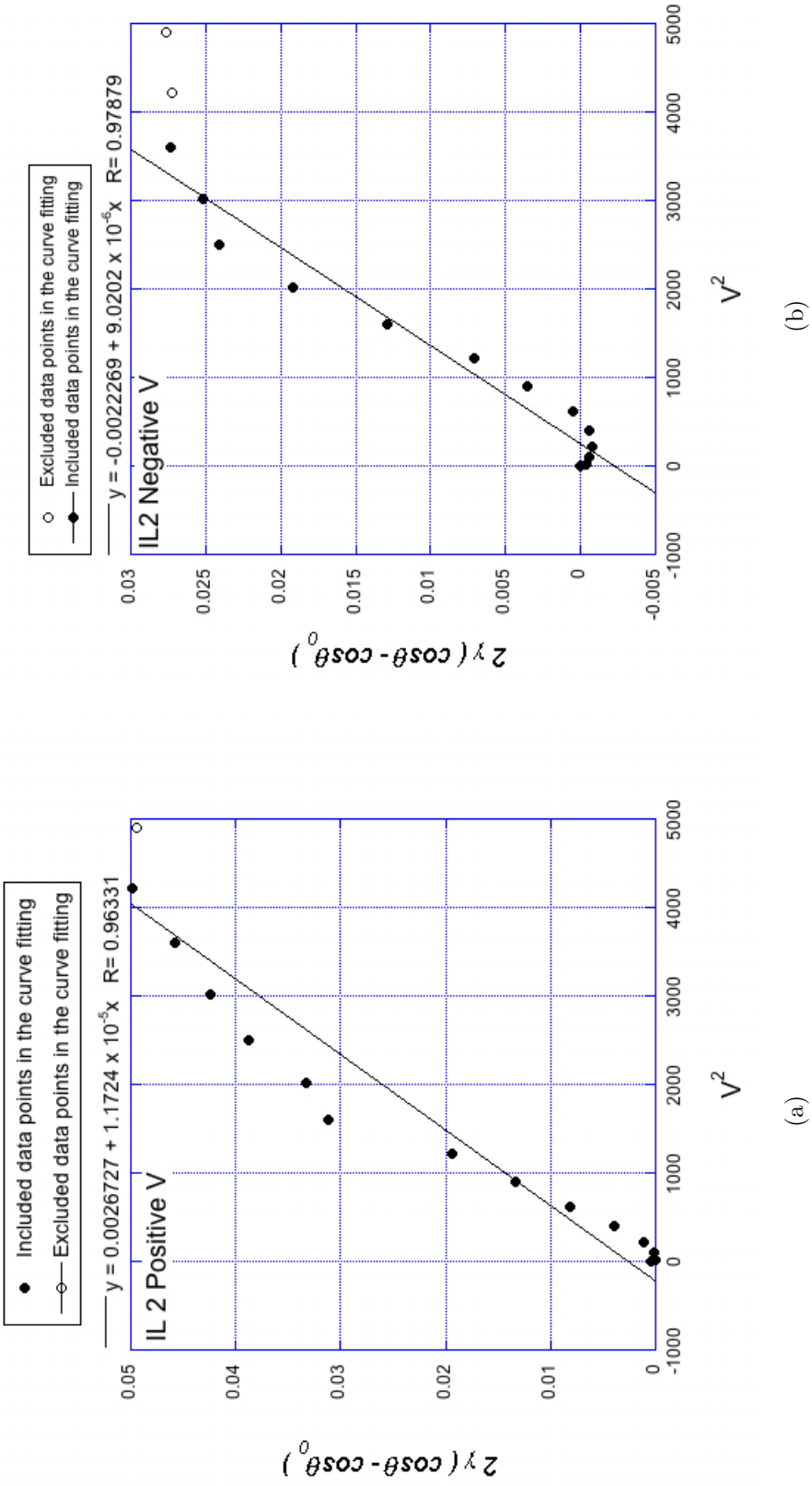

(a) (b)

Figure 2.12: $2\gamma(cos\theta - cos\theta_0)$ vs. V^2 plots of IL 2: a) for positive voltages, b) for negative voltages

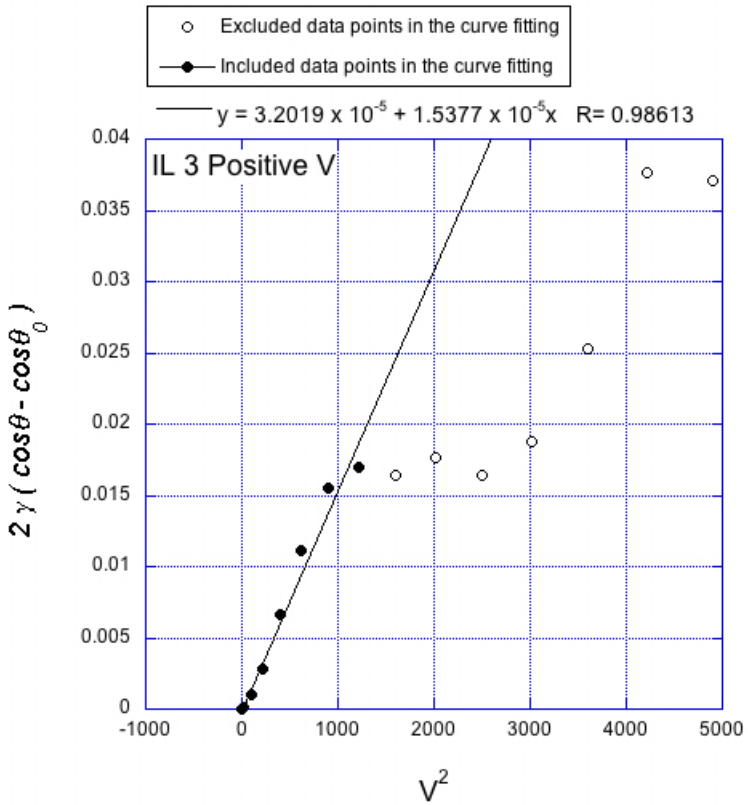

(a)

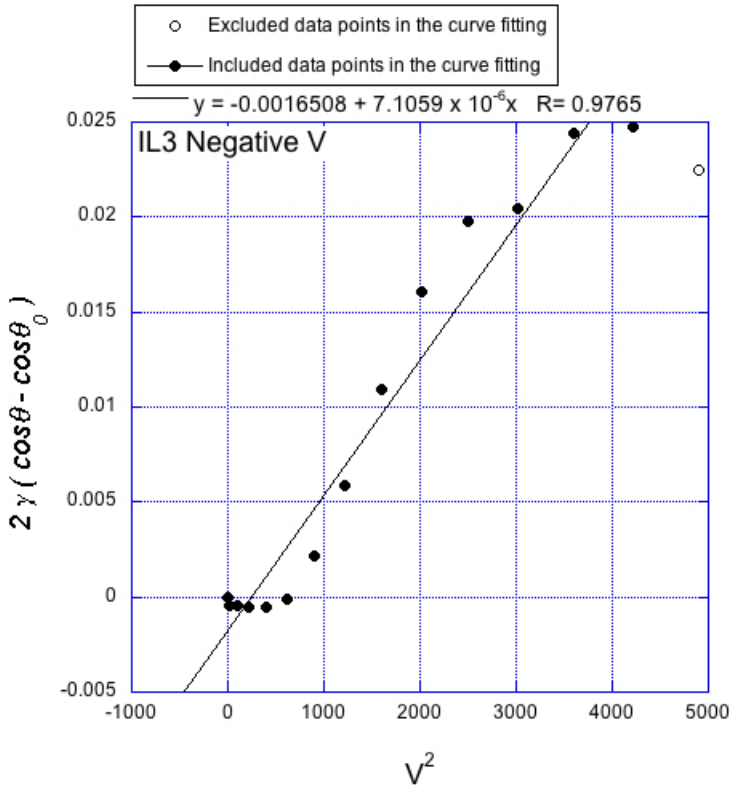

(b)

Figure 2.13: $2\gamma(cos\theta - cos\theta_0)$ vs. V^2 plots of IL 3: a) for positive voltages, b) for negative voltages

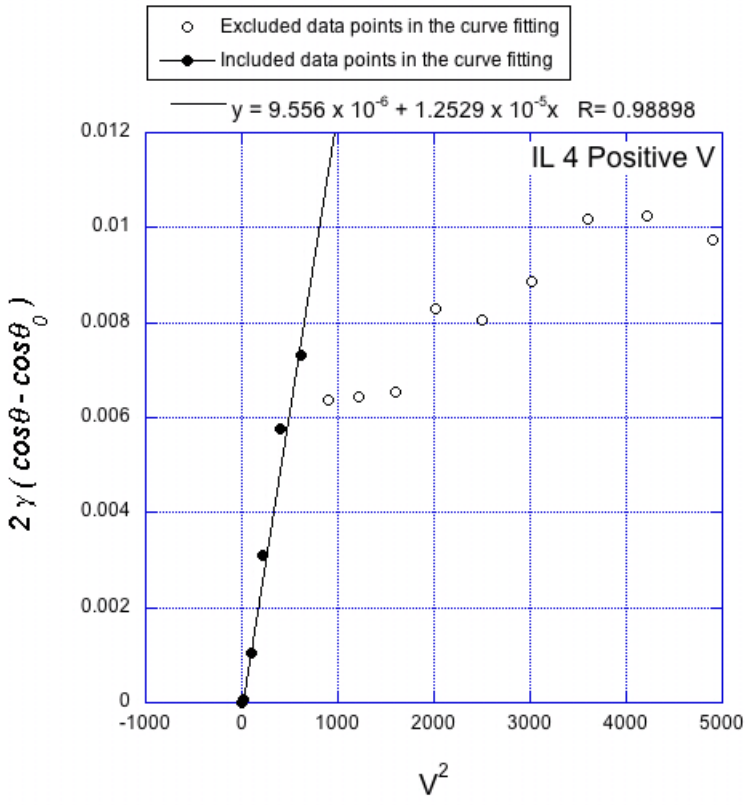

(a)

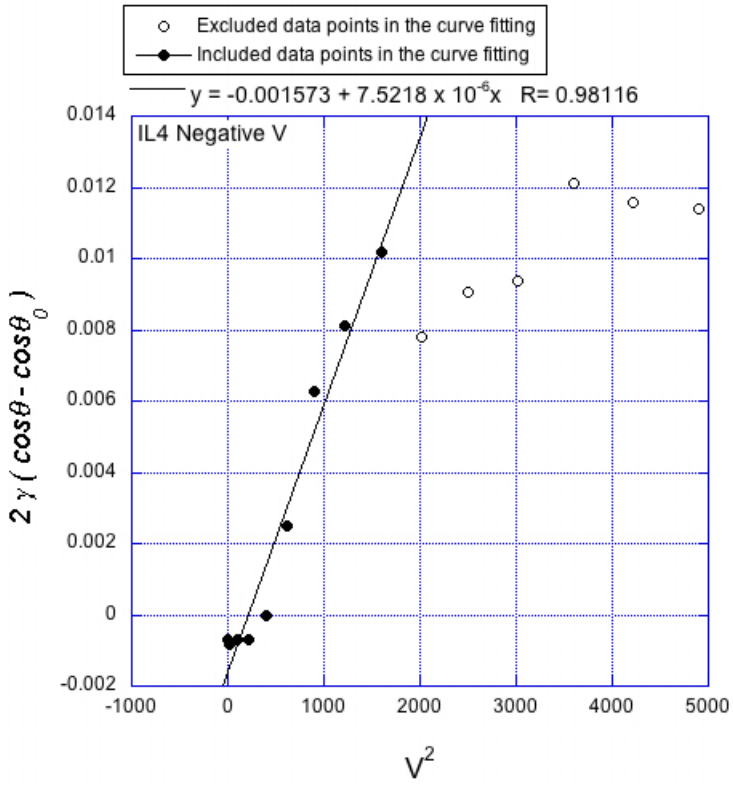

(b)

Figure 2.14: $2\gamma(cos\theta - cos\theta_0)$ vs. V^2 plots of IL 4: a) for positive voltages, b) for negative voltages

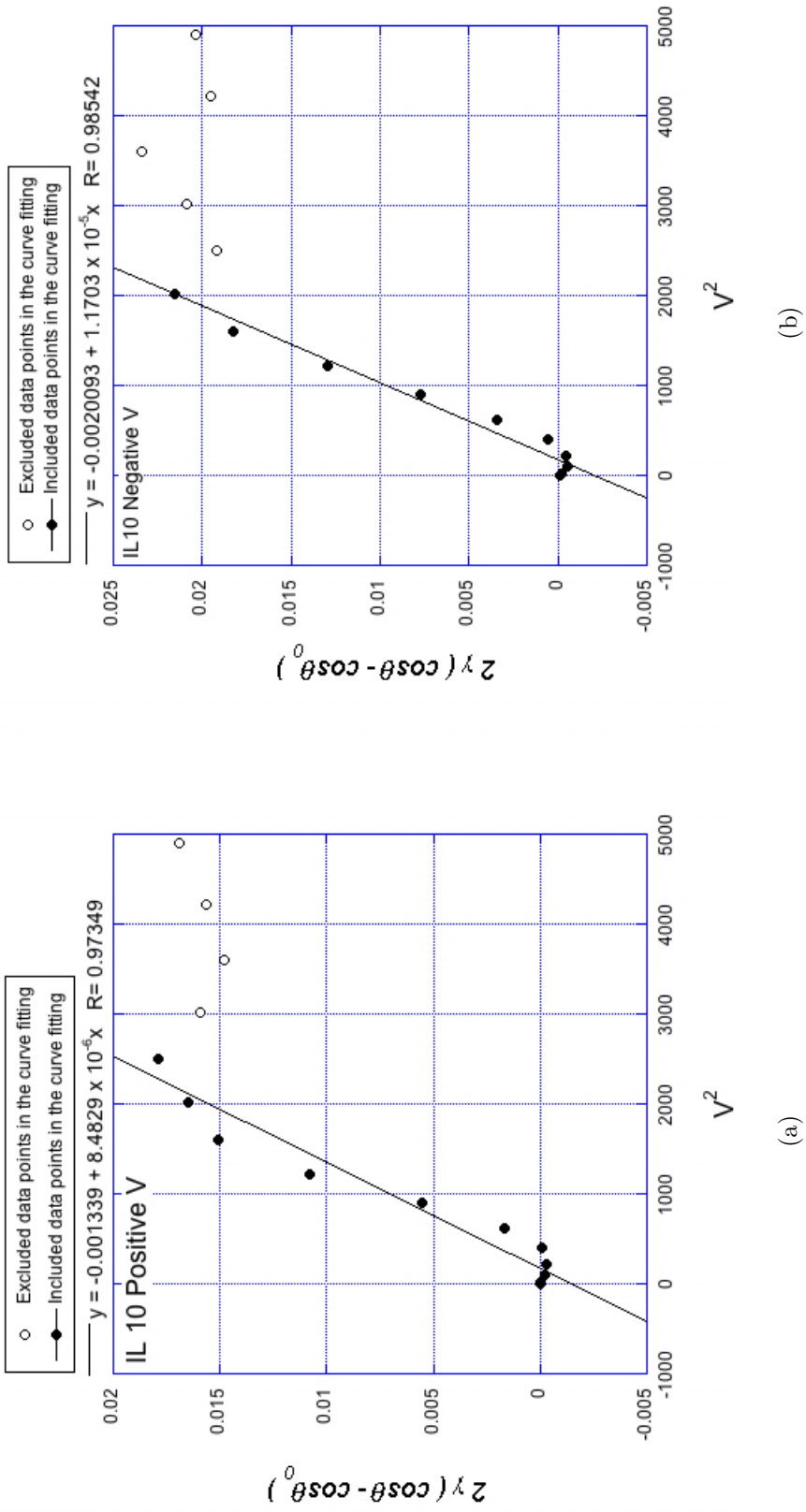

Figure 2.15: $2\gamma(cos\theta - cos\theta_0)$ vs. V^2 plots of IL 10: a) for positive voltages, b) for negative voltages

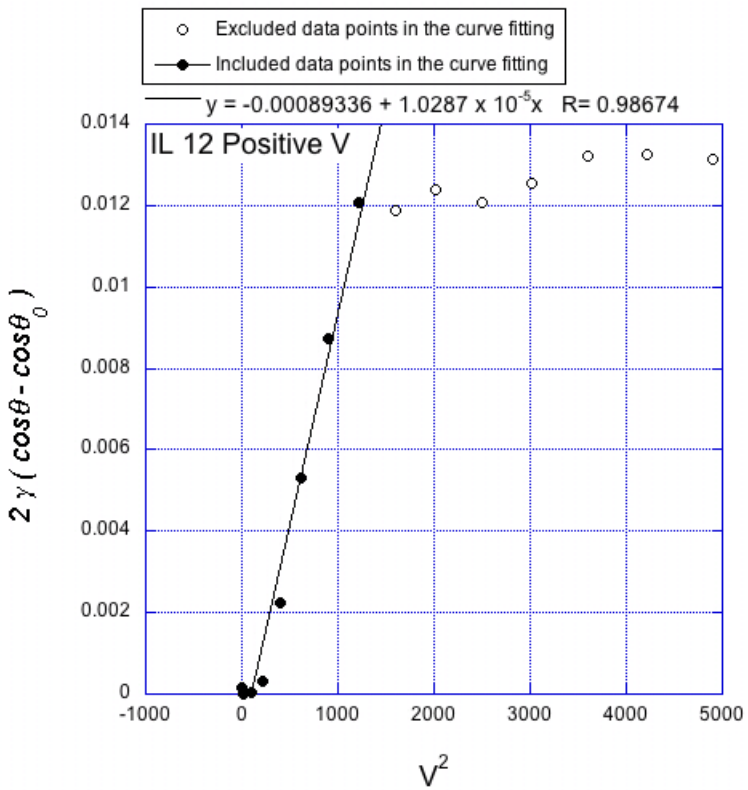

(a)

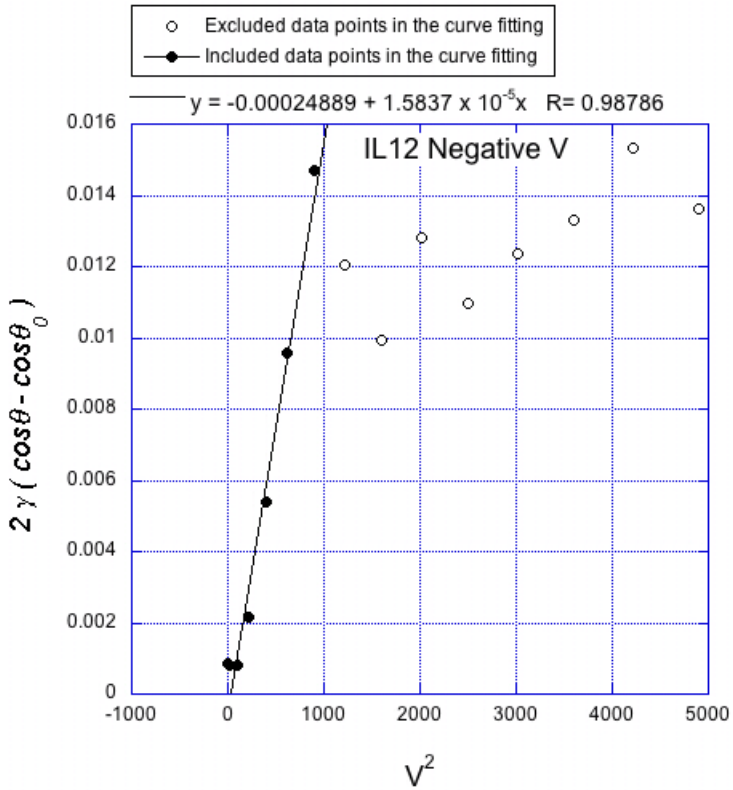

(b)

Figure 2.16: $2\gamma(cos\theta - cos\theta_0)$ vs. V^2 plots of IL 12: a) for positive voltages, b) for negative voltages

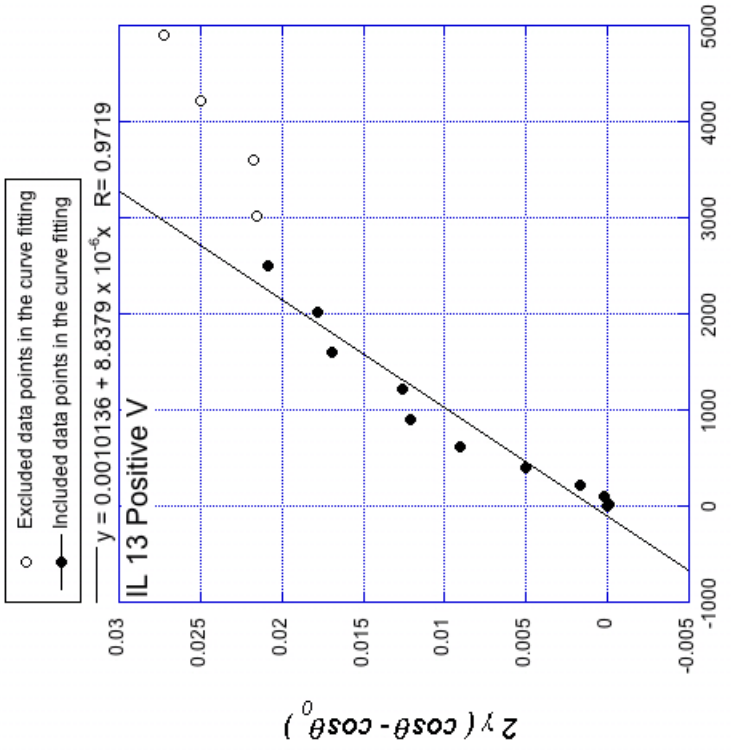

Figure 2.17: $2\gamma(cos\theta - cos\theta_0)$ vs. V^2 plots of IL 13: a) for positive voltages, b) for negative voltages

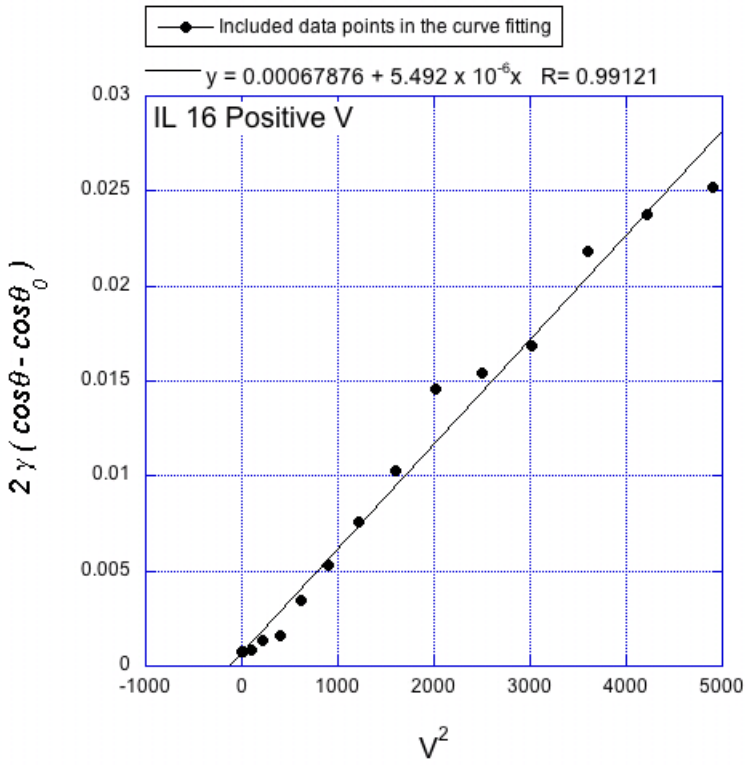

(a)

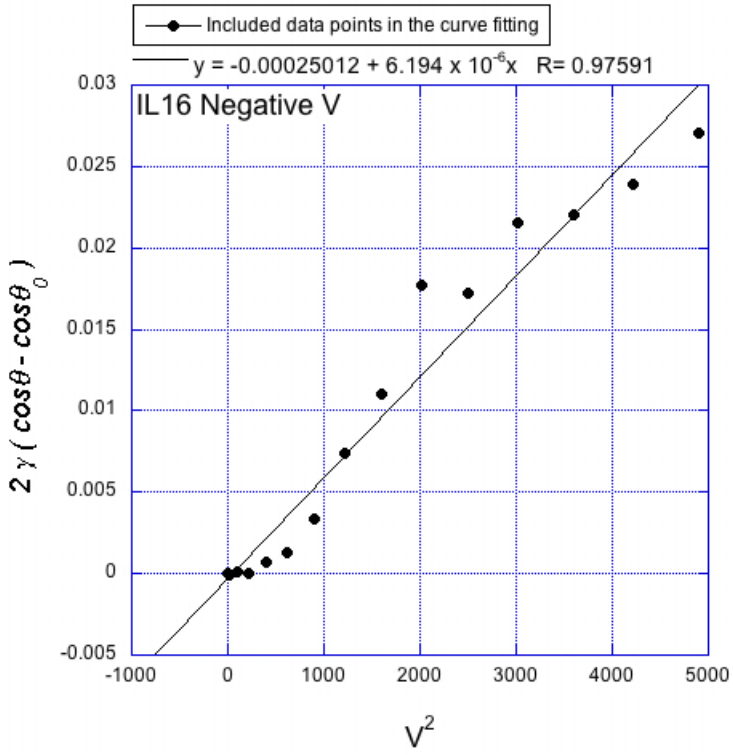

(b)

Figure 2.18: $2\gamma(cos\theta - cos\theta_0)$ vs. V^2 plots of IL 16: a) for positive voltages, b) for negative voltages

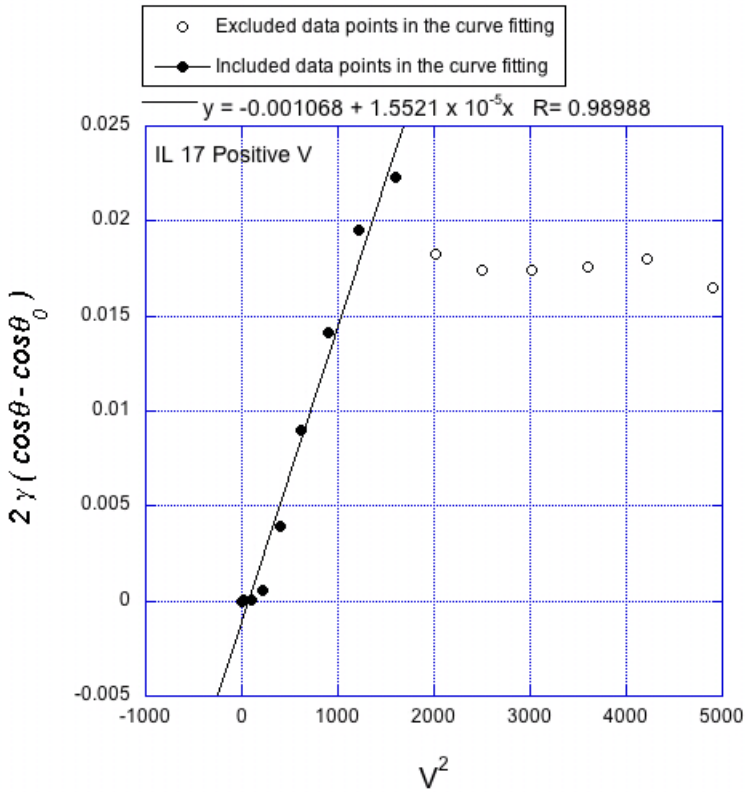

(a)

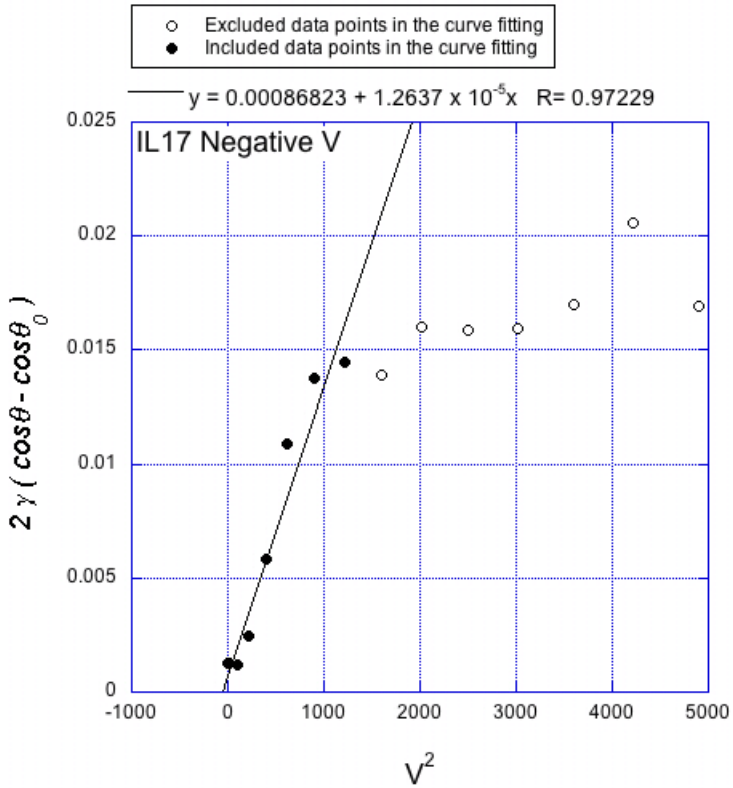

(b)

Figure 2.19: $2\gamma(cos\theta - cos\theta_0)$ vs. V^2 plots of IL 17: a) for positive voltages, b) for negative voltages

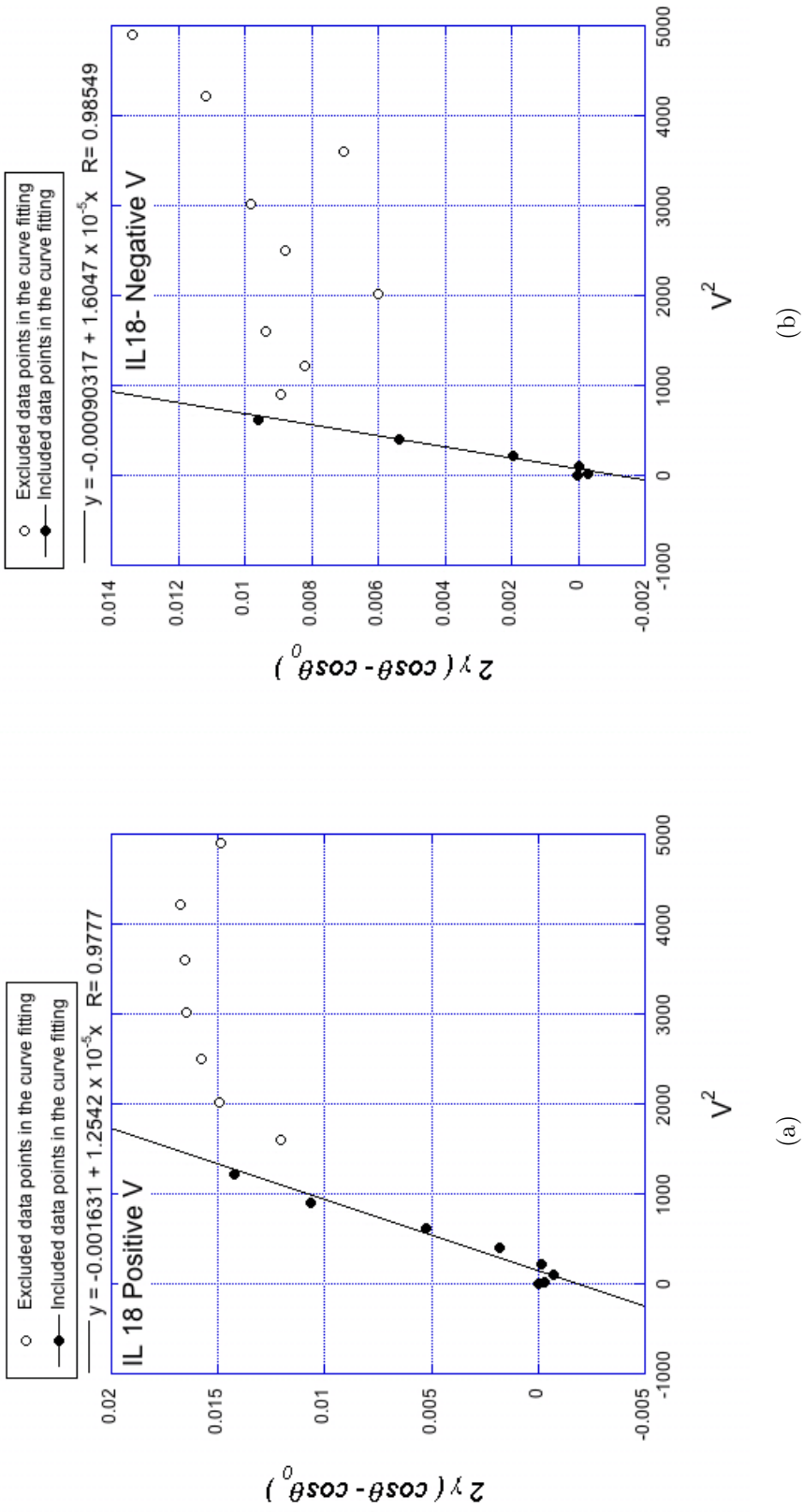

(a) (b)

Figure 2.20: $2\gamma(cos\theta - cos\theta_0)$ vs. V^2 plots of IL 18: a) for positive voltages, b) for negative voltages

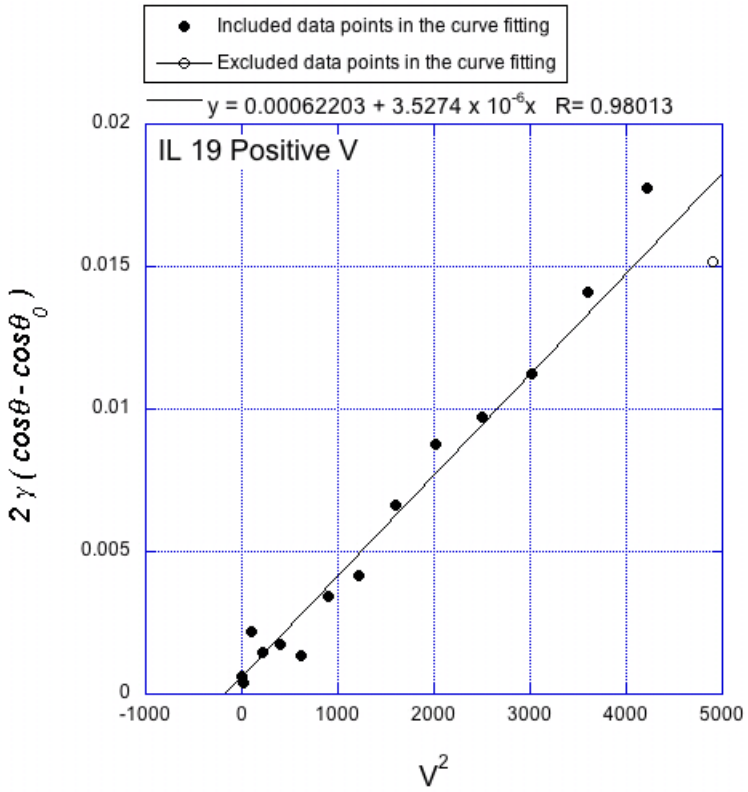

(a)

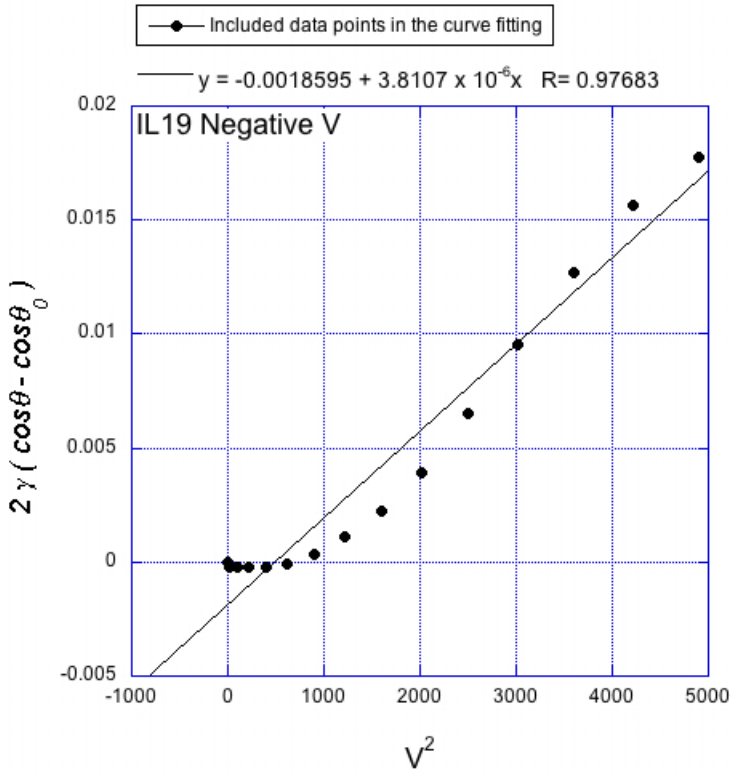

(b)

Figure 2.21: $2\gamma(cos\theta - cos\theta_0)$ vs. V^2 plots of IL 19: a) for positive voltages, b) for negative voltages

CHAPTER 3

THE EFFECT OF AC FREQUENCY ON THE ELECTROWETTING BEHAVIOR OF IONIC LIQUIDS

This chapter presents a study of electrowetting of ionic liquids (ILs) under AC voltages, where nine different ILs (including mono-, di-, and tricationic varieties) with 3 different AC frequencies (60 Hz, 1 kHz, 10 kHz) were experimentally investigated. The main foci of this study are: (i) an investigation of AC frequency dependence on the electrowetting of ILs; (ii) obtaining theoretical relationships between the relevant factors that explain the experimentally achieved frequency dependence; and (iii) a systematic comparison of electrowetting of ILs using AC vs. DC voltage fields. The apparent contact angle change ($\Delta\theta$) of the ILs was found to be directly related to the frequency of the AC voltage . This relationship was further analyzed and explained theoretically. The electrowetting properties of ILs under AC voltages were compared to that under DC voltages. All tested ILs showed greater apparent contact angle changes with AC voltage conditions than with DC voltage conditions. The effect of structure and charge density also was examined. Electrowetting reversibility under AC voltage conditions was studied for few ILs. Finally, the physical properties and AC electrowetting properties of ILs were measured and tabulated.

3.1 Introduction

Electrowetting is a well known phenomenon in which a liquid drop spreads on a solid surface upon application of an electric field across the liquid/solid interface. The spreading of a liquid drop by an electric field is often observed on

dielectric coated surfaces as well as conductive solid surfaces. In either case, one of the conventional methods to measure the extent of electrowetting is measuring the change in apparent (macroscopic) contact angle.[73] When a liquid drop on a solid surface spreads due to electric field, its apparent contact angle decreases. Since our measurements are apparent contact angles (not intrinsic contact angles), herein we will use "contact angle" to refer the "apparent contact angle." If electrowetting is performed on a smooth dielectric solid (e.g., Teflon), when the voltage is removed from the system, the contact angle will tend to approach its original value.[43] Electrowetting on dielectric (EWOD) is popular because of its usefulness in droplet based microfluidic devices or digital microfluidics.[61,62] Drop actuation using EWOD in laboratory-on-a-chip platforms is relatively trouble-free and inexpensive compared to traditional pump and micro-channel based laboratory-on-a-chip platforms. Indeed they have been used successfully in the preparation of biological samples as well as for some analytical processes.[11–16] Other than microfluidics, electrowetting is used in fluid focal lenses,[4] electrowetting displays,[6] programmable optical filters,[63] paint drying,[63] micromotors,[20] electronic microreactors,[44] and to control fluids in multichannel structures.[64] There are some significant advantages of ILs as compared to water and other aqueous electrolytes. ILs have greater stability at elevated temperatures, are liquid over a much wider temperature range, have negligible evaporation, have tunable physical properties and have selective solubility and selective extractability for various organic compounds, metal ions and biological molecules.[26,69] Also corrosion inhibition is achievable for some ILs (however diluted/hygroscopic ILs can facilitate corrosion).[85] In recent studies the electrowetting behavior of ILs was evaluated under DC conditions.[43,46–49] In addition ILs have been used under AC conditions for some EWOD based applications, such as on digital microfluidic devices,[42] electronic microreactors,[44] micro heat transfer devices,[19] and liquid-liquid extraction devices.[18]

In the previous chapter, the study of effects of IL structure on their electrowetting behavior was discussed systematically under DC conditions.[46] In this chapter, electrowetting of ILs under AC voltage at three different frequencies is discussed. Nine different ILs, including mono, di, and tricationic ILs were tested. Among them two are phosphonium based ILs, one is a pyrrolidinium based IL and the others are imidazolium based ILs. Previous studies have shown that electrowetting of water and simple electrolytes under AC voltage can have very different behaviors than with DC voltages.[1,55,86–89] However electrowetting behaviors of ILs under AC voltage conditions have not yet been studied to our knowledge. This study provides substantial information for designing and optimizing the properties of ionic liquids for electrowetting purposes. This opens up more potential applications of electrowetting based microfluidic devices which is currently limited in aqueous based solution operations.

3.1.1 Theoretical Background

Contact angle change by electrowetting can be described by a combination of Young's equation and Lippmann's equation (Equation 3.1).[46]

$$cos\theta = cos\theta_0 + \frac{c}{2\gamma}V^2 = cos\theta_0 + \frac{\epsilon\epsilon_0}{2\gamma t}V^2 \tag{3.1}$$

Here, V_D is the voltage across the dielectric layer, c is the specific capacitance (capacitance per unit area), ϵ is the relative permittivity of the dielectric layer (dielectric constant), ϵ_0 is the permittivity of free space, γ is the surface tension of the liquid, t is the thickness of the dielectric layer, θ is the contact angle at a designated voltage and/or frequency and θ_0 is the contact angle at zero external voltage. According to Equation 3.1).(1) an increase of voltage should decrease the contact angle value. However upon increasing the voltage at some point (voltage) the contact angle stops changing (Figure 1a). That point is referred to as "saturation point", and accord-

ingly the saturation voltage and saturation angle are the corresponding voltage and corresponding contact angle values respectively. It has been reported that Equation 3.1 predicts the contact angle change due to an electric field relatively well until the saturation point.[43,46]

Five quantities can be identified from contact angle vs voltage plots and used to characterize eletrowetting solvents (Figure 1a). They are as follows: θ_0 is the contact angle at zero voltage, θ_S and V_S are the saturation contact angle and saturation voltage respectively. $\Delta\theta$ is the apparent contact angle change ($\Delta\theta = \theta_0$ - θ) at any voltage and/or frequency. Finally, $\Delta\theta_S$ is the maximum apparent contact angle change ($\Delta\theta_S = \theta_0$ - θ_S).

3.2 Experimental Section

The acronyms, chemical names and structures of the ionic liquids used in this work are shown in Figure 3.2 and some of their relevant physical properties are listed in Table 1. All of the tested ILs were synthesized in our laboratory as reported previously[48,66,71,90] except for $[bmpy][NTf_2]$, $[3C_6C_{14}P][DCA]$ and $[3C_6C_{14}P][NTf_2]$. $[bmpy][NTf_2]$ was purchased from Sigma-Aldrich (St. Louis, MO). $[3C_6C_{14}P][DCA]$ and $[3C_6C_{14}P][NTf_2]$ were provided by CYTEC (www.cytec.com, West Paterson, NJ). Both $[3C_6C_{14}P][DCA]$ and $[3C_6C_{14}P][NTf_2]$ are phosphonium based ILs, $[bmpy][NTf_2]$ is a pyrrolidinium based IL and the rest are imidazolium based ILs. $[(bim)_2C_{10}][NTf_2]$ is a dicationic ionic liquid, $[(beim)_3a][NTf_2]$ is a tricationic ionic liquid with a rigid core, while $[(bimC_{10})_2im][NTf_2]$ is a flexible, linear tricationic ionic liquid and the rest of ILs are monocationic ionic liquids. Before the experiments each tested IL was kept in a vacuum oven 12-18 hours with phosphorous pentoxide (P_2O_5) at room temperature to minimize the water content. The final water content of each IL as measured by Karl Fischer titration is, 1.56% for $[bmim][Cl]$, 990 ppm for $[bmim][PF_6]$, 470 ppm for

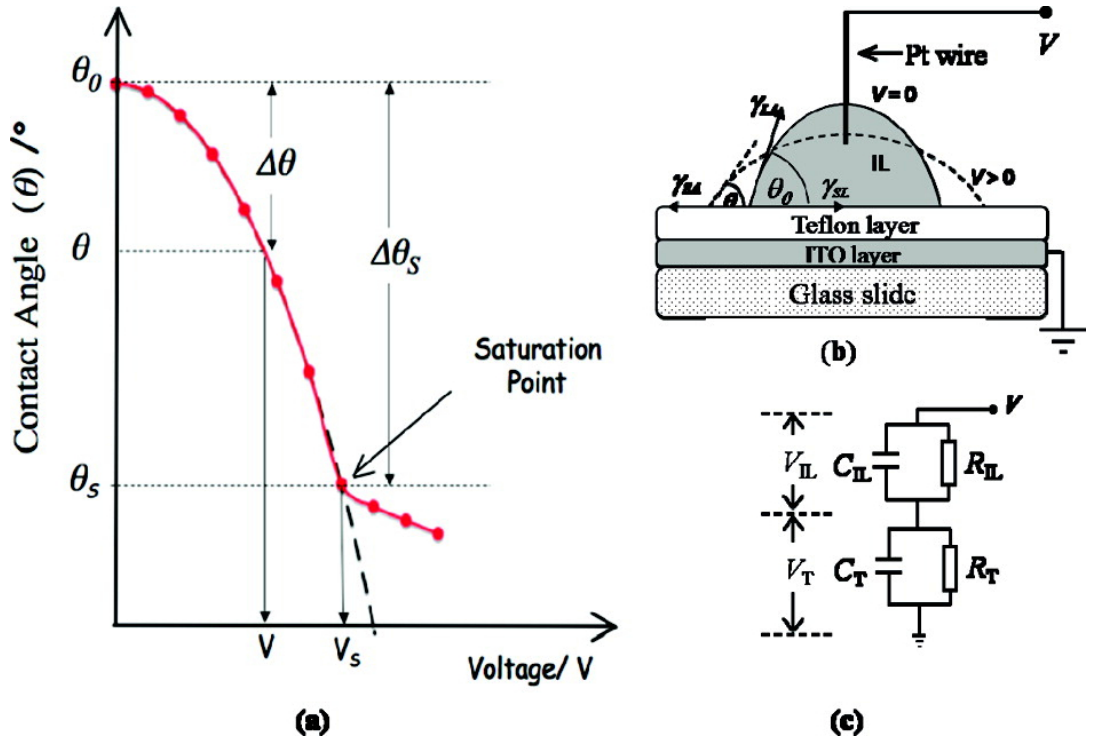

Figure 3.1: a) An idealized electrowetting curve obtained by plotting the contact angle of a liquid drop on a dielectric surface versus voltage. b) Experiment setup for electrowetting measurements. Solid line represents the drop shape at zero external voltage. Dashed line represents the drop shape at a given external voltage.c) Equivalent circuit model for the electrowetting experiment

$[bmim][NTf_2]$, 320 ppm for $[bmpy][NTf_2]$, 0.29% for $[3C_6C_{14}P][DCA]$, 420 ppm for $[3C_6C_{14}P][NTf_2]$, 480 ppm for $[(bim)_2C_{10}][NTf_2]$, 980 ppm for $[(bimC_{10})_2im][NTf_2]$ and 810 ppm for $[(beim)_3a][NTf_2]$. The substrate preparation and electrowetting experiments were performed in a similar manner to that reported elsewhere.2 First, 30 nm thick Indium-tin-oxide (ITO) pre-coated unpolished float glass slides were used as purchased (www.delta-technologies.com, Stillwater, MN). They were dip coated with an amorphous fluoropolymer layer (Teflon). The Teflon solution was prepared by dissolving 4% (w/v) of Teflon AF1600 (www2.dupont.com, Wilmington, DE) in Fluoroinert FC75 solvent (www.fishersci.com Barrington, IL). The approximate dipping speed of the custom made dipcoater was 0.78±0.03 mm/s. Dipping was stopped for 5 seconds, once 3/4 of the slide was dipped in the solution, and then the slide was raised at the same speed. The coated slides were then heat treated serially for 6 min at 112 °C, 5 min at 165 °C and 15 min at 328 °C in an oven. Teflon coated glass slides were then allowed to reach room temperature, washed thoroughly with acetone and deionized water and air-dried. Then the electrowetting experiment was conducted using a contact angle goniometer (CAM 101, www.ksvltd.com, Monroe, CT).

A capillary tube was used to place a drop of ionic liquid ($\approx$ 5 μL) on top of the Teflon layer (Figure 3.1b). Since ILs are viscous, a micro pipette cannot be used to place/measure the ionic liquid drop. For a specific IL volume variation is approximately $\pm$ 1 μL. The variation in volumes between different ILs was $\pm$ 2 μL. However this variation affects neither the contact angle of the drop nor the apparent contact angle change by electrowetting. [See Figure 3.3]. The volume and the contact angle of the drop were calculated using CAM 200 software (www.ksvltd.com, Monroe, CT). The AC voltage was applied in 5 V increments starting from 0 V, using a waveform generator (Agilent Model 33220A) connected to a voltage amplifier (Trek

Model PZD 350). One electrode was attached to a Pt wire (36 gauge), which was inserted to the drop while the ground electrode was attached to the ITO layer. The voltage was increased in 5 V increments until the IL drop burned, decomposed or oscillated. For each voltage value, the contact angle was measured. This procedure was repeated for each IL at three different frequencies, 60 Hz, 1 kHz and 10 kHz. DC electrowetting experiments were conducted as reported in our previous work on the DC electrowetting of ILs (from 0 V to ± 70 V).[46]

The volume and the contact angle of the drop were measured for water, a water miscible IL ($[bmim][Cl]$) and a water immiscible IL ($[bmim][NTf_2]$) with time. First a drop of liquid ($\approx 5\mu L$) was placed on the Teflon layer. Then pictures were taken at 5-minute interval for 45 minutes, without applying any external voltage. Subsequently, the volume and contact angle of the drop were calculated and the volume versus time curves and contact angle versus time curves were plotted. The impact of water on the AC electrowetting of ILs was evaluated using both a water-miscible IL (i.e., $[bmim][Cl]$) and a water-immiscible IL (i.e., $[bmim][NTf_2]$). 16 %, 48 % and 80 % water containing, $[bmim][Cl]$ + water, (w/w) solutions were prepared. Then electrowetting experiments were conducted at 1 kHz for the water containing solutions as well as for the pure DI water. For the water immiscible IL, 0.5 mL of $[bmim][NTf_2]$ was added to 5 mL of water, shaken for 2 min and then allowed to settle for one hour. The water layer was then decanted from the clearly observed two layers. The electrowetting experiments were conducted on the remaining $[bmim][NTf_2]$ layer at all three frequencies (i.e., 60 Hz, 1 kHz and 10 kHz). All the experiments were conducted in ambient conditions 23 ± 1 °C and all the AC voltages are reported in V_{RMS} values, unless otherwise noted. In regard to their safety, all of the tested ILs are non-flammable.

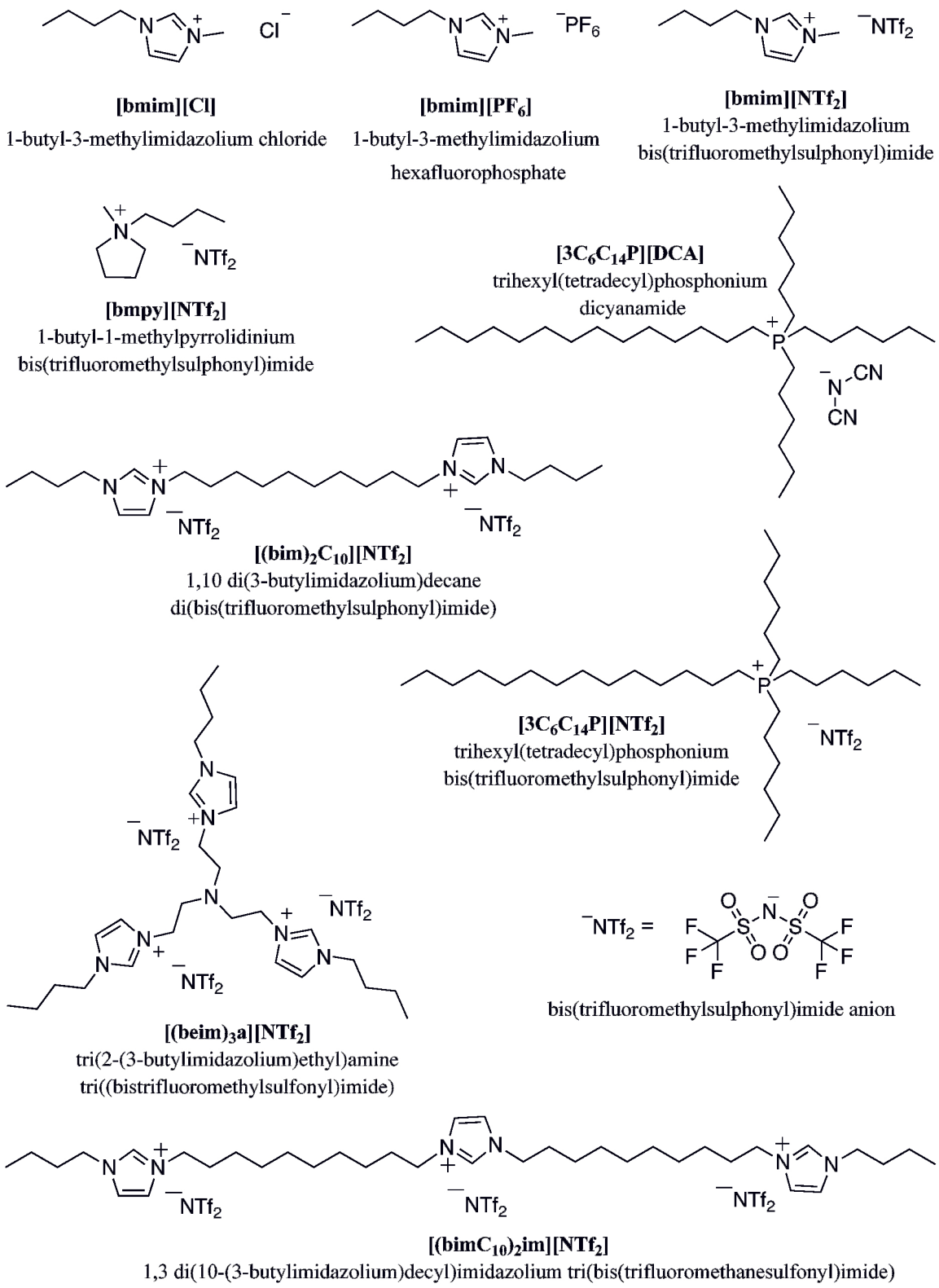

Figure 3.2: Structures, acronyms, and chemical names of the investigated ionic liquids

Table 3.1: Physical Properties of the Studied Ionic Liquids[a]

	$[bmim]$ $[Cl]$	$[bmim]$ $[NTf_2]$	$[bmim]$ $[NTf_2]$	$[bmpy]$ $[NTf_2]$	$[3C_6C_{14}P]$ $[NTf_2]$	$[3C_6C_{14}P]$ $[DCA]$	$[(bim)_2C_{10}]$ $[NTf_2]$	$[(beim)_3a]$ $[NTf_2]$	$[(bimC_{10})_2im]$ $[NTf_2]$
MW (g/mol)	174.7	284.2	419.4	422.4	764.0	493.8	884	1311.2	1435.3
MP (°C)	65	-8	-4		$(> -76 < -22)$			-47.5	-53.17
d (g/cm3)	1.10	1.36	1.43	1.40	1.06	0.90	1.401	1.41	1.54
RI	1.523	1.411	1.427		1.451	1.484	1.483	1.451	1.44
η (cSt)	1701	170	36		219	269	146	1580	2400
$\sigma(10^{-4}S/cm)$	0.3	14.6	40.6	22	2.1	0.9			
TS(°C)	145		185		380	360		308	350
γ (dyn/cm)	60.7	44.8	32.8	35.2	31.7	40.8	37.5	43.2	40.4
WM	M	I	I	I	I	I	I	I	I

[a]Structures and names of the ILs are shown in Figure 3.2. For measurement techniques and data sources see Ref [2]

MW = Molecular Weight MP = Melting Point d = density

RI = Refractive Index η = Viscosity at 30 °C σ = conductivity at 25 °C

TS =Thermal Stability, temperature at 1 % mass decrease of sample γ = Surface Tension

WM =Water Miscibility, M= Miscibile, I= Imiscible

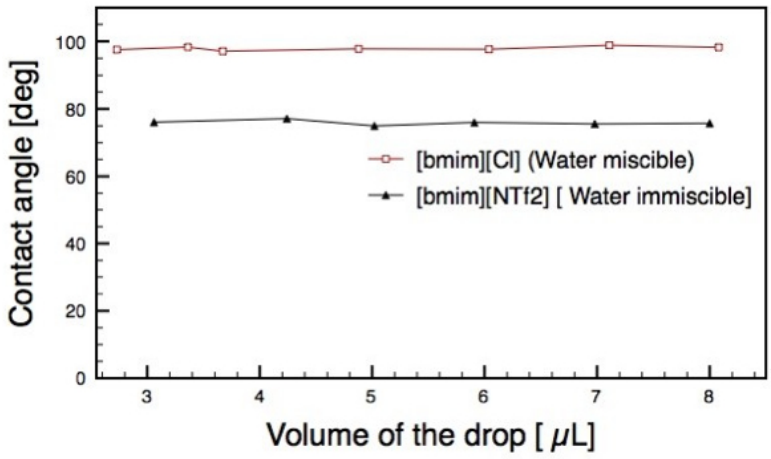

(a)

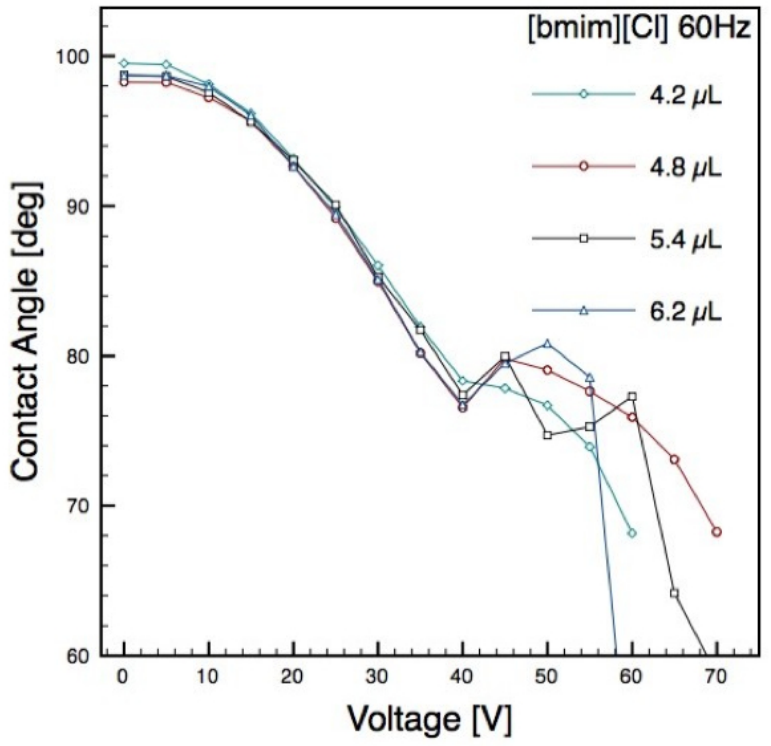

(b)

Figure 3.3: Effect of the volume of the drop on electrowetting, a) Contact angle versus volume of $[bmim][Cl]$ and $[bmim][NTf_2]$ at zero external voltage, b) Electrowetting curves of $[bmim][Cl]$ at 60 Hz with different drop volumes

3.3 Results and Discussion

3.3.1 Initial Contact Angle (θ_0)

The θ_0 is the contact angle at zero external voltage therefore, it refers both apparent and intrinsic contact angle if the solid surface is ideally smooth. On such ideal surfaces, θ_0 can be described using the Young equation, where: $\theta_0 = \cos^{-1}[(\gamma_{SL}\text{-}\gamma_{SA})/\ \gamma_{SA}]$, where γ_{SL}, γ_{SA} and γ_{SA} are liquid/air, air/solid and solid/liquid interfacial tensions respectively (Figure 1b).[46,91] It has been reported that, for a series of liquids, only the surface tension of the liquid can affect its $\theta_0$value in identical experimental conditions.[46] Table 2.2 lists the θ_0 values for all ILs. It is observed that different ILs have different θ_0 values. ILs in this study can be broadly categorized in to three different groups by means of their surface tension values. The surface tensions of $[bmim][Cl]$ and $[bmim][PF_6]$ are higher than 44 dyn/cm [See Table 1], while $[bmim][NTf_2]$ and $[3C_6C_{14}P][NTf_2]$ have surface tension values lower than 34 dyn/cm. The surface tensions of the other five ILs lie between 34 dyn/cm and 44 dyn/cm. It was observed that, $[bmim][Cl]$ and $[bmim][PF_6]$ have higher $\theta_0$values (98° and 90° respectively) than all other ILs (see Table 2.2). Similarly, $[bmim][NTf_2]$ and $[3C_6C_{14}P][NTf_2]$ have lower $\theta_0$values (75° and 72° respectively) than the other ILs, while other five ILs have intermediate $\theta_0$values (between 77° and 80°). Therefore it can be concluded that the $\theta_0$value correlates directly with the surface tension of the IL, i.e., the higher the surface tension of the IL, the higher the $\theta_0$value obtained.

3.3.2 θ, $\Delta\theta$, V_S, θ_S and $\Delta\theta_S$ Values

Figure 3.4 shows the electrowetting curves of $[3C_6C_{14}P][DCA]$ at different voltage and frequency conditions. It was observed that, at a given voltage the $\Delta\theta$ values of $[3C_6C_{14}P][DCA]$ with AC voltage were always substantially larger than those with DC voltage (at 60 V_{AC} and 10 kHz, $\Delta\theta$ is more than 5 times larger than the $\Delta\theta$ with

Table 3.2: Saturation Angles of Studied Ionic Liquids

	$[bmim]$ $[Cl]$	$[bmim]$ $[PF_6]$	$[bmim]$ $[NTf_2]$	$[bmpy]$ $[NTf_2]$	$[3C_6C_{14}P]$ $[DCA]$	$[3C_6C_{14}P]$ $[NTf_2]$	$[(bim)_2C_{10}]$ $[NTf_2]$	$[(beim)_3a]$ $[NTf_2]$	$[(bimC_{10})_2im]$ $[NTf_2]$
θ_0	98 ± 1	90 ± 1	75 ± 1	79 ± 1	77 ± 1	72	79 ± 1	78 ± 1	80
	θ_S	θ_S	θ_S	θ_S	θ_S	θ_S	θ_S	θ_S	θ_S
DC + ve	80	78	68	71	62	55	64	57	66
DC - ve	84	73	65	66	68	58	60	52	65
60 Hz	77	73	56	58	31	38	32	31	39
1 kHz	58	46	37	42	21	22	30	29	30
10 kHz	53	35	26	40	11	10	39	26	41;29

Table 3.3: Electrowetting properties of studied ILs

Ionic Liquid	θ_0 [deg]		θ_S [deg]	$\Delta\theta_S$ [deg]	V_S [V]
$[bmim]$ $[Cl]$	98±2	DC + ve	80	17	50
		DC - ve	84	13	60
		60 Hz	77	22	40
		1 kHz	58	42	55
		10 kHz	53	45	40
$[bmim]$ $[PF_6]$	90±1	DC + ve	78	11	35
		DC - ve	73	16	60
		60 Hz	73	17	35
		1 kHz	46	44	70
		10 kHz	35	56	40
$[bmim]$ $[NTf_2]$	75±1	DC + ve	68	7	25
		DC - ve	65	10	40
		60 Hz	56	19	35
		1 kHz	37	39	70
		10 kHz	26	49	40
$[bmpy]$ $[NTf_2]$	79±1	DC + ve	71	8	30
		DC - ve	66	13	30
		60 Hz	58	21	35
		1 kHz	42	38	60
		10 kHz	40	39	30
$[3C_6C_{14}P]$ $[DCA]$	77±1	DC + ve	62	16	40
		DC - ve	68	10	30
		60 Hz	31	46	110
		1 kHz	21	55	115
		10 kHz	11	65	65
$[3C_6C_{14}P]$ $[NTf_2]$	72	DC + ve	55	17	30
		DC - ve	58	14	30
		60 Hz	38	34	60
		1 kHz	22	50	75
		10 kHz	10	62	70
$[(bim)_2C_{10}]$ $[NTf_2]$	79±1	DC + ve	64	15	35
		DC - ve	60	20	35
		60 Hz	32	47	105
		1 kHz	30	49	75
		10 kHz	39	41	40
$[(beim)_3a]$ $[NTf_2]$	78±1	DC + ve	57	20	70
		DC - ve	52	25	70
		60 Hz	31	46	70
		1 kHz	29	50	85
		10 kHz	26	53	60
$[(bimC_{10})_2im]$ $[NTf_2]$	80	DC + ve	66	14	30
		DC - ve	65	15	35
		60 Hz	39	42	60
		1 kHz	30	50	85
		10 kHz	41/29	39/51	50/65

+60 V_{DC}). In other words, lower contact angles (θ) can be obtained when using AC voltages as compared to those obtained for DC voltages. Furthermore, it appears that an increase in the AC frequency leads to a further increase in the $\Delta\theta$ value, i.e., at higher frequencies, lower θ values are obtained. The behavior is apparent for $[3C_6C_{14}P][DCA]$ at 60 V. It has five different contact angle values; 14°, 42°, 50°, 65° and 66° at 10 kHz AC, 1 kHz AC, 60 Hz AC, and (+) or (-) DC voltages respectively. Similar behavior was observed for the all tested ILs. [Figures $3.13 - 3.20$].

Figure 3.9 shows the $\Delta\theta_S$ of all ILs under both AC and DC voltage conditions and Table 3.2 lists the corresponding θS. It appears that in general $\Delta\theta_S$ increases (i.e., θ_S decreases) with increasing frequency. Also, it is observed that, θ_S in AC conditions is always smaller than that of DC conditions. Finally it was observed that the V_S under DC voltage conditions is generally lower than it is with AC conditions. (See Table 3.3).

Our observations (vidae supra) can be explained using a model similar to that reported by Chatterjee et al.[59] First, the voltage across the dielectric (Teflon) layer, V_D, was determined using the model. (Figure 3.1c shows the equivalent circuit model for the sessile drop electrowetting experiment). Then, it was combined with the Young-Lippmann equation (Equation 3.1) to establish the relationship with contact angle (θ), in a way similar to that described by Kumar et al.[55] The final derived relationship is: (see section 3.3.3 for the step by step derivation of this expression).

$$\theta = F(V, f, \gamma, \sigma, \epsilon_{IL}, d) \tag{3.2}$$

It shows that the contact angle (θ) is a function of externally controlled factors [i.e., applied external voltage (V) and frequency (f)] as well as some physical properties of the IL itself [i.e., surface tension (γ), conductivity (σ), dielectric constant (ϵ_{IL}) and double layer thickness (d)].

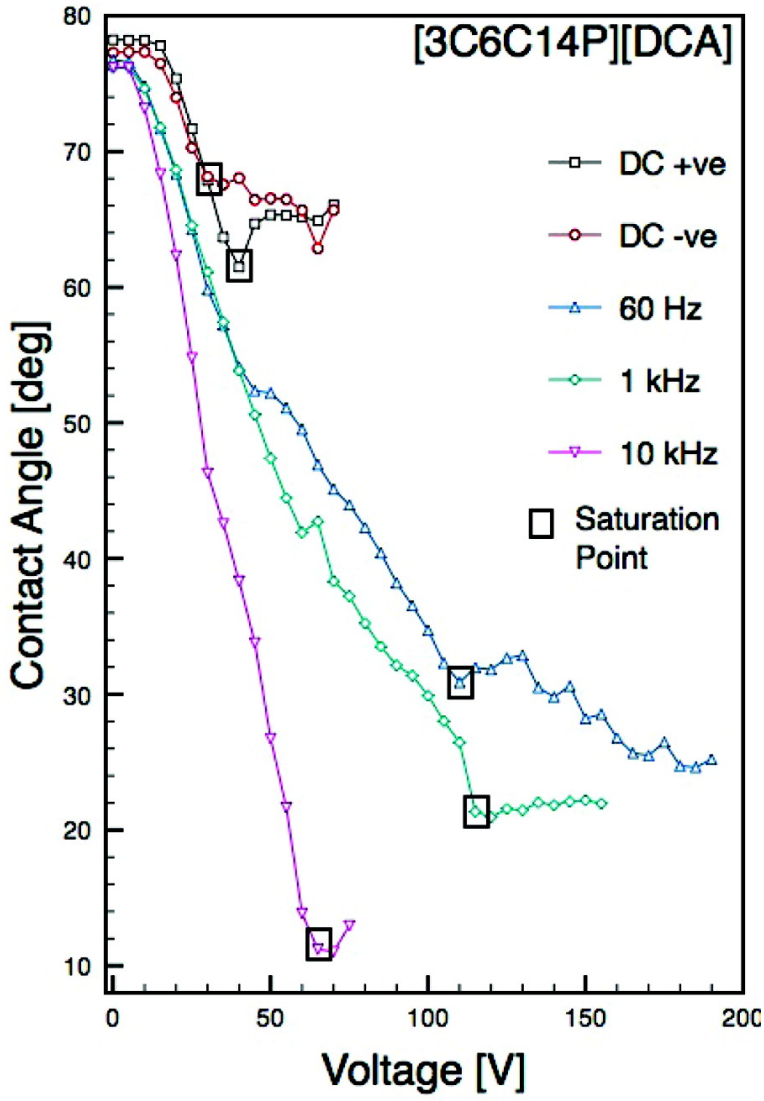

Figure 3.4: Electrowetting curves of $[3C_6C_{14}P][DCA]$ with DC and AC voltage conditions

For a given IL, ϵ_{IL}, ρ, γ and d are constants. During the entire experiment the distance between the Pt tip and the Teflon surface remains constant. Therefore according to equation 3.2 for a given IL, θ depends only on f and V. This phenomenon can be easily visualized by the electrowetting curves of $[3C_6C_{14}P][DCA]$in Figure 3.4. Applying +60 V DC voltage, θ changes from 77° to 65°, which is due to the basic electrowetting effect described by Young and Lippmann's equation (3.1). While

keeping the voltage constant, if the frequency is increased to 1 kHz, the contact angle further decreases (42°). Additional increases in the frequency to 10 kHz continue to suppress the contact angle to 14°. This justification is valid for every IL studied (see Table 3.2-3.3).

According to equation 3.2, at a fixed V and fixed f, ILs with different ϵ_{IL}, ρ, γ and d should generate different contact angles values (θ). Our experimental results agree with this as well. For example, the contact angles of the studied ILs at 1 kHz and 50 V are, 66° for $[bmim][Cl]$, 57° for $[bmim][PF_6]$, 44° for $[bmim][NTf_2]$, 44° for $[bmpy][NTf_2]$, 47° for $[3C_6C_{14}P][DCA]$, 36° for $[3C_6C_{14}P][NTf_2]$, 43° for $[(bim)2C10][NTf_2]$, 48° for $[(beim)_3a][NTf_2]$ and 54° for $[bimC10)2im][NTf_2]$. Apart from the above-mentioned observations, there is another important phenomenon observed with the $\Delta\theta_S$ values. The $\Delta\theta_S$ values of $[bmim][Cl]$, $[bmpy][NTf_2]$ and $[(bimC_{10})_2im][NTf_2]$ increase when the frequency increases from 60 Hz to 1 kHz, but it remained constant when the frequency increases from 1 kHz to 10 kHz. (see Figure 3.5). Also for $[(beim)_3a][NTf_2]$ those values at all three frequencies differ from one another by less than 4°. This phenomenon may be due to: 1) the presence of critical frequency (f_C), 2) the effect of ordinary contact angle saturation, or 3) both.

3.3.2.1 Effect of the critical frequency (f_C)

It is reported that at their f_C liquids tends to change from conductive to dielectric behavior.[56,59] When the frequency is lower than f_C, liquids behave as conductors, and when the frequency is higher than f_C liquids behave as insulators. For our system, f_C, can be written as:[59]

$$f_C = F(R_{IL}, C_{IL}, C_T) \tag{3.3}$$

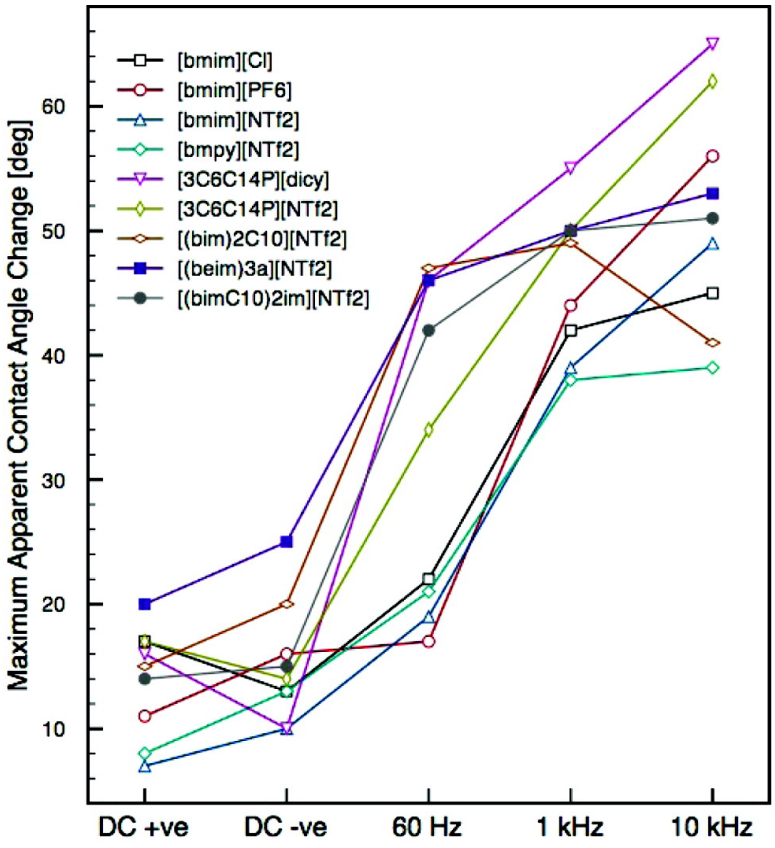

Figure 3.5: Maximum apparent contact angle change, $\Delta\theta_S$, of ILs at $\pm$ DC voltages and three different frequencies of AC voltage

(See, section 3.3.3 for the step by step derivations). where, C is the capacitance and R is the resistance. The subscripts "IL" and "T" indicate the IL and Teflon layers respectively. Since different ILs have different R_{IL} and C_{IL} values, according to equation 2.3, f_C values of each IL should differ from one another. When increasing the frequency, θ starts to decrease. However after $f{=}f_C$, the liquid becomes dielectric in nature and as a consequence the reduction in θ should stop or should exhibit very little change. Since the f_C for each IL will be different, the reduction of θ between different frequencies should vary.

3.3.2.2 Effect of ordinary contact angle saturation

Ordinary contact angle saturation is observed for both AC and DC electrowetting experiments. It has many origins as well as many proposed mechanisms and is not yet fully understood.[1] The primary focus on this study was not the understanding of the contact angle saturation or the effect of critical frequency. Therefore we can not quantify the contributions of these two possible effects on the above observed phenomenon.

3.3.3 Derivation of Equations

3.3.3.1 Definition of Terms

d = double layer thickness of the IL

v = volume of the drop

t = thickness of the Teflon layer

ρ = resistivity of IL

γ = surface tension of IL

σ = conductivity of IL

ϵ_0 = permittivity of free space

ϵ = dielectric constant

f = frequency of the applied voltage

$\omega = 2\pi f$

V_D = voltage across the dielectric (Teflon) layer ; V = rms voltage

$A_i = \pi r^2 sin^2\theta = \frac{1}{X_i}$ = area between the drop and the Teflon layer (Figure 3.6)

$A_i^1 = \pi[r^2 - (L + rcos\theta)^2]$ = area of horizontal cross section that goes through the Pt wire (Figure 3.6)

L = distance from Pt tip to the Teflon Surface (Figure 3.6)

v = volume of the drop

$r = [\frac{3v}{\pi(1-cos\theta)^2(2+cos\theta)}]^{\frac{1}{3}}$ = radius of the curvature of the drop

C = capacitance

R = resistance

Z = impedence

$g = \frac{1}{R}$ = conductance

$j = \sqrt{-1}$. The subscripts "IL" and "T" (e.g., C_{IL}, C_T, etc...) indicate the IL and Teflon layers respectively.

3.3.3.2 Equation 3.2 Derivation

Figure 2.1 shows the equivalent circuit for the sessile drop electrowetting experiment. Let Z_{IL} and Z_T be the impedance of the ionic liquid and Teflon layer respectively. Then elementary electric circuit modeling indicate that,

$$Z_{IL} = \frac{1}{g_{IL} + j\omega C_{IL}}; Z_T = \frac{1}{g_T + j\omega C_T}$$

Therefore, the voltage across the Teflon (dielectric) layer is:

$$V_D = \frac{Z_T}{Z_{IL} + Z_T}$$

$$V_D = \frac{1 + j\omega R_{IL} C_{IL}}{1 + \frac{R_{IL}}{R_T} + j\omega R_{IL}(C_{IL} + C_T)} V$$

Since the resistivity of Teflon is $\approx 1 \times 10^{16} \Omega m$,

$$\frac{R_{IL}}{R_T} \to 0$$

$$V_D = \frac{1 + j\omega R_{IL} C_{IL}}{1 + j\omega R_{IL}(C_{IL} + C_T)} V$$

In order to make the denominator real, the denominator and numerator were multiplied by the complex conjugate of the denominator. Then,

$$V_D = \frac{[1 + \omega^2 R_{IL}^2 C_{IL}(C_{IL} + C_T)] - j\omega R_{IL} C_T}{1 + \omega^2 R_{IL}^2 (C_{IL} + C_T)^2} V$$

Considering only the amplitude of V_D,

$$V_D = [V_D . V_D^*]^{\frac{1}{2}}$$

$$V_D = \frac{[[1 + \omega^2 R_{IL}^2 C_{IL}(C_{IL} + C_T)]^2 + \omega^2 R_{IL}^2 C_T^2]^{\frac{1}{2}}}{1 + \omega^2 R_{IL}^2 (C_{IL} + C_T)^2} . V \tag{3.4}$$

Inserting V_D in equation 3.1 gives,

$$cos\theta = cos\theta_0 + \frac{\epsilon_T \epsilon_0}{2\gamma_{IL} t} . \frac{[[1 + \omega^2 R_{IL}^2 C_{IL}(C_{IL} + C_T)]^2 + \omega^2 R_{IL}^2 C_T^2]}{[1 + \omega^2 R_{IL}^2 (C_{IL} + C_T)^2]^2} . V^2 \tag{3.5}$$

According to equation 3.5, for a given IL, θ is a function of $f, \gamma_{IL}, R_{IL}, C_{IL}, C_T$, and V, which can be represented as,

$$\theta = F(f, R_{IL}, \gamma_{IL}, C_{IL}, C_T, V) \tag{3.6}$$

However, R_{IL}, C_{IL} and C_T are, in terms, functions of θ. Since the area between the drop and the Teflon layer (A_i) is a function of contact angle θ. R_{IL} and C_{IL} both have A_i and A_i^1 terms (Figure 3.6), but C_T includes only the A_i term (A_i and A_i^1 both are functions of θ).

$$A_i = \pi r^2 sin^2\theta \tag{3.7}$$

Resistance of an imaginary (dy) thick horizontal slice of the drop can be written as,

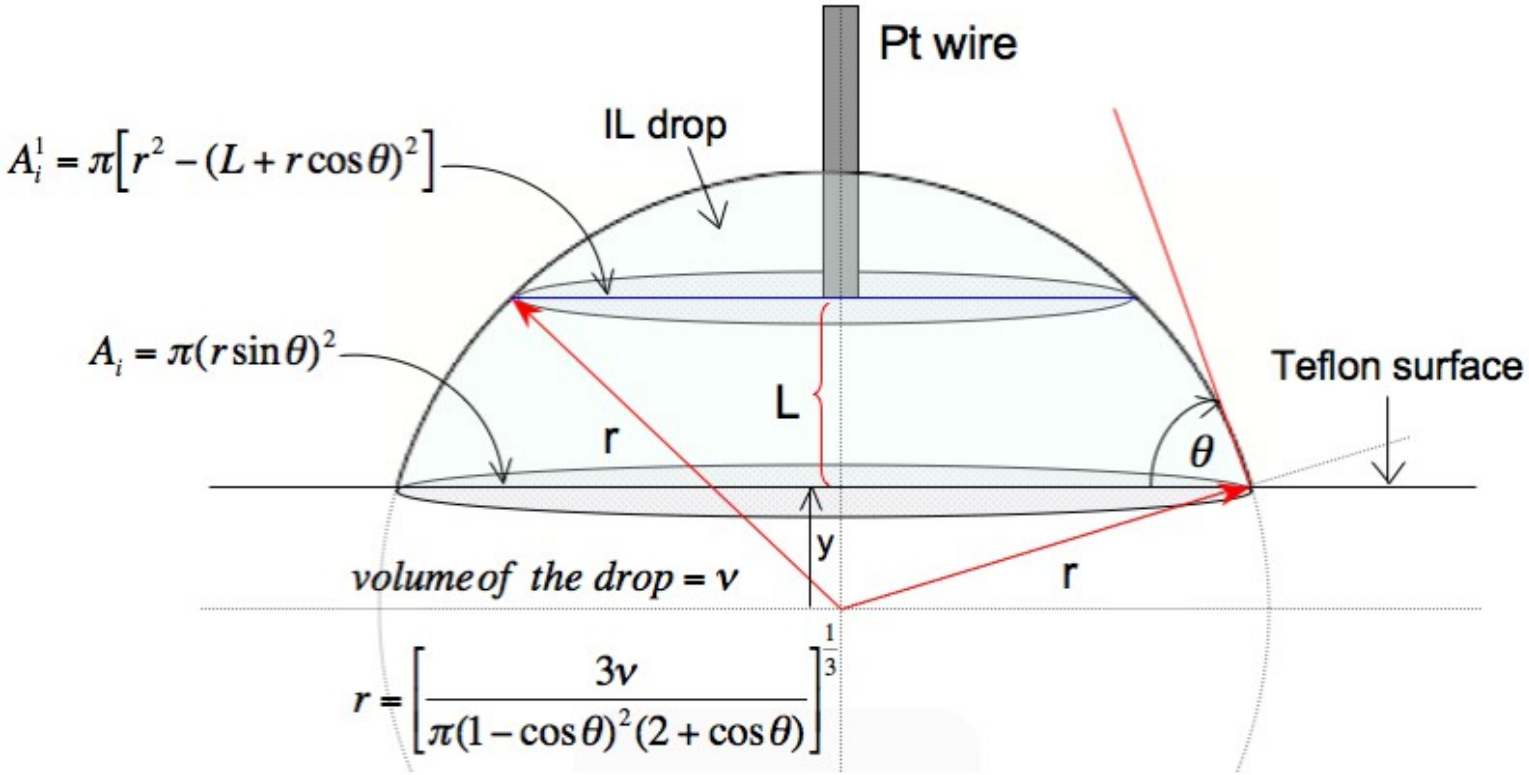

Figure 3.6: Modeled ionic liquid drop shape at a given voltage and/or frequency

Here the drop is assumed to be a spherical cap. A_i corresponds to the contact area of the liquid drop on Teflon surface. A_i^1 corresponds to the area of horizontal cross section that goes through the Pt wire. r corresponds to the radius of the drop (spherical cap) with contact angle (θ) and volume ($v = 5\mu L$)

$$R = \rho\frac{dy}{A} = \rho\frac{dy}{\pi(r^2 - y^2)};$$

where, $y = rsin\theta$ (See Figure 3.6)

Therefore, R_{IL} can be written as,

$$R_{IL} = \int_{y}^{L+y} \rho\frac{1}{\pi(r^2 - y^2)}dy$$

$$R_{IL} = \int_{y}^{L+y} \rho\frac{1}{\pi(r^2 - y^2)}dy$$

$$R_{IL} = \frac{1}{2\pi\sigma r}.ln|\frac{(r + rcos\theta + L)(1 - cos\theta)}{(r - rcos\theta - L)(1 + cos\theta)}|$$

L is a constant for a given experiment, therefore above equation can be re-written as,

$$R_{IL} = F(\theta, \sigma) \tag{3.8}$$

If the double layer thickness of a given IL is d, then C_{IL} can be considered as L/d number of capacitors in series and can be given as,

$$\frac{1}{C_{IL}} = \frac{1}{C_1} + \frac{1}{C_2} + ... + \frac{1}{C_{\frac{L}{d}}}$$

$$\frac{1}{C_{IL}} = \frac{d}{\epsilon_{IL}\epsilon_0}\left[\frac{1}{A_i} + \frac{1}{A_{i+1}} + ... + \frac{1}{A_{\frac{L}{d}}}\right]$$

$$C_{IL} = \frac{\epsilon_{IL}\epsilon_0}{d\left[\frac{1}{A_i} + \frac{1}{A_{i+1}} + ... + \frac{1}{A_{\frac{L}{d}}}\right]}$$

Since ϵ_0 is a constant,

$$C_{IL} = F(\epsilon_{IL}, d, \theta) \tag{3.9}$$

The capacitance of the Teflon layer (C_T), can be given as,

$$C_T = \epsilon_T\epsilon_0\frac{A_i}{t}$$

Since both ϵ_0 and t are constants, above equation can be rewritten as,

$$C_T = F(\theta) \tag{3.10}$$

Combining equation 3.6, 3.8, 3.9 and 3.10 gives,

$$\theta = F(V, f, \gamma, \sigma, \epsilon_{IL}, d) \qquad (3.2)$$

3.3.3.3 Equation 3.3 derivation

According to equation 3.4,

$$\frac{V_D}{V} = \frac{[[1 + (2\pi f)^2 R_{IL}^2 C_{IL}(C_{IL} + C_T)]^2 + (2\pi f)^2 R_{IL}^2 C_T^2]^{\frac{1}{2}}}{1 + (2\pi f)^2 R_{IL}^2 (C_{IL} + C_T)^2} \tag{3.11}$$

at critical frequency (i.e., $f = f_C$),

$$|\frac{V_D}{V}| = \frac{1}{\sqrt{2}}$$

then, equation 3.11 becomes,

$$\frac{1}{\sqrt{2}} = \frac{[[1 + (2\pi f)^2 R_{IL}^2 C_{IL}(C_{IL} + C_T)]^2 + (2\pi f)^2 R_{IL}^2 C_T^2]^{\frac{1}{2}}}{1 + (2\pi f)^2 R_{IL}^2 (C_{IL} + C_T)^2} \tag{3.12}$$

According to equation 3.12, f_C can be written as a function of C_T, C_{IL} and R_{IL}.

$$f_C = F(C_T, C_{IL}, R_{IL}) \qquad (3.3)$$

3.3.4 Anion Effects

Figure 3.7a shows the electrowetting curves for $[bmim][Cl]$, $[bmim][PF_6]$ and $[bmim][NTf_2]$ at 1 kHz. These three ILs are monocationic and have a common cation, $bmim^+$. The size of the anion and charge delocalization of the anion decreases in

the order of $NTf_2^- > PF_6^- > Cl^-$(diameters NTf_2^- 7.57, PF_6^- 5.10, Cl^- 3.62Å).[74] According to Figure 3.7a, θ_0 increases in the same order, giving the highest θ_0 for the IL with the smallest anion (Cl^-) and giving the lowest $\theta_0$for the IL with the largest anion (NTf_2^-). This is mainly due to differences in the surface tensions of the ILs (Table 1). It has been reported that, if the size and/or the charge delocalization of an anion (say X) is smaller than those of another anion (say Y), then the surface tension of IL with X anion is larger than that of the corresponding IL with the Y anion.[46] Therefore, Figure 3.7a represents the dependence of θ_0 on the size and charge delocalization of anion.

Figure 3.7b shows the electrowetting curves of $[bmim][Cl]$, $[bmim][PF_6]$ and $[bmim][NTf_2]$ at 1 kHz which are overlaid normal to θ_0 value of $[bmim][Cl]$. According to Figure 3.7b the $\Delta\theta$ and $\Delta\theta_S$ values are approximately same for the three ILs. It has been reported that the anion has a significant effect on the $\Delta\theta_S$ value with positive DC voltages but not with negative DC voltages due to the anion and Teflon surface interactions in positive DC voltage experiments.[46] In AC voltage conditions the Teflon surface and anion interactions are minimal.[55,86,89] Therefore, as expected for all frequencies with AC voltage, the $\Delta\theta$ and $\Delta\theta_S$ values are comparable for $[bmim][Cl]$, $[bmim][PF_6]$ and $[bmim][NTf_2]$.

3.3.5 Cation Effects

Figure 3.8a shows the electrowetting curves of $[bmpy][NTf_2]$, $[bmim][NTf_2]$ and $[3C6C14P][NTf_2]$ at 1 kHz. $[bmpy][NTf_2]$, $[bmim][NTf_2]$ and $[3C_6C_{14}P][NTf_2]$ all have a common anion: $[NTf_2]$. Since $[3C_6C_{14}P][NTf_2]$ has the largest cation, it has the lowest surface tension among the three ILs (Table 1). Even though, the $[bmpy]$ cation and the $[bmim]$ cation are approximately same size, the $[bmpy]$ cation has a point charge whereas the $[bmim]$ charge is delocalized over the imidazole ring. As

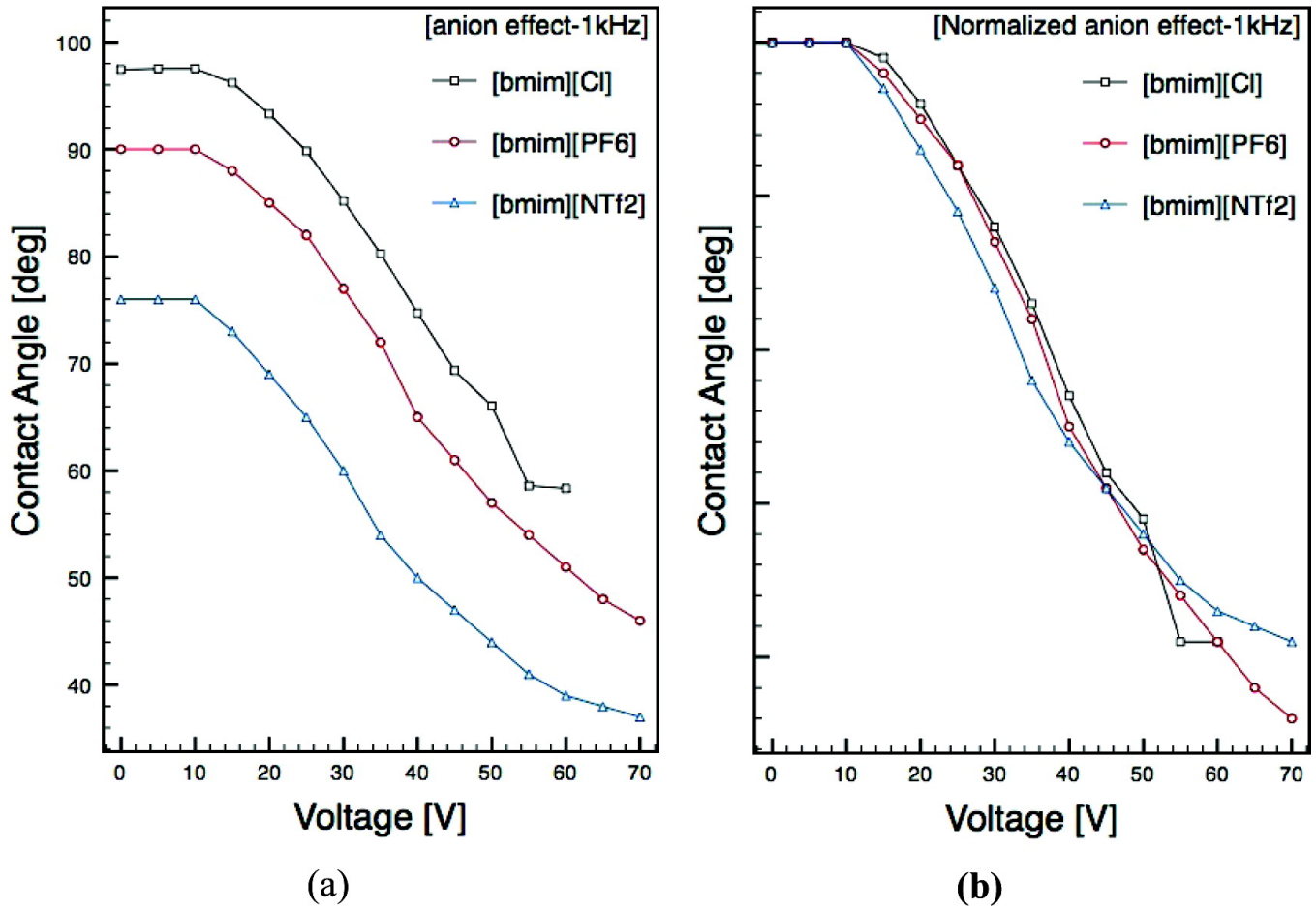

Figure 3.7: Effect of anion: a) electrowetting curves of $[bmim][Cl]$, $[bmim][PF_6]$ and $[bmim][NTf_2]$ at 1 kHz, (b) electrowetting curves of $[bmim][Cl]$, $[bmim][PF_6]$, and $[bmim][NTf_2]$ at 1 kHz were overlaid normal to the maximum θ_0 value

a consequence $[bmpy][NTf_2]$ has slightly larger surface tension value than that of $[bmim][NTf_2]$. These differences in surface tensions reflect on the $\theta_0$values (Figure 3.8a). This result is consistent with that of the anion effect which discussed in previous section. Figure 3.8b shows the electrowetting curves for $[bmpy][NTf_2]$, $[bmim][NTf_2]$ and $[3C_6C_{14}P][NTf_2]$ at 1 kHz, which are overlaid normal to their maximum $\theta_0$values. According to Figure 3.8b, all ILs have approximately the same $\Delta\theta$ values. Therefore it can be concluded that different cations have little effect on $\Delta\theta$ values. In contrast to the $\Delta\theta$, $\Delta\theta_S$ of $[3C_6C_{14}P][NTf_2]$ is 11° more than the $\Delta\theta_S$ of $[bmpy][NTf_2]$ and $[bmim][NTf_2]$ ILs. This observation can be explained by looking at stability of the ILs at higher voltages. ILs $[bmpy][NTf_2]$ and $[bmim][NTf_2]$ only stable up to 70 V and 65 V at 1 kHz respectively, after which they tend to decompose or burn. However $[3C_6C_{14}P][NTf_2]$ is stable at voltages even over 135 V (Table 3.4). Reasons for this decomposition or burning are discussed in the following section.

3.3.6 Stability of the ILs under AC Voltages

The voltages at which ILs remain stable, are listed in Table 3.4. It is observed that, at higher frequencies, ILs become more vulnerable to decomposition. As an example, $[(beim)_3a][NTf_2]$ remains stable up to 150 V when the frequency is 60 Hz, while at 1 kHz and 10 kHz it remains stable up to 140 V and 70 V respectively (Table 3.4). A 10 fold increase in the frequency caused $[(beim)_3a][NTf_2]$ to decompose at approximately half of the voltage (75V versus 145V). This probably is related to the "sonication effect" which is known to break cells and/or molecules using high frequency sound waves. In fact Oxley et al., have shown ILs do decompose when sonicated with 20 kHz frequency sound waves.[92] Apart from that, electrolysis of water which contained in ionic liquids or an electric breakdown could also cause decomposition of ILs at higher voltages. In comparison to ILs, it is observed that water

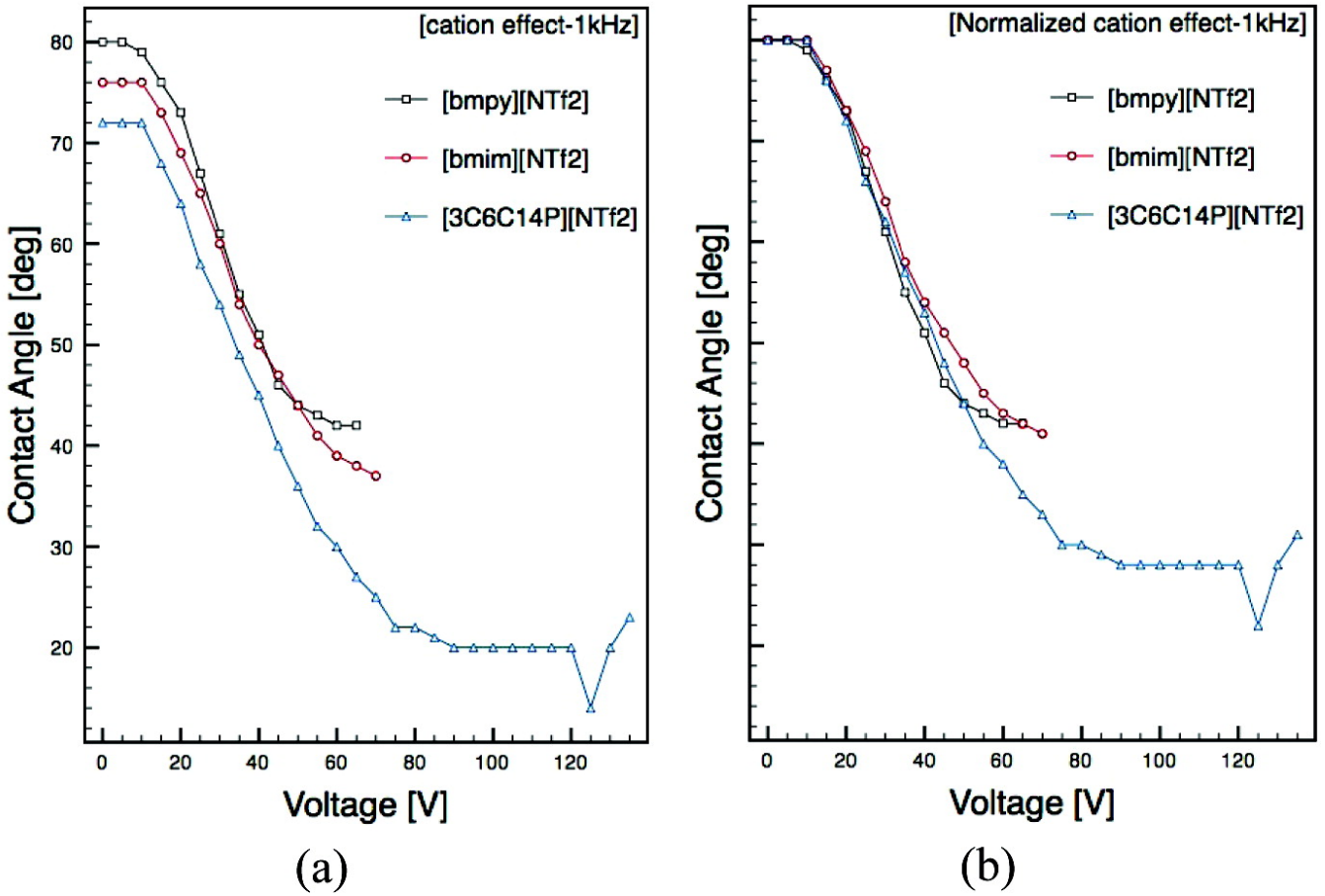

Figure 3.8: Efect of cation: a) electrowetting curves of $[bmpy][NTf_2]$, $[bmim][NTf_2]$ and $[3C_6C_{14}P][NTf_2]$ at 1 kHz, b) electrowetting curves of$[bmim][Cl]$, $[bmim][PF_6]$, and $[bmim][NTf_2]$ at 1 kHz were overlaid normal to the maximum θ_0 value

Table 3.4: Stability of ILs in AC Voltage[a]

ionic liquid	maximum voltage at which liquid remains stable/V		
	60 Hz	1 kHz	10 kHz
$[bmim][Cl]$	60	55	40
$[bmim][PF_6]$	70	70	38
$[bmim][NTf_2]$	70	70	45
$[bmpy][NTf_2]$	65	65	35
$[3C_6C_{14}P][DCA]$[b]	190	155	75
$[3C_6C_{14}P][NTf_2]$[b]	140	135	85
$[(bim)_2C_{10}][NTf_2]$	110	100	50
$[(beim)_3a][NTf_2]$	150	140	70
$[(bimC_{10})_2im][NTf_2]$	125	120	75
$water$[c]	25	100	230

[a]These values are for 260 nm thick Teflon layer electrowetting experiment. [b]Did not decompose, but sparking was observed for these ILs. [c]Did not decompose, but oscillations were observed.

oscillates more readily at low frequencies than at higher frequencies (Table 3.4). This may be due to the low viscosity of water and its resonance frequency.[93]

3.3.7 Evaporation

It was observed that the water drop completely evaporated when it is exposed to the atmosphere for 45 mins, whereas, the volume of water-immiscible IL, $[bmim][NTf_2]$, was unchanged after 45 mins. The volume of water-miscible IL, $[bmim][Cl]$, was slightly increased due to absorption of water from the atmosphere [See Figure 3.9.a]. Similarly, the contact angle of the water drop changed rapidly with time, however the contact angle of all ILs remained constant for the entire experimental time [See Figure 3.9a] This clearly shows the importance of using IL as the medium of EWOD based devices, which can be fabricated without any sealing and for long time period operations.

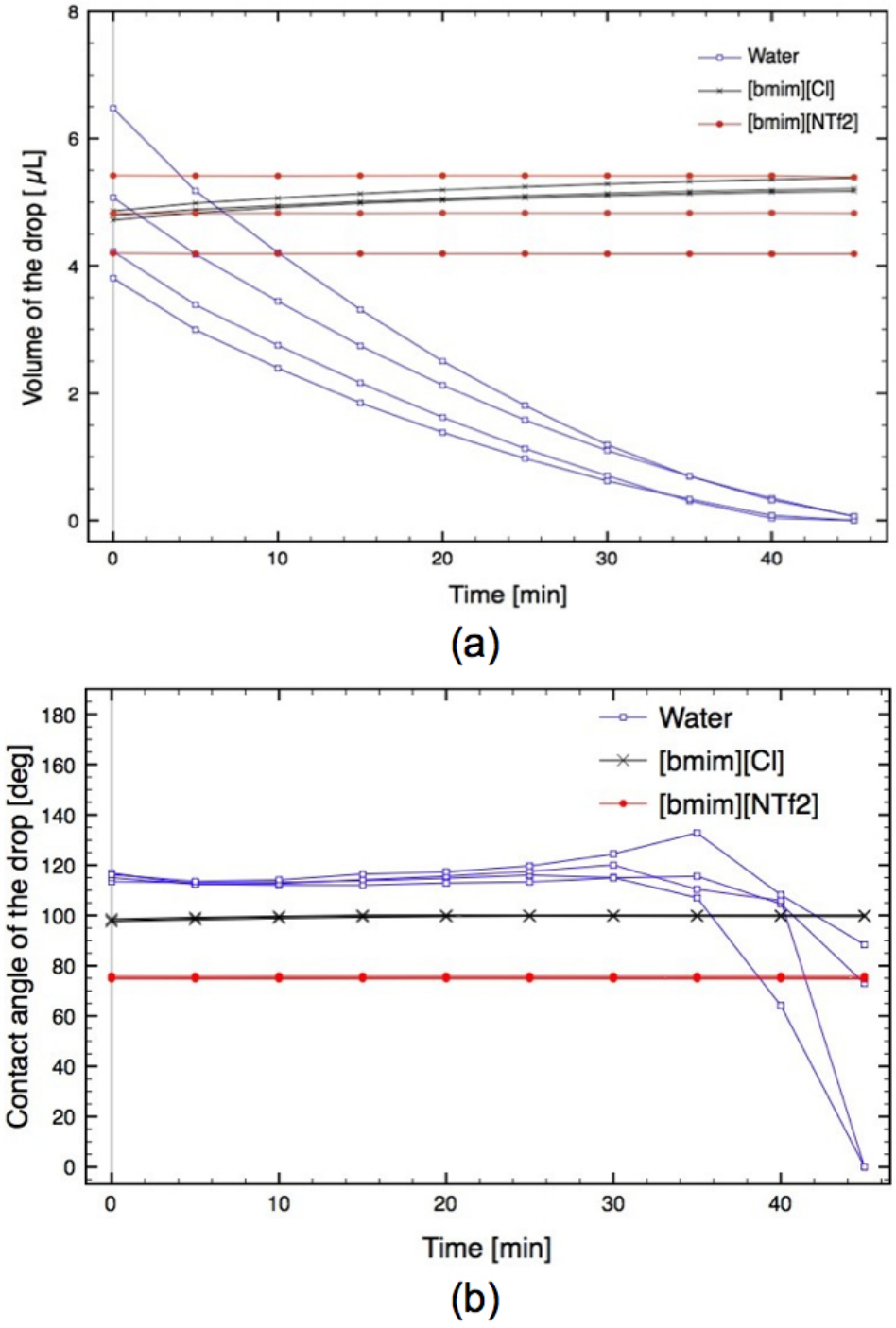

Figure 3.9: Evaporation of ILs and water drops with time, a) drop volume vs. time, b) contact angle vs. time

3.3.8 Effect of Water

Generally all liquids contain water to a certain extent. ILs are no exception. In the final step of IL synthesis, water and the other solvents were removed using a rotary evaporator as explained in the Experimental Section. To further minimize their water content, $\sim$ 0.5 mL of each IL was stored in a vacuum oven for 12-18 hours with phosphorous pentoxide (P_2O_5) at room temperature. Figure 3.10a shows the electrowetting curves of $[bmim][Cl]$, DI water and 16%, 48% and 80 % (w/w) water containing $[bmim][Cl]$ solutions at 1 kHz frequency. According to Figure 3.10a an increase in the water content of $[bmim][Cl]$ will result in an upward shift in the electrowetting curves towards that of pure water. Increasing the water percentage will increase the surface tension of a water miscible IL[46,84] and that will cause the electrowetting curves to shift upwards. Electrowetting curves of $[bmim][NTf_2]$ and its water saturated solution tested at 60 Hz, 1 kHz and 10 kHz frequencies, are shown in Figure 3.10b. For each frequency, approximately same curves can be observed for both $[bmim][NTf_2]$ and its water saturated analogue. Therefore it can be concluded that a water has negligible effect on the AC electrowetting of water immiscible ILs. These results agree well with previous results published on effect of water on the DC electrowetting of ILs.[46]

3.3.9 Reversibility

The reversibility of two ILs ($[bmim][Cl]$ and $[bmim][NTf_2]$) were tested at 1 kHz. Figure 3.11 (a) and (b) represent the electrowetting curves of $[bmim][Cl]$ and $[bmim][NTf_2]$ in 3 different experiments. The open symbols represent the contact angles of the ILs, five seconds after the voltage is switched off. The electrowetting process of these two ILs seems to be reversible to a great extent, i.e., the drop returns close to its original contact angle value, the difference between original contact an-

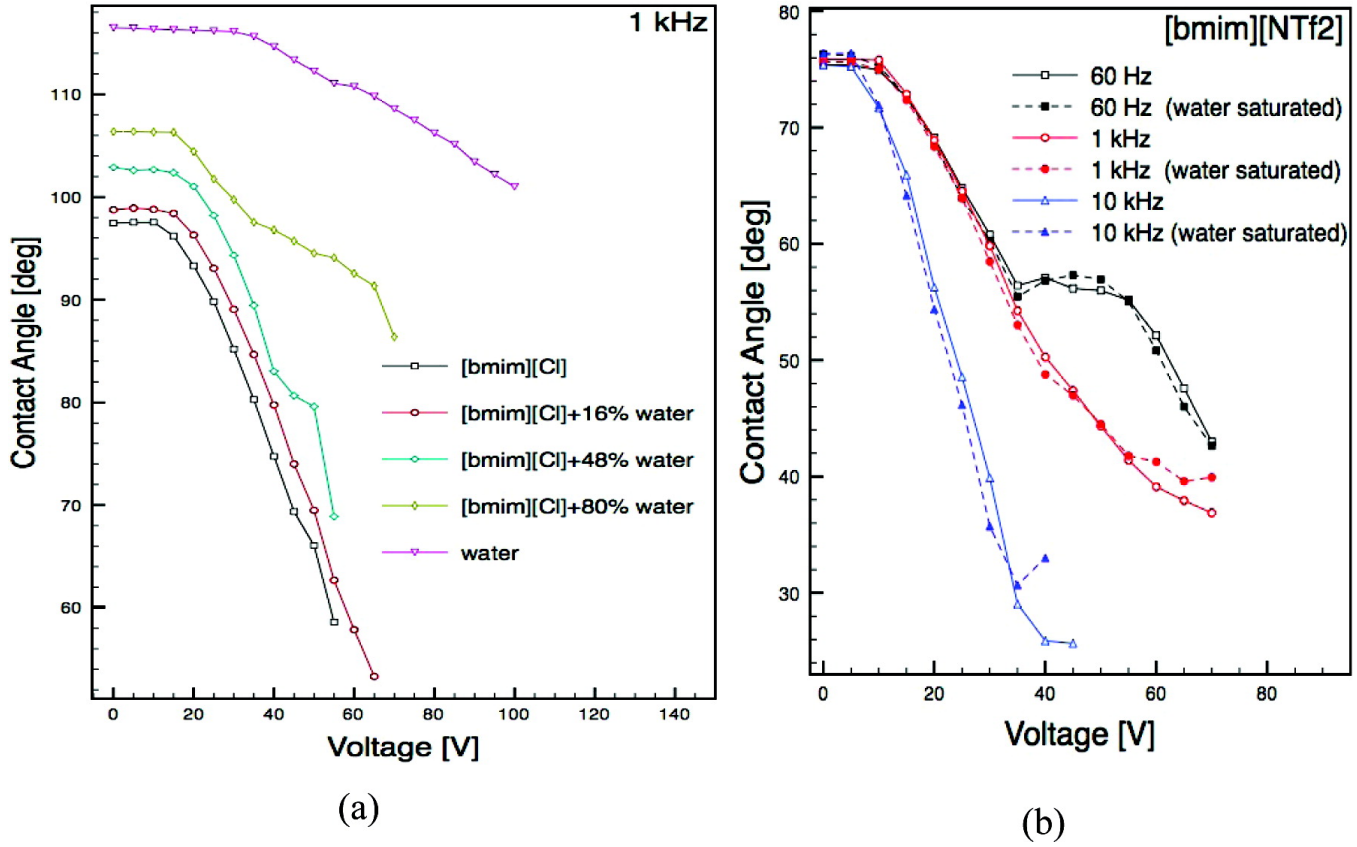

Figure 3.10: Effect of water content on electrowetting, a) Electrowetting curves of $[bmim][Cl]$ and its diluted solutions at 1 kHz fequency. (b)Electrowetting curves of $[bmim][NTf_2]$ and water saturated $[bmim][NTf_2]$ at 60 Hz, 1 kHz and 10 kHz frequencies

gle and the return contact angle values are approximately $\sim 3^{\circ} \sim 4^{\circ}$. Recent work by Restolho et al. demonstrated irreversibility of ILs in electrowetting at DC voltages.[49] Differences between our systems and theirs may be due to two reasons, (1) Surface roughness: reversibility is greatly affected by the surface roughness, with smoother surfaces having greater reversibility. However, there's no indication about their surface coating technique or surface treatments, therefore its difficult to compare the two systems. (2) Reversibility also can be affected by ion adsorption to the surface. It has been reported that in AC electrowetting ion adsorption to the surface is less than that in DC conditions.[86,89] Hence, better reversibility under AC voltage is logical. However, Restolho et al suggested that "the irreversibility (or reversibility) of the electrowetting process is a consequence of the experimental procedure and does not reflect an intrinsic characteristic of the ionic liquid".[49] Here we confirm that statement and we believe that surface enhancement is more important in order to get higher reversibility than the changing the IL properties.

3.3.10 Edge Instability / Satellite Droplets

It has been reported that for aqueous electrolytes, edge instability is common under AC conditions, i.e., small satellite droplets form next to the parent droplet.[1,86,94] However with ILs satellite droplets were not observed. This is another advantage of ILs over aqueous electrolytes.

3.3.11 Deviation of Curves

In addition to the above-mentioned observations, it was found that, when the electrowetting curves are overlaid at their maximum $\theta_0$values, at low frequency (60 Hz) normalized curves tends to coincide until their saturation points. Conversely at

high frequency (10 kHz) the normalized curves seem to deviate from one another. [See Figure 3.12].

3.4 Conclusions

The apparent contact angle change ($\Delta\theta$) obtained by electrowetting was higher under AC voltage conditions than with DC voltage conditions for all ILs tested. The frequency of the AC voltage was directly related to $\Delta\theta$. Some ILs had 4 to 5 times larger $\Delta\theta$ with AC voltage conditions than with DC voltage conditions. At higher voltages, ILs seems to be more stable at lower frequencies than higher frequencies. ILs did not evaporate regardless of the length of the study, but all water drops completely evaporated in 45 minutes or less. Edge instability/ satellite-droplets were not observed for ILs in either AC or DC experiments. Reported physical properties and the AC electrowetting data of ILs can be used to optimize their use in EWOD based applications.

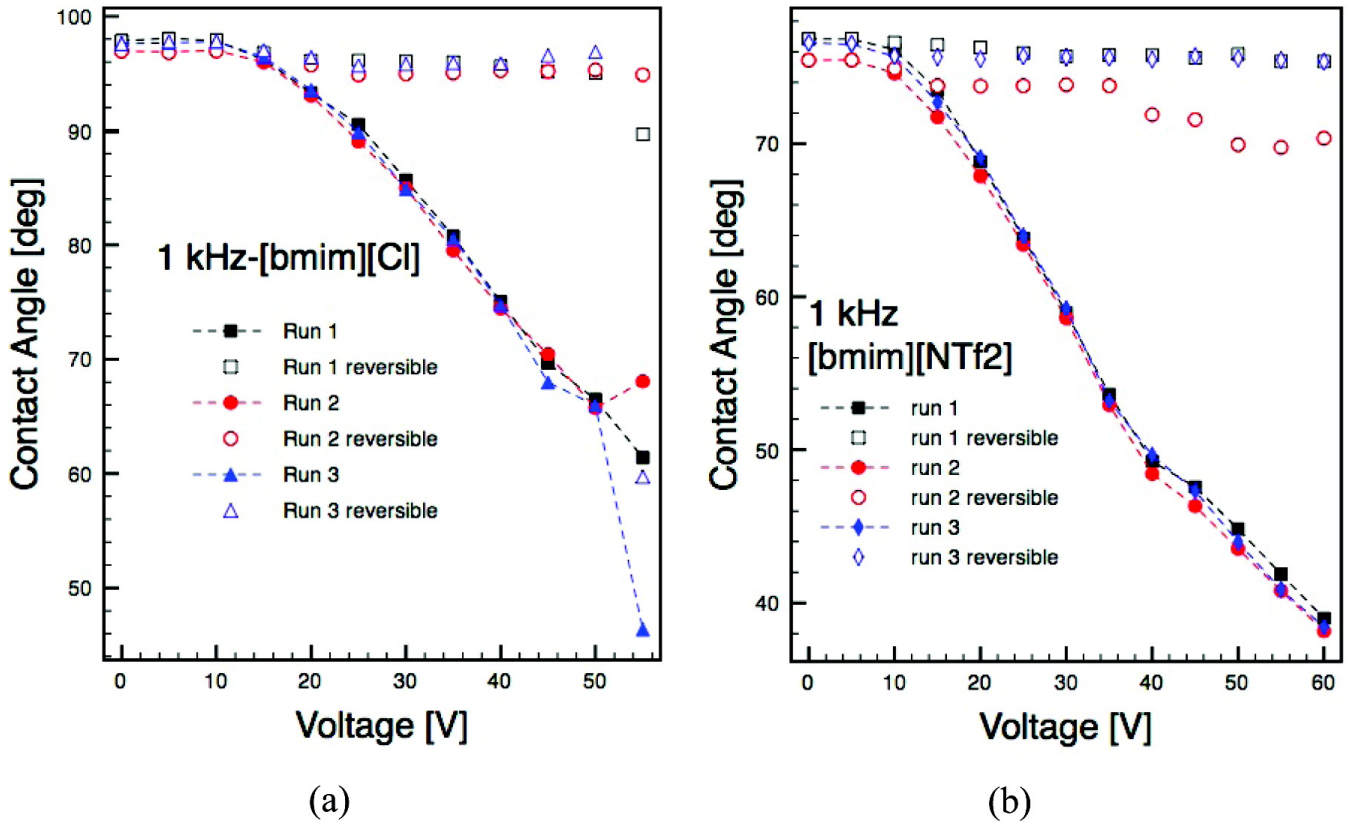

Figure 3.11: Reversibility of ionic liquids at 1 kHz: a) $[bmim][Cl]$, b) $[bmim][NTf_2]$

Solid symbols represent contact angle at designated voltage and frequency. Open symbols represent the contact angles of the ILs, five seconds after the voltage is switched off.

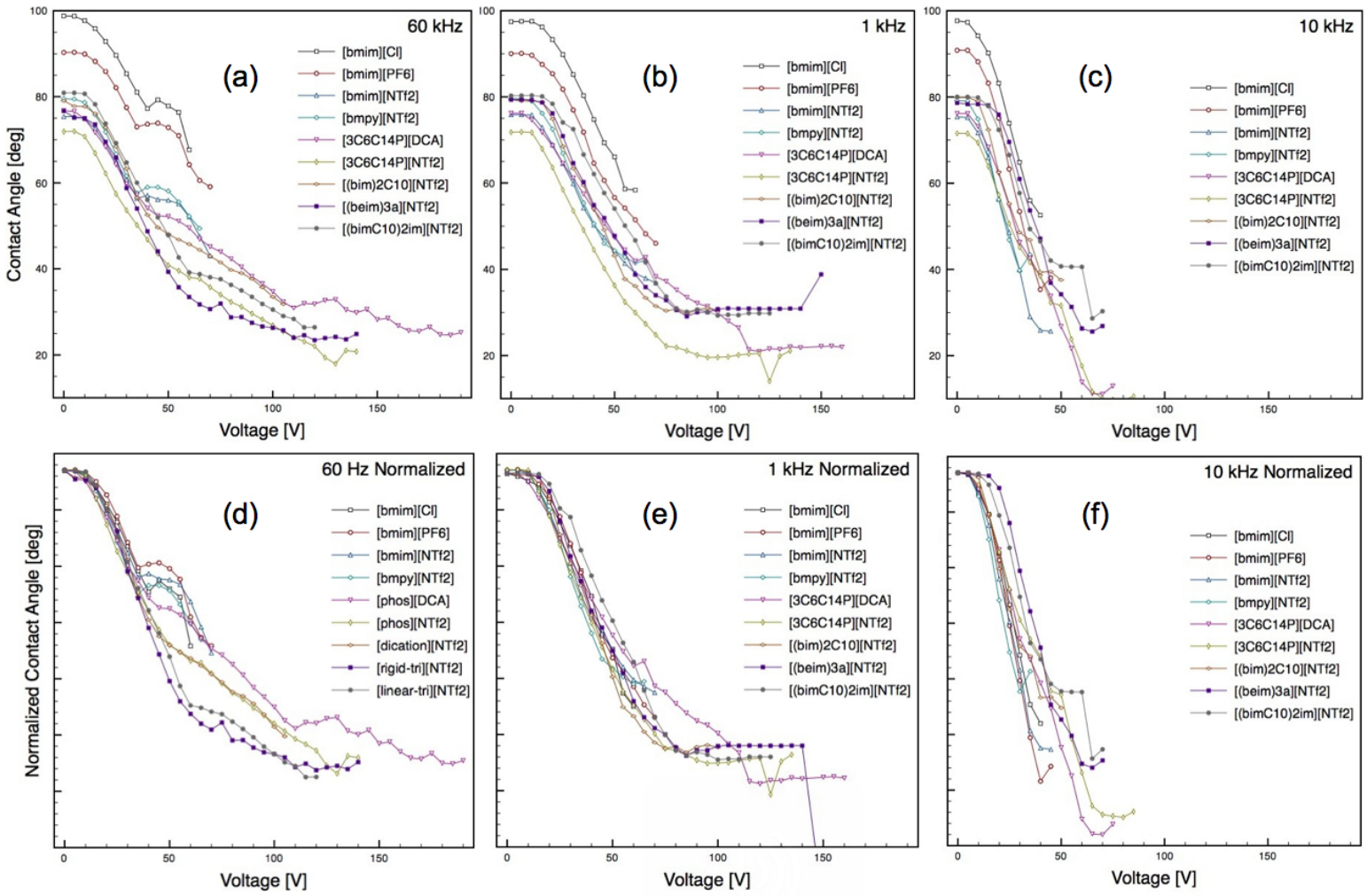

Figure 3.12: Deviation of electrowetting curves. Electrowetting curves at: a) 60 Hz, b) 1 kHz and c) 10 kHz. Electrowetting curves were overlaid normal to maximum θ_0 value at: d) 60 Hz, e) 1 kHz and f) 10 kHz

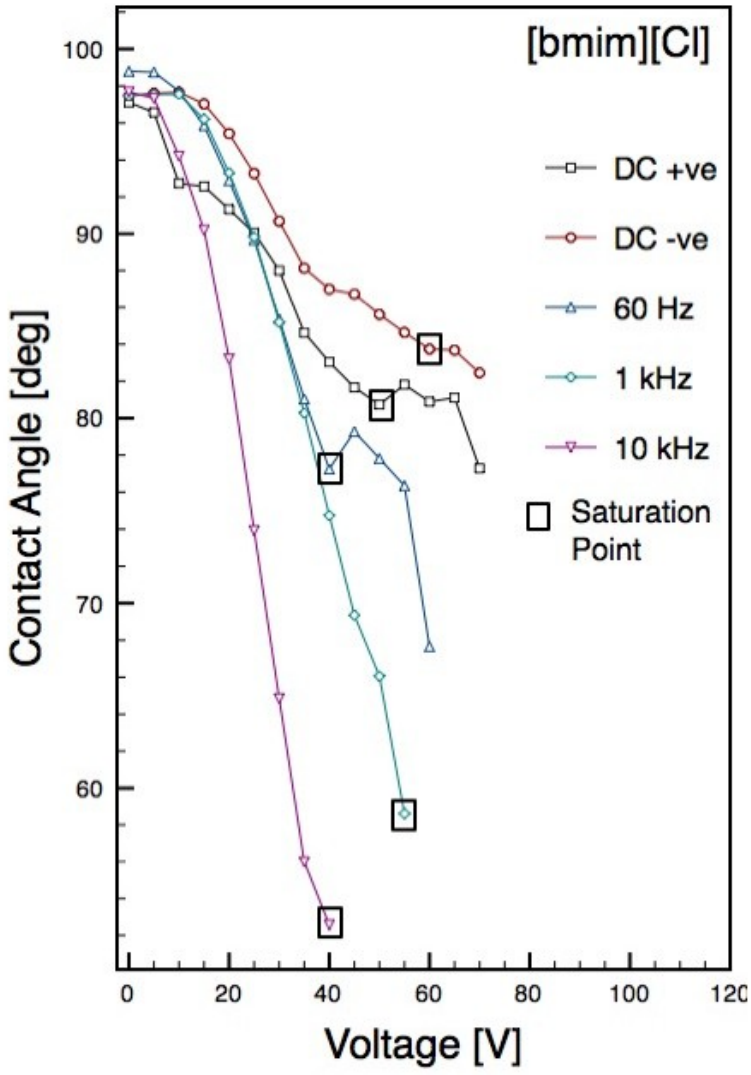

Figure 3.13: Electrowetting curves of $[bmim][Cl]$

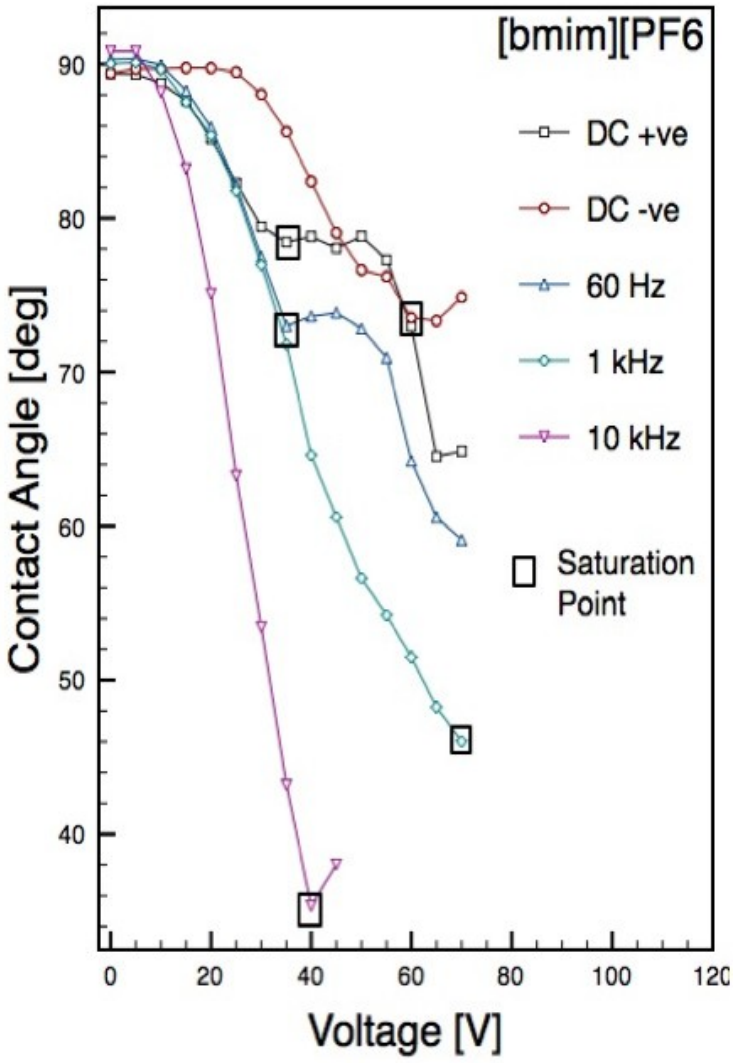

Figure 3.14: Electrowetting curves of $[bmim][PF_6]$

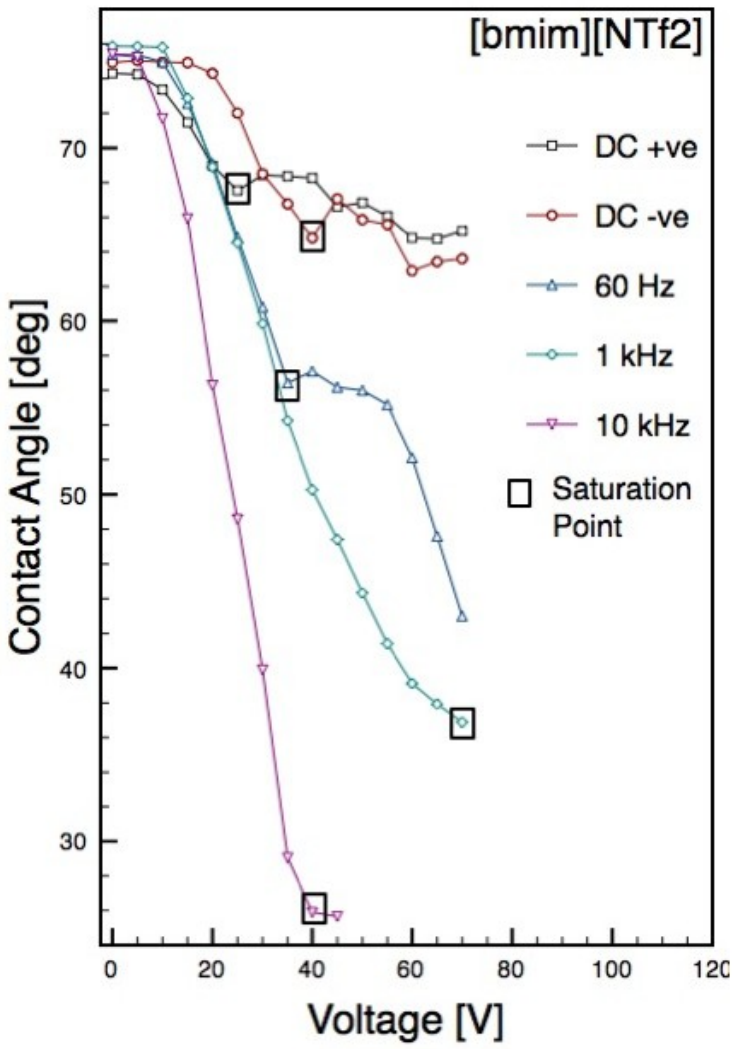

Figure 3.15: Electrowetting curves of $[bmim][NTf_2]$

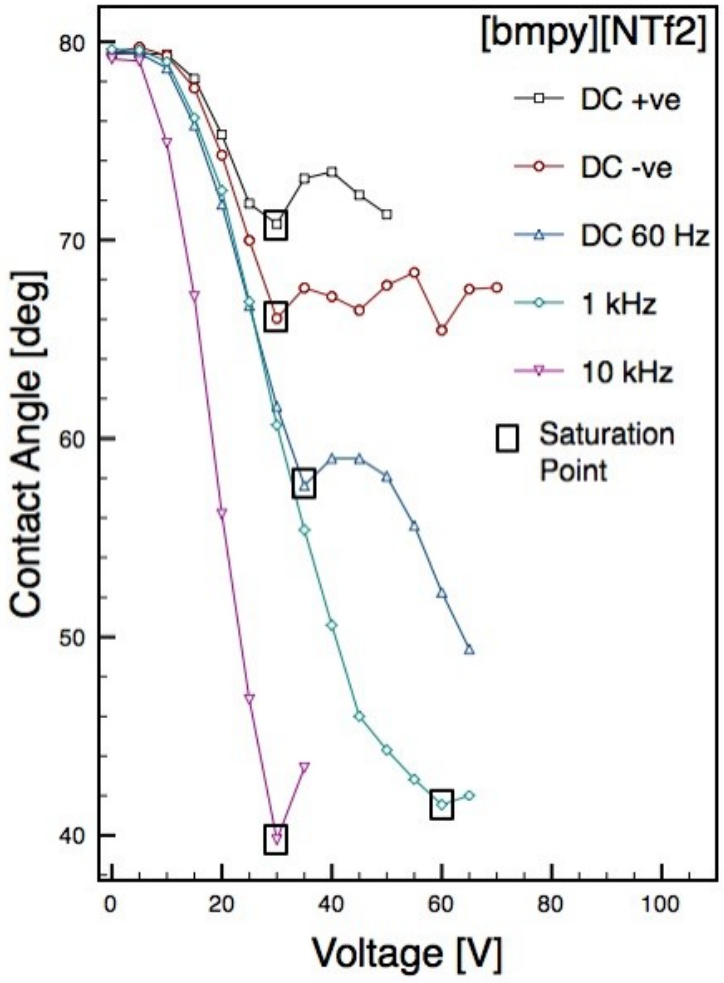

Figure 3.16: Electrowetting curves of $[bmpy][NTf_2]$

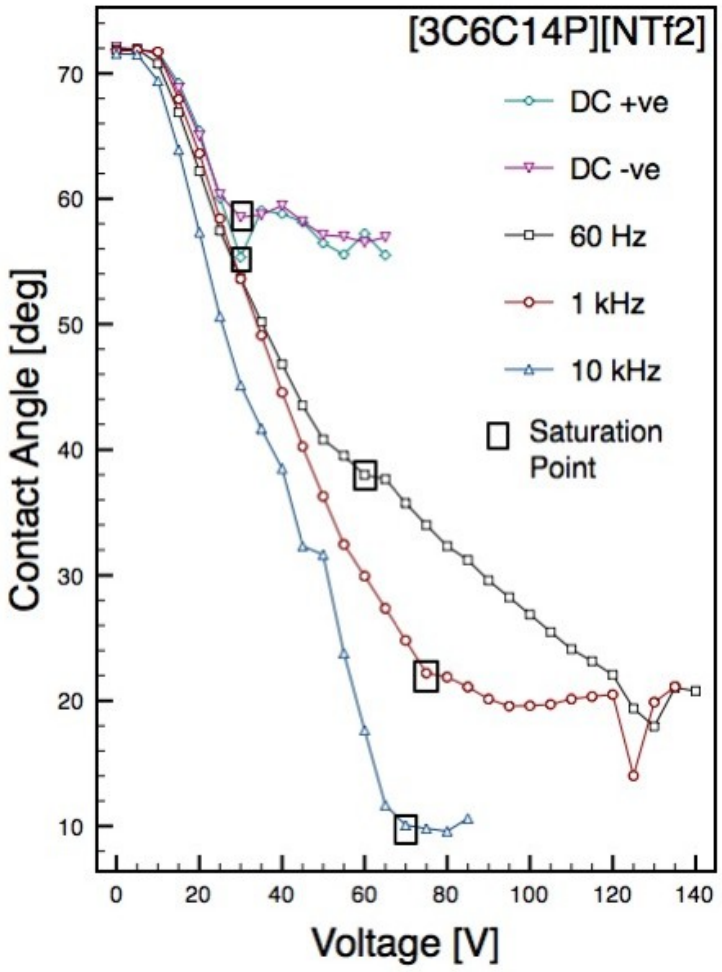

Figure 3.17: Electrowetting curves of $[3C_6C_{14}P][NTf_2]$

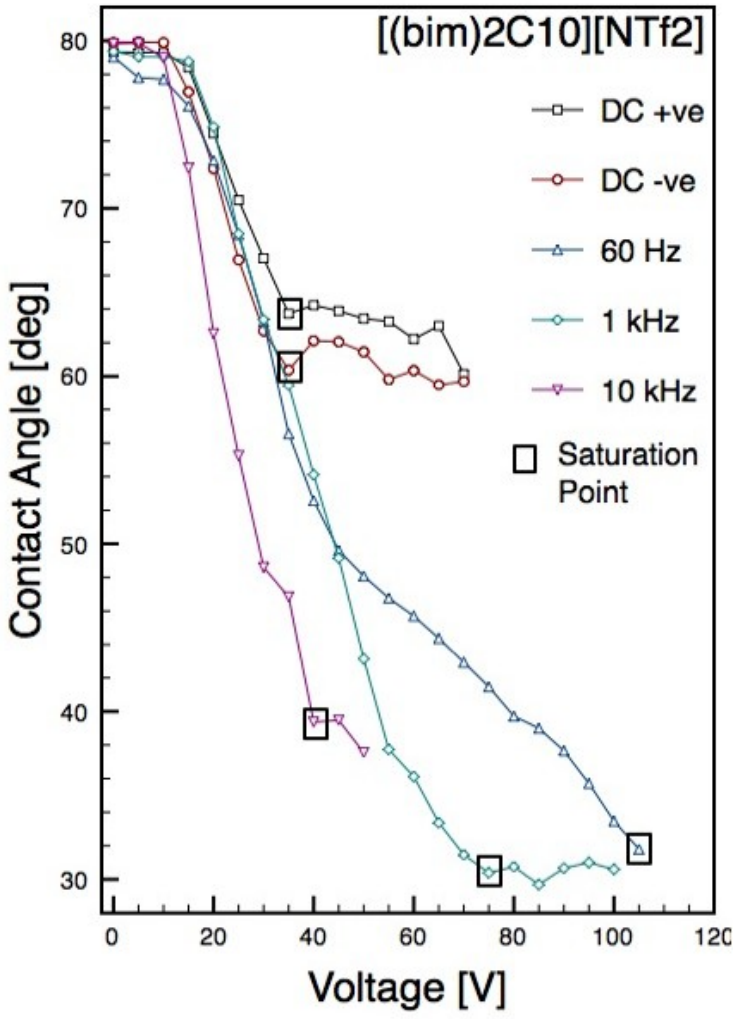

Figure 3.18: Electrowetting curves of $[(bim)_2C_{10}][NTf_2]$

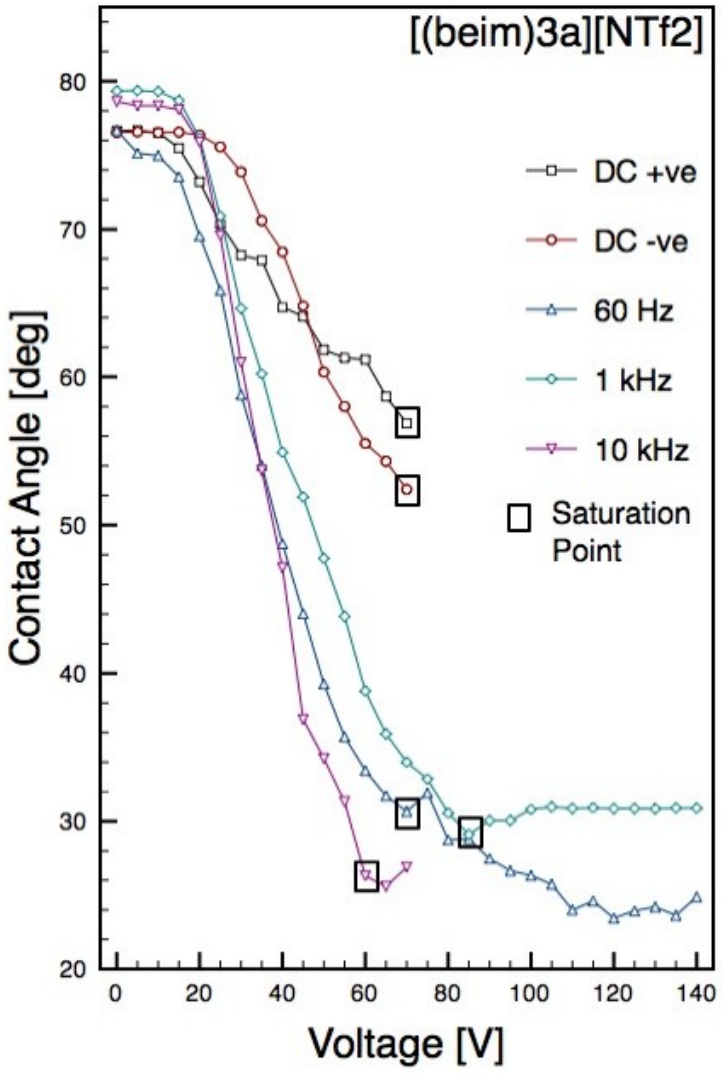

Figure 3.19: Electrowetting curves of $[(beim)_3a][NTf_2]$

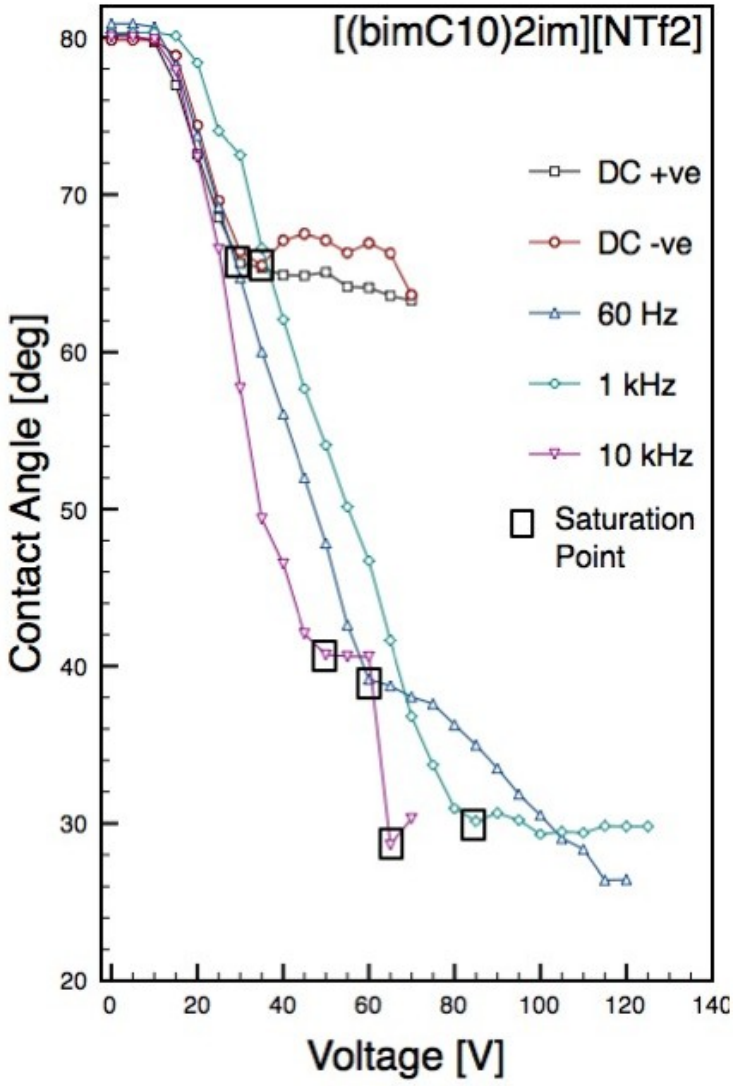

Figure 3.20: Electrowetting curves of $[(bimC_{10})_2im][NTf_2]$

CHAPTER 4

A TUNABLE IONIC LIQUID BASED RC FILTER USING ELECTROWETTING

RC filters are used to discriminate unwanted frequency elements of a specific signal. In this chapter we report a new concept for a tunable RC filter. The concept was demonstrated by developing a tunable RC filter "consisting of an ionic liquid drop placed on a dielectric layer." Cut-off frequency of the filter can be altered and controlled by changing the drop shape via electrowetting. The dielectric layer and the solid-liquid interface behave as serially connected capacitors, where the total capacitance is a function of drop shape (or contact angle). The drop shape, hence the total capacitance can be instantly controlled by electrowetting. The change in the capacitance will change the cut-off frequency of the filter. For a 5 μL ionic liquid drop, the achieved "tunability range" was 4.5 - 9.8 kHz. This demonstrates that the new concept is attainable. This RC filter system could potentially be used as a detecting technique.

4.1 Introduction

A resistor-capacitor (RC) filter is an electronic circuit, which is used to discriminate unwanted frequency elements of a specific signal. The cut-off frequency (f_C) value of a filter typically is a function of R (resistor) and C (capacitor) values. Therefore changing either the R value, the C value or both can alter the f_C value. Hence almost all tunable RC filters have been using the same principle of tuning resistor value or capacitor value to tune f_C value.[95]

It's well known that a solid-liquid interface can act as a capacitor in the presence of an external electric field. If a liquid drop is placed on a dielectric surface such as Teflon, then that system can be modeled as a series of capacitors.[1] Thus the total value of the capacitance is a combination of solid-liquid interface capacitance and dielectric layer capacitance.[1] The total capacitance is a function of the area between drop and the dielectric layer,[2,55] and this area is dependent on the shape of the drop or the contact angle.[55,96] The shape (or the contact angle) of the drop can be controlled by electrowetting,[1] therefore the total capacitance can be easily tuned by electrowetting. If this system is serially connected to a traditional resistor then one can produce a simple RC filter with tunable f_C values. We used the system explained above to demonstrate the concept of a new type of tunable RC filter. The RC filter effect has been observed for both sessile drops and parallel plate type in previous electrowetting/dielectrophoretic experiments.[2,55–59] However those studies had no intention of developing a workable RC filter, rather they explained their experimental observations using the RC filter effect. Here we report a novel liquid drop based tunable RC filter. This kind of liquid RC filter system can easily be combined with most microfluidic devices to analyze data online and has several applications, such as: 1) to determine approximate water and other impurity contents of different ionic liquids, 2) to detect ionic liquids synthesized on microfluidic chips,[50] 3) as a detector in microfludic liquid-liquid extraction chips.[18]

4.2 Experimental Section

The ionic liquid (IL), 1-butyl-3-methylimidazolium bis(triflouromethylsulphonyl) imide, is commonly abbreviated $[bmim][NTf_2]$ (Figure 4.1) was synthesized in our laboratory as reported previously.[46] Before use, the IL was kept in a vacuum oven for 18 hours with phosphorous pentoxide (P_2O_5) at room temperature to minimize the

water content. The final water content of the IL, measured by Karl Fischer titration was 470 ppm. The experimental setup for the RC filter is shown in Figure 4.2. Unpolished float glass slides coated with 30 mm indium-tin-oxide were purchased from Delta Technologies Ltd., (Stillwater, MN). Then they were dip coated with Teflon solution prepared by dissolving 4% (w/v) of Teflon AF1600 (www2.dupont.com) in Fluoroinert FC75 solvent (www.fishersci.com). The approximate dipping speed of the custom made dipcoater was set to 0.78±0.03 mm/s. Once 75% of the slide was dipped in the solution, dipping was stopped for 5 seconds, and then the slide was raised at the same speed. The coated slides were kept in an oven for 6 min at 112 $^{\circ}C$, 5 min at 165 $^{\circ}C$ and 15 min at 328 $^{\circ}C$. Finally, Teflon coated glass slides were allowed to reach room temperature, then washed thoroughly with acetone and deionized water and air-dried. The resulted Teflon coating thickness was 260 ± 10 nm, as measured by a Tencor Alphastep 200 Profilometer. A drop of ionic liquid (5.0 ±0.5 μL) was placed on top of the Teflon layer using a capillary tip. The volume and the contact angle of the drop were calculated using CAM 200 software (www.ksvltd.com). A waveform generator (Agilent Model 33220A) connected to a voltage amplifier (Trek Model PZD 350) was used as the signal source for the experiments. The ground electrode was connected to the ITO layer using an Al contact pad, the IL drop was always placed 5 cm apart from this Al contact pad. The other electrode was connected to a 82 $k\Omega$ resistor. The resistor was serially connected to one end of a Pt wire (32 gauge) and the other end of the wire was dipped in the IL drop. In this way, the wired system is an analogue to a low-pass type RC filter (Figure 4.2b). The distance between Pttip and Teflon surface was set to 0.8 mm. First, 30 V_{rms} sinusoidal signal was supplied to the system, increasing the frequency from 20 Hz to 18.5 kHz logarithmically with a 140 s sweep time. Output signal data was collected using a PC based oscilloscope

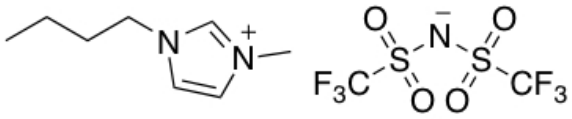

Figure 4.1: The structure and the acronym of 1-butyl-3-methylimidazolium bis(trifluoromethylsulphonyl)imide ionic liquid

(www.picotech.com). This procedure was repeated for 50 V_{rms} and 70 V_{rms} sinusoidal signals.

4.3 Results and Discussion

To make a practical, tunable, liquid RC filter an ionic liquid, $[bmim][NTf_2]$ was used. Use of $[bmim][NTf_2]$ has several practical advantages: 1) having negligible or no vapor pressure so that evaporation is not a concern and no special sealing or packaging is needed for the filter,[46] 2) resistance to vibrations and satellite drop formation, particularly compared to water or aqueous electrolytes,[2] 3) a lower viscosity than most ILs so that response times are faster than other ILs,[46] 4) the apparent contact angle change ($\Delta\theta$) of $[bmim][NTf_2]$ due to frequency (not voltage) is lower than that of other ILs,[2] 5) ion adsorption to the Teflon surface is minimal for $[bmim][NTf_2]$, since it contains a bulky $[NTf_2^-]$ anion,[2,46] and 6) negligible effect of water when compare to other ionic liquids.[2,46]

Typically frequency versus gain plots are used to characterize RC filters, in which the intersection point of the curve and the -3 dB line represents the f_C of the filter. Figure 4.3 shows frequency versus gain plot of the IL based low-pass RC filter.

It can be observed from the plot that at 10 V_{rms} the obtained f_C is 9.8 kHz, whereas at 30V, 50 V and 70 V the obtained f_C's are 8.2 kHz, 6.1 kHz and 4.5 kHz respectively. At higher voltages, lower f_C is obtained. Cut-off frequency (f_C) depen-

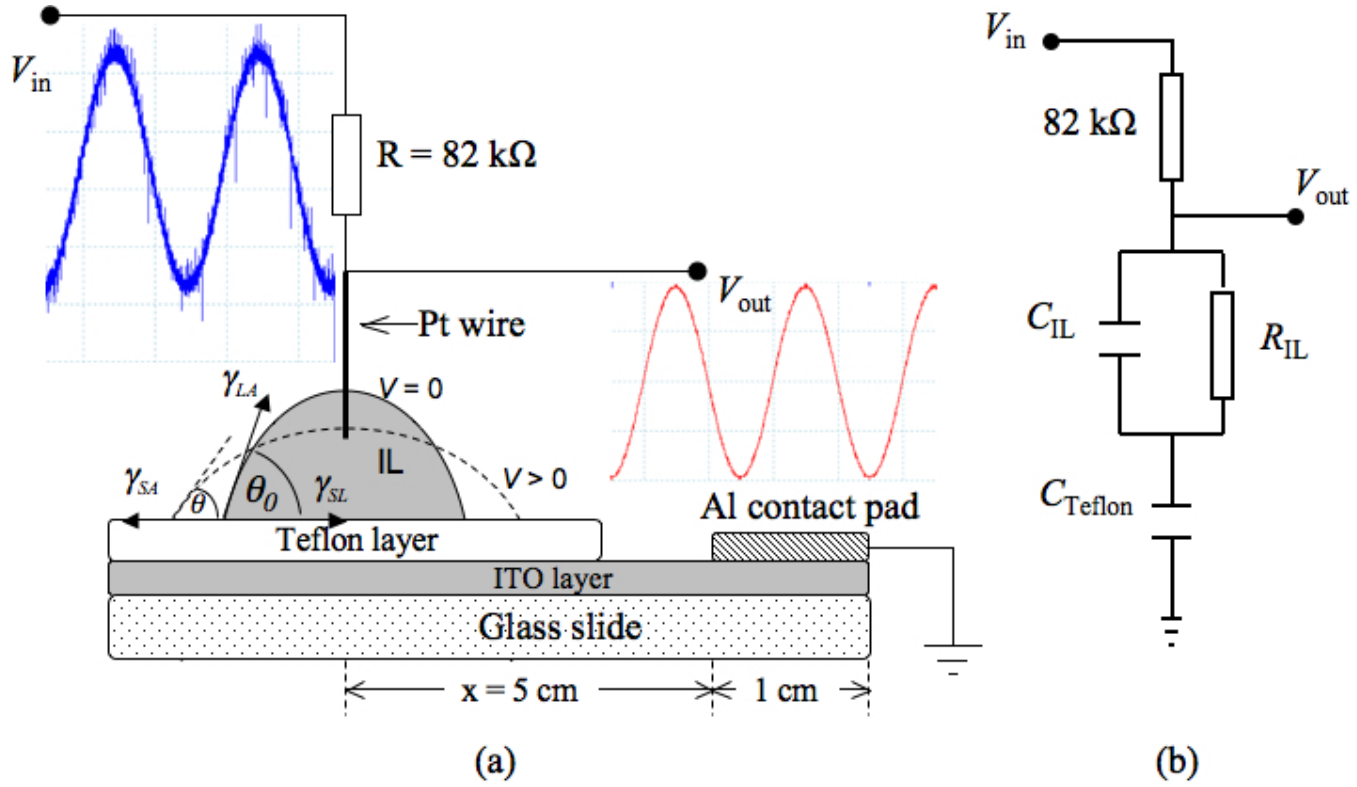

Figure 4.2: Ionic liquid based RC filter: a) experiment setup, b) equivalent circuit model

θ_0 is the contact angle at zero external voltage, θ is the contact angle at any given voltage and frequency. For ionic liquid $[bmim][NTf_2]$, $\theta_0 = \sim 75°$, $\theta_{(1kHz,30V)} = \sim 58°$, $\theta_{(1kHz,50V)} = \sim 43°$, $\theta_{(1kHz,70V)} = \sim 35°$. γ_{SA}, γ_{LA} and γ_{SL} are solid-air, liquid-air and solid-air interfacial tensions respectively. The sinusoidal signal in left (blue color) is an unfiltered signal with noise. The filtered signal is shown on the right (red color).

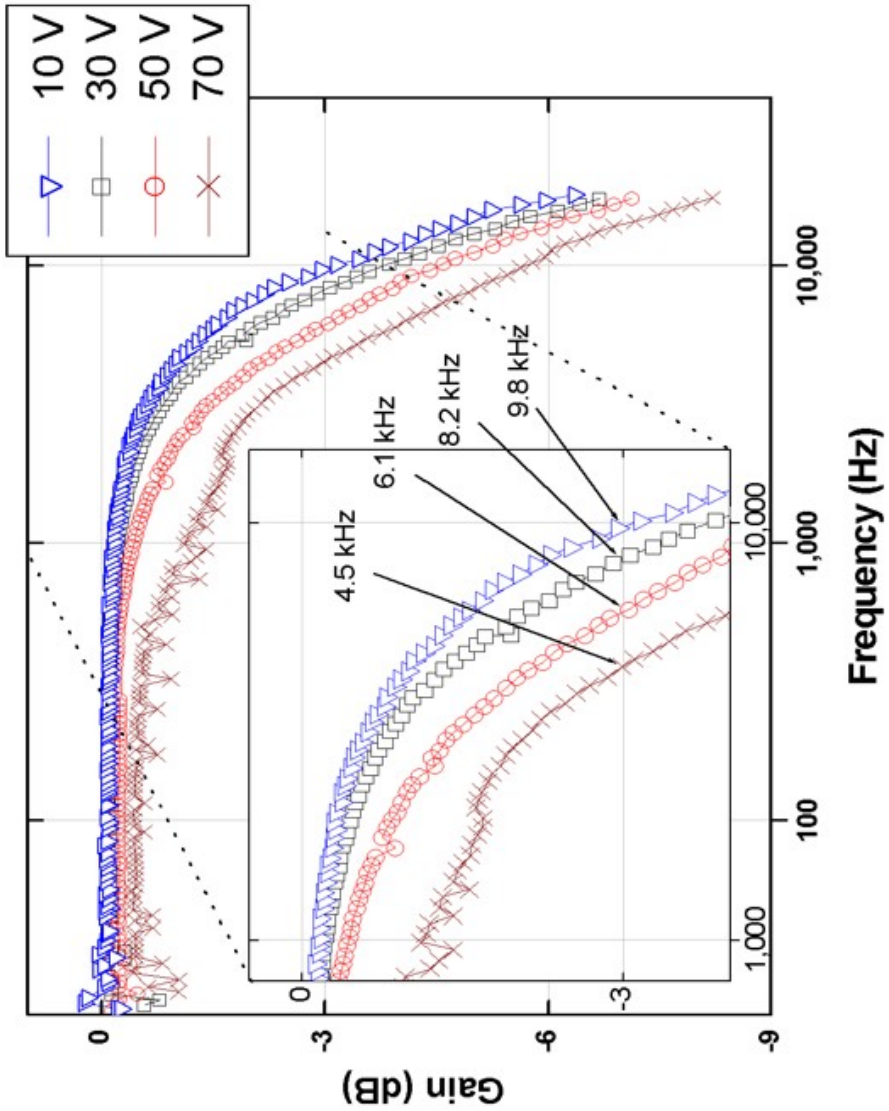

Figure 4.3: Frequency vs. gain plot for the ionic liquid based RC filter

dence on electrowetting voltage (V_{in}) can be explained by formulating a relationship between V_{in} and f_C. (See section 4.1 for the step by step derivation) The final derived relationship states that for a given IL,

$$f_C = f(V_{in}) \tag{4.1}$$

When the applied voltage (V_{in}) increases θ will decrease as described by the Young-Lippmann equation.[1] As a consequence, the contact area of the drop on the Teflon surface (A) will increase,3, 4 thus increase the total capacitance of the system. Finally increase in capacitance will result in decrease in f_C value. The performance and the range f_C of the RC filter can be optimized by altering or controlling any of the following factors: 1) the value of the resistor (R) can be changed, 2) the total capacitance of the filter can be easily changed by changing the drop size, here we used a 5 μL drop. Note that there are reported examples of drops as large as 25 - 50 μL and as small as few tens of picoliters used to demonstrate electrowetting,[1,43] 3) since different ILs have different capacitances due to their structure and the nature of their functional groups, the IL itself can be changed depending on the required capacitance value,[81] Also, the $\Delta\theta$ is different for different ILs i.e., some ILs exhibit higher $\Delta\theta$ at a given voltage, while other ILs show lower $\Delta\theta$ at the same voltage.[42,43,46] Therefore, if one needs a wide tunability range of f_C it is desirable to use the first type of ILs, and for fine tunability the latter types of ILs are desirable, 4) the C_{total} value also can be controlled by changing the dielectric layer material. Here we used Teflon as our dielectric layer, since it shows good reversibility and ease of use. However, Teflon layers usually have small pin holes in them, and electrons can penetrate through these holes creating a leakage current, this can reduce the performance of the filter. Coating another dense dielectric material like SiO_2 beneath the Teflon layer can minimize the leakage current,[60] 5) the voltage, which requires achieving a certain $\Delta\theta$ can be

reduced by reducing the thickness of the dielectric layer. In our work we used a 260 nm dielectric layer. Previous studies have shown the use of thinner dielectric layers than 260 nm.[60] However most thin dielectrics exhibit numerous failure modes.[97] Hence one should decrease the dielectric thickness with analysis of reliability for better operation. If the reliable thinner dielectric is achievable, then that may allow the use of even lower voltage to tune the f_C values, 6) the resistivity of the ITO coating in this study was higher than that of the connecting wires ($\sim$100 Ω/cm). Thus it behaves more like an extra resistor in the system, and the resistance value depends on the position of the IL drop, which affects the f_C value. Therefore distance from the Al contact pad to the drop position (i.e., x in Figure 4.2a) was kept constant (5 cm) for every experiment. Using gold or silver coated glass slides this effect can be minimized, 7) the amount of connecting wires used should be minimized, since at higher frequencies the impedance coming from these wires can affect the system, 8) this filter can be assembled in oil instead of air, which would provide more contact angle change giving a larger cut-off frequency range. This liquid drop RC filter system has low tunability range compared to traditional solid state electronic RC filter systems.[98] However, liquid drop RC filter systems have many potential applications where traditional solid-state electronic RC filters cannot be used. One potential application would be determination of water content in water miscible ionic liquids. Previous studies show, water has significant role in water miscible ionic liquids, where contact angles vary with the amount of absorbed water. Since different contact angles provide different f_C values, this RC filter system can easily be used to determine the water content of water miscible ionic liquids. In addition, this RC filter system can be easily integrated with microfluidics chips and can be used as a detector when synthesizing ionic liquids on chip and in microfluidic liquid-liquid extractions. Finally one another advantage of this RC filter is its ability of continuous tunability. Most tunable RC filters have multiple discrete

switches to achieve different capacitances,[99,100] hence their corresponding f_C values are discrete. Where as in our RC filter, the f_C values are continuous due to its continuous change of capacitance.

4.4 Equation 4.1 Derivation

Note that the terms used in this section were defined in section 3.3.3.1. Figure 4.4 shows the equivalent circuit for the ionic liquid based RC filter.

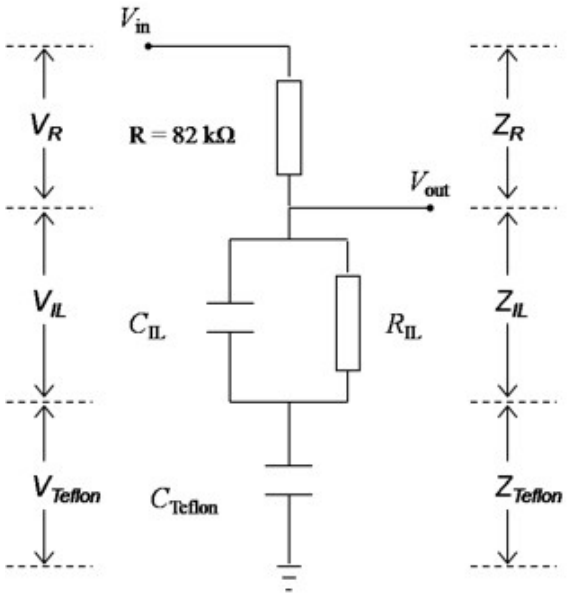

Figure 4.4: Equivalent circuit for the ionic liquid based RC filter (More detailed version of Figure 4.2.a)

Let Z_R,Z_{IL} and Z_T be the impedance of the resistor (82 Ω), ionic liquid and Teflon layer respectively and let V_R, V_{IL} and V_T be the voltages across the resistor (82 Ω), ionic liquid and Teflon layer respectively. Then elementary electric circuit modeling indicate that,

$$Z_R = R; \qquad Z_{IL} = \frac{1}{g_{IL} + j\omega C_{IL}}; \qquad Z_T = \frac{1}{g_T + j\omega C_T}$$

$$V_{in} = V_R + V_{IL} + V_T$$

$$V_{out} = V_{IL} + V_T$$

Therefore, the output voltage (V_{out}) is:

$$V_{out} = \left[\frac{Z_{IL} + Z_T}{Z_R + Z_{IL} + Z_T}\right] V_{in}$$

$$V_{out} = \left[\frac{\frac{1}{g_{IL}+j\omega C_{IL}} + \frac{1}{g_T+j\omega C_T}}{R + \frac{1}{g_{IL}+j\omega C_{IL}} + \frac{1}{g_T+j\omega C_T}}\right] V_{in}$$

$$\frac{V_{out}}{V_{in}} = \left[\frac{g_{IL} + j\omega(C_T + C_{IL})}{g_{IL} - R\omega^2 C_{IL}C_T + j\omega(g_{IL}RC_T + C_T + C_{IL})}\right]$$

In order to make the denominator real, the denominator and numerator were multiplied by the complex conjugate of the denominator. Then,

$$\frac{V_{out}}{V_{in}} = \left[\frac{g_{IL} + j\omega(C_T + C_{IL})}{g_{IL} - R\omega^2 C_{IL}C_T + j\omega(g_{IL}RC_T + C_T + C_{IL})}\right]$$

In order to make the denominator real, the denominator and numerator were multiplied by the complex conjugate of the denominator. Then,

$$\frac{V_{out}}{V_{in}} = \frac{\begin{array}{c}[g_{IL}(g_{IL} - R\omega^2 C_{IL}C_T) + \omega^2(C_T + C_{IL})(g_{IL}RC_T + C_T + C_{IL})] \\ + j\omega[(C_T + C_{IL})(g_{IL} - R\omega^2 C_{IL}C_T) - g_{IL}(g_{IL}RC_T + C_T + C_{IL})\end{array}}{1 + \omega^2 R_{IL}^2 (C_{IL} + C_T)^2}$$

$$\left|\frac{V_{out}}{V_{in}}\right| = \left[\left[\frac{V_{in}}{V_{out}}\right] \cdot \left[\frac{V_{in}}{V_{out}}\right]^*\right]^{\frac{1}{2}}$$

Considering only the amplitude,

$$\left|\frac{V_{out}}{V_{in}}\right| = \left[\frac{\left[[g_{IL}(g_{IL} - R\omega^2 C_{IL}C_T) + \omega^2(C_T + C_{IL})(g_{IL}RC_T + C_T + C_{IL})]\right]^2 + \omega^2\left[[(C_T + C_{IL})(g_{IL} - R\omega^2 C_{IL}C_T) - g_{IL}(g_{IL}RC_T + C_T + C_{IL})\right]^2}{[1 + \omega^2 R_{IL}^2(C_{IL} + C_T)^2]^2}\right]^{\frac{1}{2}}$$

$R = 82k\Omega$ = constant, $g_{IL} = \frac{1}{R_{IL}}, \omega = 2\pi f$ at cut off frequency (i.e., at $f = f_C$); $\left|\frac{V_{in}}{V_{out}}\right| = \frac{1}{\sqrt{2}}$ Substituting these values to above equation f_C can be written as a function of R_{IL},C_{IL} and C_T.

$$f_C = F(R_{IL}, C_{IL}, C_T) \tag{4.2}$$

According to the equation 3.8; $R_{IL} = F(\theta, \sigma)$ however, for a given IL σ is a constant. Therefore equation C.5 re-written as,

$$R_{IL} = F(\theta) \tag{4.3}$$

According to the equation 3.9; $C_{IL} = F(\theta, \epsilon_{IL}, d)$ however, for a given IL ϵ_{IL}, d are constants. Therefore equation C.6 re-written as,

$$C_{IL} = F(\theta) \tag{4.4}$$

Equation 3.10 says;

$$C_T = F(\theta)$$

Young-Lippmann equation describes the relationship between contact angle (θ) and voltage across the dielectric (Teflon) layer (V_T),

$$cos\theta = cos\theta_0 + \frac{\epsilon\epsilon_0}{2\gamma t}V_T^2$$

Since, $V_{in} = V_R + V_{IL} + V_T$; Young-Lippmann equation can be re-written as,

$$\theta = F(V_{in}) \tag{4.5}$$

Therefore combining equation 4.2, 4.3, 4.4, 3.10 and 4.5, it is reasonable to state that the cut-off frequency (f_C) is a function of the input voltage (V_{in}). i.e.,

$$f_C = f(V_{in}) \qquad (4.1)$$

CHAPTER 5

A LOW COST, ELECTROWETTING ON DIELECTRIC (EWOD) BASED LIQUID DROP DETECTOR, VALIDATED WITH INDUSTRIAL BIOCIDES

This chapter presents the development of an analytical detector, which can be used to detect virtually any substance dissolved in a liquid (e.g., water, alcohol, mixtures, etc). This device was fabricated by modifying an electrowetting on eielectric (EWOD) based experiment setup. When a liquid drop is placed on a dielectric surface, the system act as a RC filter. It generates a cut-off frequency when a range of sinusoidal signals are passed through the system. The cut-off frequency is a function of conductivity, surface tension, dielectric constant, double layer of the liquid drop as well as applied voltage. Since different liquids and solutions have different physical properties, each liquid/solution has a unique cut-off frequency (f_C); this is the basic principle behind this detector. Different amounts of benzalkonium chloride (BAC) dissolved in water, cetyltrimethyl-ammonium chloride (CTAC) in water and CTAC dissolved in ethylene glycol solutions were tested with the detector to prove the proposed principle. The Detector seems to be an universal sensor and can be used as a stand alone detector or potentially be coupled with HPLC systems and droplet based microfluidic lab-on-a-chip systems such as EWOD based microfluidic chips.

5.1 Introduction

A RC-filter is an electronic circuit which composed of resistors and capacitors. RC filters are used to refine signals by attenuating the unwanted frequency elements. Typically, the cut-off frequency of a such a filter is a function of the resistor's and

the capacitor's values. A liquid drop resting on a dielectric surface can be modeled as resistor-capacitor network, therefore acting as a RC-filter.[8] In such a system, the dielectric layer and solid-liquid interface are acting as serially connected capacitors plus the liquid drop acts as a resistor connected in parallel to the latter capacitor. Adding extra traditional resistor to this system one can develop a liquid drop based RC filter.[8] The cut-off frequency (f_C) generated by this kind of RC filter is a function of conductivity(σ), dielectric constant(ϵ), surface tension (γ), double layer thickness (d) of the liquid and the applied voltage(V_{in}) [i.e., $f_C = F(\sigma, \epsilon, \gamma, d, V_{in})$]. Different liquids have different σ, ϵ, γ and d values, which means the f_C generated by a certain liquid is unique. Consider a solution prepared by dissolving an analyte in a pure liquid. In that solution the σ, ϵ, γ and d values are different from those values of the pure liquid, and accordingly the generated f_C value for the solution also is different from that of the pure liquid. Depending on the properties of the analyte and the concentration of the analyte the change of f_C can vary. Therefore the relationship between σ, ϵ, γ, d values and f_C can easily be used to detect the analyte. A detector is developed based on that relationship. Section 5.1.1 will elaborate the theoretical background of the relationship.

The existence of RC filter type behavior in EWOD/dielectrophoretic (DEP) experiments were reported in many previous publications.[2,55–59] After noting this behavior and by modifying the traditional EWOD experiment setup, we developed an ionic liquid based tunable RC filter.[8] It is notable that none of the previous studies focused on detecting analytes using the RC filter effect. In this study, we use a liquid tunable RC filter,[8] with minor modifications to fabricate a detector/sensor. In the tunable RC filter only one liquid (an ionic liquid) is used, therefore the σ, ϵ, γ and d values become constants. Therefore, f_C depend only on V_{in}; and by changing V_{in},

the f_C values can be tuned. However in the detector, V_{in} is kept constant and several liquids (analytes) are detected by the change in f_C.

Like most other detectors (UV-vis, conductivity, refractive index, etc...) prior to the detection, the analyte should be isolated from interfering compounds. As an example, if one needs to detect A^+ ions, in a solution consisting of A^+ and B^+ using a conductivity detector, before the sample introduction to the detector A^+ must be isolated from B^+ using a separation technique such as chromatography, extraction, precipitation, etc. The same basic principle applies to this detector.

Aqueous solutions of benzalkonium chloride (BAC) were utilized as initial test mixtures. BAC is a mixture of alkylbenzyldimethylammonium chlorides with even-numbered alkyl chain lengths which range from $n - C_8H_{17}$ to $n - C_{18}H_{37}$. BAC is a popular biocide which is used as a preservative in over 155 commercial cosmetic, disinfectant and ophthalamic products.[101] Each homolog of BAC has different bactericidal activities,[102] therefore the United States Pharmacopeia−National Formulary (USP−NF) regulates the percentage of each homolog of BAC.[103]

As a second test analyte cetyltrimethyl-ammonium chloride (CTAC) dissolved in water is evaluated. CTAC, also known as cetrimonium chloride or hexadecyl trimethyl ammonium chloride is an antiseptic, antistatic agent and fabric softner, typically used in shampoos and hair conditioners. CTAC is used as an active agent over 1000 commercial products.[104] Due to its lack of a chromophore uv-vis detectors are not effective in detection of CTAC, therefore conductimetric, refractive index(RI), evaporative light scattering (ELS) and mass spectrometry (MS) based detection methods are used.[105] Each of these detection methods have their own disadvantages: RI and ELS are low sensitive methods, MS is an very expensive method. Detection of aqueous solutions of CTAC with our detector seems to be highly sensitive and in-

expensive. In addition to aqueous solutions of CTAC, different amounts of CTAC dissolved in ethylene glycol (EG) were tested to determine the effect of solvent.

5.1.1 Theoretical Background

Experiment setup for the detector is shown in Figure 5.1.a. The equivalent circuit model for the detector is shown in Figure 5.1.b. In these figures R is a traditional resistor (82 $k\Omega$). R_a and C_a are resistance and capacitance values caused by the analyte drop respectively. C_T is the capacitance value due to the Teflon layer. Fundamental calculations show that, for this kind of system, the f_C value obtained is a function of R_a, C_a and C_T as represented in the following equation, (see section 5.5 for a step by step derivation).

$$f_C = F(R_a, C_a, C_T) \tag{5.1}$$

However, as described in Section 3.3.3.2, R_a is a function of the conductivity(σ) of the analyte and the contact angle(θ) of the analyte drop. Therefore at constant V_{in},

$$R_a = F(\sigma, \theta) \tag{5.2}$$

Also, as described in Section 3.3.3.2, C_a is a function of the dielectric constant (ϵ), double layer thickness(d) of the analyte and the contact angle(θ) of the analyte drop. Therefore at constant V_{in},

$$C_a = F(\epsilon, d, \theta) \tag{5.3}$$

The Young-Lippmann equation (eq. 2.1) and Young's law (eq. 2.2) can be used to establish a relationship between θ, ϵ and surface tension γ of the analyte. Therefore at constant V_{in},

$$\theta = F(\gamma, \epsilon) \tag{5.4}$$

Therefore at constant V_{in} and by combining equation 5.1, 5.2, 5.3 and 5.4; f_C can be written as,

$$f_C = F(\sigma, \epsilon, d, \gamma) \tag{5.5}$$

According to equation 5.5, f_c is a function of σ, ϵ, d and γ; which means a change of one or more above properties, could change the f_C value.

5.2 Experimental Section

The experimental setup for the detector is shown in Figure 5.1. Unpolished float glass slides coated with 30 nm thick indium-tin-oxide (ITO) were purchased from Delta Technologies Ltd., (Stillwater, MN). After that they were dip coated with Teflon solution prepared with 4% (w/v) of Teflon AF1600 (www2.dupont.com) in Fluoroinert FC75 solvent (www.fishersci.com). A custom made device was used to perform dipcoating, where the approximate dipping speed was set to 0.78±0.03 mm/s. Once 75% of the slide was dipped in the solution, dipping was stopped for 5 seconds, and then the slide was raised at the same speed. The coated slides were allowed to condition in an oven for 6 min at 112 $^{\circ}C$, 5 min at 165 $^{\circ}C$ and 15 min at 328 $^{\circ}C$. Once Teflon coated glass slides reached room temperature, they were washed thoroughly with acetone and deionized water and air-dried. A Tencor Alphastep 200 Profilometer was used to measure the thickness of the coated Teflon layer thickness, which was 260 ± 10 nm.

A drop of analyte (5.0 ±0.5 μL) was placed on top of the Teflon layer using a micropippete. A 32 gauge Pt wire was inserted tino the analyte drop in a way that the distance between Pt tip and Teflon surface was exactly 0.8 mm. The other end of the Pt wire was connected to a 82 kΩ resistor. The input signal was fed through this resistor. The ITO layer is used as the ground electrode of the system.

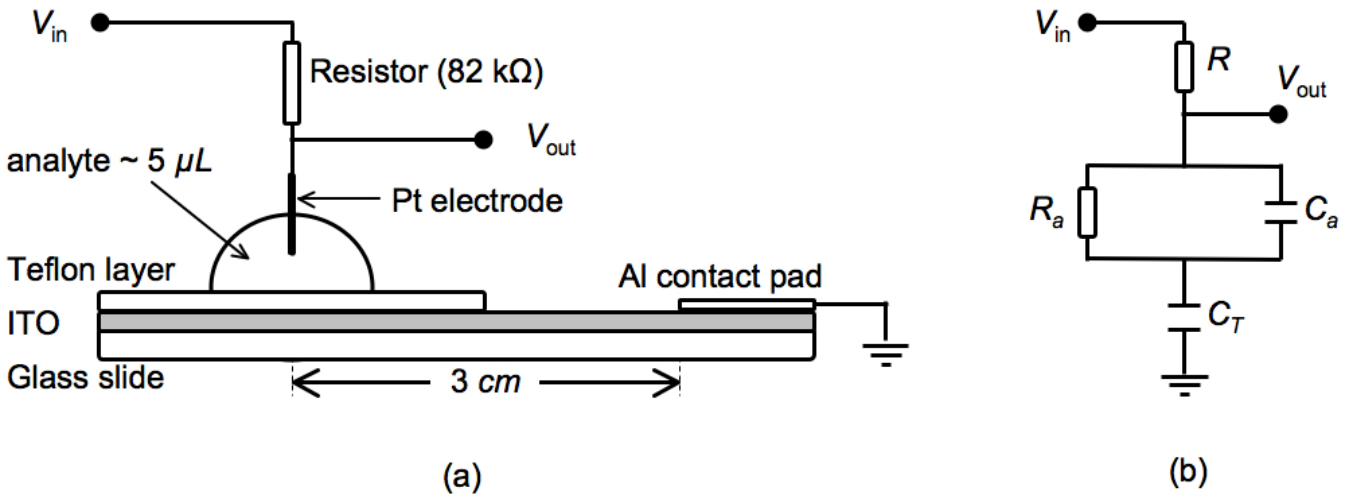

Figure 5.1: Schematic of the detector and modeled circuit. a) Experiment setup of the detector. b) Modeled circuit of the detector, where: R is a resistor, C is a capacitor, subscripts "a" and "T" denote analyte and the Teflon layer respectively

An aluminium contact pad was used to make the connection between the ITO layer and the system. The analyte drop always kept 3 cm apart from the Al contact pad to minimize the error caused by the ITO resistance (see Figure 5.1a). In this way, the wired system can be modeled as the circuit as shown in Figure 5.1b. A sinusoidal signal generated by a waveform generator (Agilent Model 33220A) connected to a voltage amplifier (Trek Model PZD 350) was used as the input signal. The amplitude of the signal was kept at 50 V_{RMS} at all times. The frequency of the signal was increased logarithmically from 200 Hz to 140 kHz with a 50 s sweep time. Input and output data were collected from a PC based oscilloscope (www.picotech.com). A *gain* vs. *frequency* plot was used to extract the f_C of the analyte. The experiments were monitored with a contact angle goniometer (CAM 101, www.ksvltd.com).

Benzalkonium chloride (BAC) reference standard was purchased as 10 % (w/v) aqueous solution from the United States Pharmacopeia (store.usp.org). As per the catalog, the homolog distribution of the reference standard was 0.1% C10, 68% C12, 25% C14 and 5% C16 and <0.1% C18 in weight percentages. Standard solutions of 0, 10, 20, 40,...,120 ppm aqueous solutions of BAC were prepared and tested with the detector using 5 μL sample volumes. Each BAC sample was tested at least 4 times using 3 different glass slides.

Cetyltrimethyl-ammonium chloride (CTAC) was purchased from Sigma-Aldrich (St. Louis, MO). 0, 20,...,80 ppm standard CTAC aqueous solutions were prepared and tested with the detector. To study the effect of solvent; 0, 100, 200,...1000 ppm CTAC/ethylene glycol (EG) solutions were tested. Each test utilized a 5 μL sample volume.

1000 ppm CTAC in EG solution was used to study the effect of droplet shape. Contact angles were measured for selected frequency values (i.e, 199.5, 354.8, 640.9, 1122, 1995, 3548, 6309, 11220, 19952, 35481, 63095 and 112202 Hz) using the contact

angle goniometer. All aqueous solutions were prepared with DI water (resistivity-$18 M\Omega.cm$) and all experiments were performed in room temperature ($22\pm1^{\circ}$) unless otherwise noted.

5.3 Results and Discussion

Experimentally, a plot of $frequency$ versus $gain$ ($20.log|V_{in}/V_{out}|$) is used to find the f_C of a specific system. In such a plot, the intersection point of the curve and -3dB line defines as f_C.

5.3.1 Benzalkonium Chloride (BAC) Detection

Figure 5.2a shows the $frequency$ versus $gain$ plots for selected BAC solutions. It can be observed that, each solution has a different f_C value and the concentration of BAC is inversely proportional to the f_C value (note that frequency axis in Figure 5.2a is logrithamic in scale). Figure 5.2b shows the relationship between f_C and the concentration of BAC. Clearly f_C has a very good linear relationship with the concentrations of BAC solutions (see Figure 5.2b).

Lower limit of detection (LLD) was calculated using following equation,[106]

$$LLD = \frac{3.s_{y/x}}{slope} \tag{5.6}$$

where,

$$s_{y/x} = \left[\frac{\sum(Y_i - Y_{r,i})^2}{n-2}\right]^{1/2}$$

X_i = concentration of analyte

Y_i = analytical signal measured by the detector

$Y_{r,i}$ = analytical signal predicted by the regression line

n = number of data points

$slope$ = gradient of the calibration plot

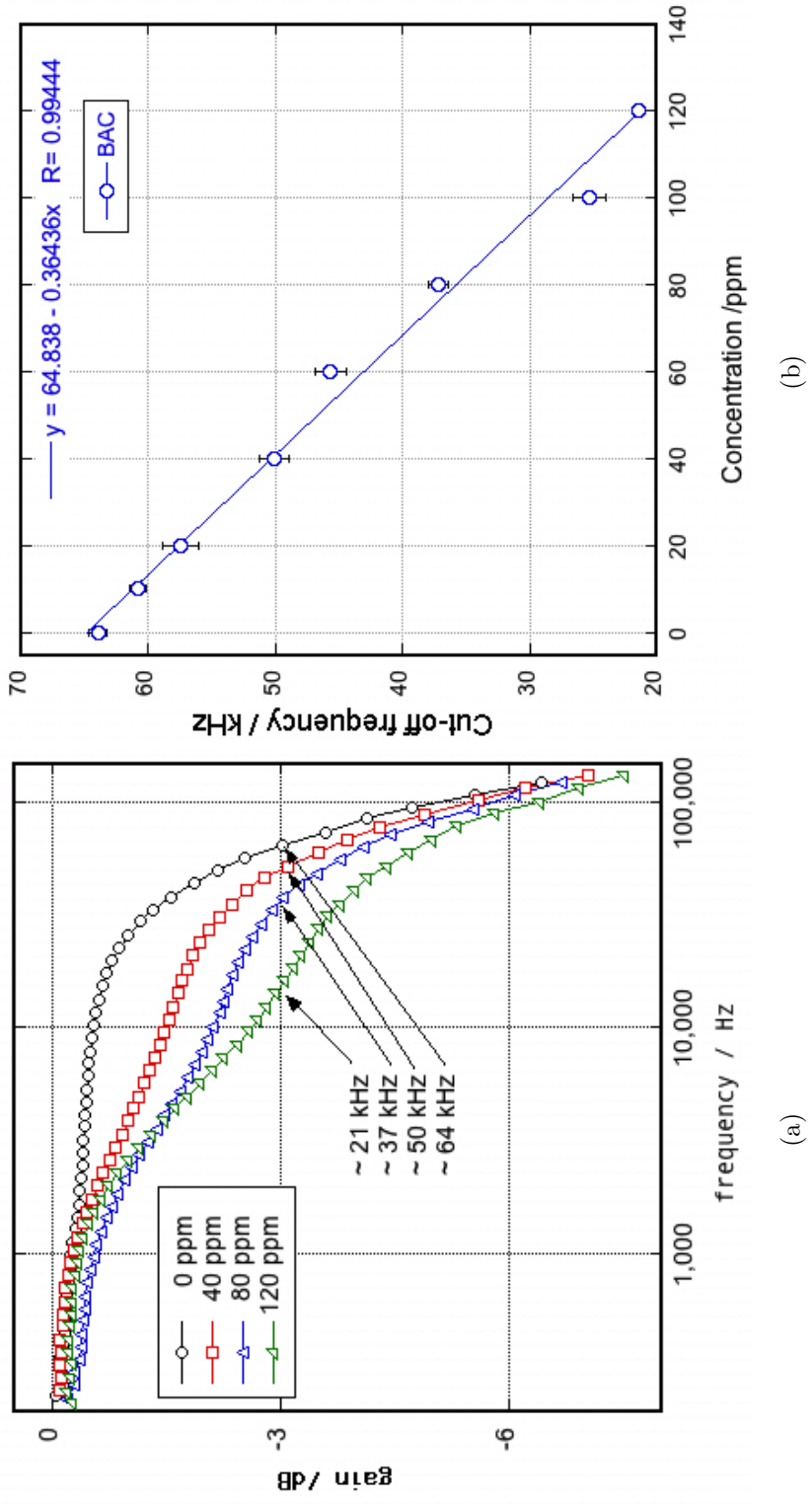

Figure 5.2: a) *gain* vs. *frequency* plots of selected BAC solutions, b) f_C values extracted from Figure 5.2a were plotted against concentration values of BAC solutions in order to use as a calibration curve

Table 5.1 shows the calculations of the LLD. It seems that LLD of 13 ppm can be achieved for BAC using this detector. EWOD detector can further be improved in order to obtain much lower LLD's as discussed in section 5.3.5.

5.3.2 Cetyltriethyl-ammonium Chloride (CTAC) Detection

Different concentrations of CTAC/water solutions were tested with the EWOD detector. To study the effect of solvent, different concentrations of CTAC in ethylene glycol (EG) also were tested. Figure 5.3 shows the calibration plots obtained for CTAC solutions prepared with DI water and EG. Equation 5.6 was used to calculate the LLD's for both CTAC in water and EG. Table 5.2 shows the LLD calculations. Obtained LLD for CTAC/water was $\simeq$ 4ppm, whereas LLD for CTAC/EG was $\simeq$ 110ppm. It seems that solvent plays a big role in LLD. This may be due to the conductivity differences of CTAC in two solvents. Since EG is much viscous than water, the conductivity of CTAC/EG is much lower than that of CTAC/water. Also the linear dynamic range (LDR) for CTAC/water lies between 0-80ppm, whereas that of CTAC/ EG lies between 0-1000ppm. In a way this is a great phenomenon to detect CTAC in wide range of concentrations, if one needs low LLD he can use less viscous solvent, whereas if one needs wide LDR he can use high viscous solvent. Since, LLD of CTAC aqueous solutions is $\simeq$ 4 ppm, the EWOD detector is ideal for the industrial applications. Due to lack of chromophores popular uv-vis detectors can not be used to detect CTAC directly.

5.3.3 Contact Angle of the Analyte Drop

It was observed that, during the frequency sweep, an analyte drop adjusts itself to different shapes. To investigate that phenomenon, the contact angle of a 1000ppm-CTAC/EG drop recorded for selected frequencies during an experiment.

Table 5.1: LLD Calculations for BAC

concentration of BAC solution X_i /ppm	detector response (f_C) Y_i / kHz	f_C predicted by regression line $Y_{r,i}$ / kHz	$(Y_i - Y_{r,i})^2$/	$(kHz)^2$
0	64	65	1	
10	61	61	0	
20	57	57	0	
40	52	51	1	
60	45	43	4	
80	37	36	1	
100	25	28	9	
120	21	21	0	
$\sum(Y_i - Y_{r,i})^2$			16	$(kHz)^2$
$s_{y/x} = [\sum(Y_i - Y_{r,i})^2/(n-2)]^{1/2}$			1.6	kHz
$LLD = 3.s_{y/x}/slope$			13	ppm

n = number of data points

slope = |-0.36 kHz/ppm|

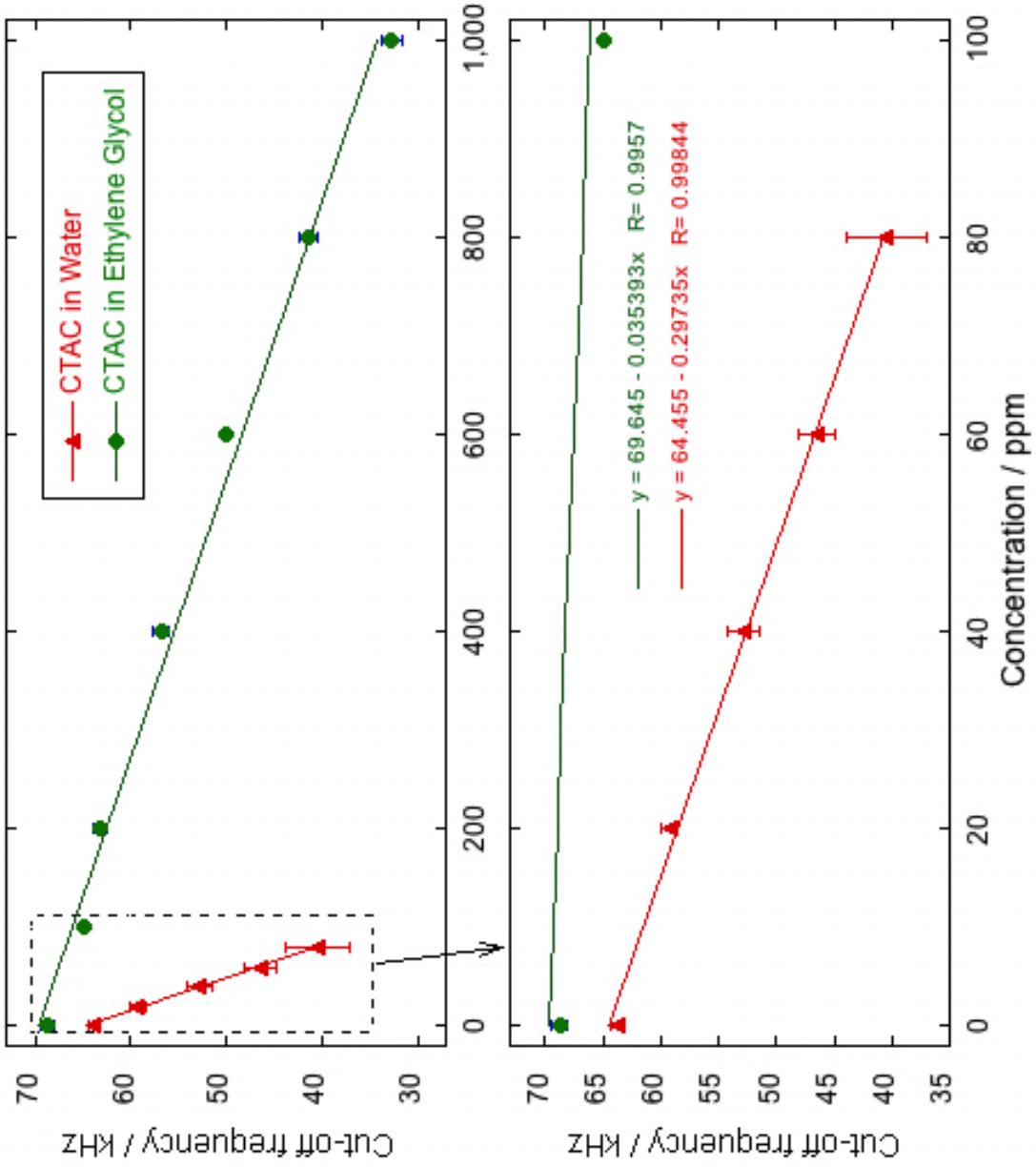

Figure 5.3: Calibration Plot

Table 5.2: Comparison of LLD's CTAC/Water vs. CTAC/EG

concentration of CTAC solution X_i / *ppm*	CTAC in water			CTAC in ethylene glycol		
	f_C	f_C predicted by regression line		f_C	f_C predicted by regression line	
	Y_i / kHz	$Y_{r,i}$ / kHz	$(Y_i - Y_{r,i})^2$	Y_i / kHz	$Y_{r,i}$/ kHz	$(Y_i - Y_{r,i})^2$
0	63.81	63.89	0.01	68.74	69.40	0.44
20	59.26	59.1	0.03			
40	52.81	52.63	0.03			
60	46.42	46.00	0.18			
80	40.50	40.89	0.15			
100				64.94	66.05	1.24
200				63.24	62.45	0.63
400				56.81	55.75	1.13
600				49.93	48.32	2.59
800				41.42	41.14	0.08
1000				32.72	34.19	2.15
$\sum(Y_i - Y_{r,i})^2$			0.39			8.26
$s_{y/x} = [\sum(Y_i - Y_{r,i})^2/(n-2)]^{1/2}$			0.36			1.29
$LLD = 3.s_{y/x}/slope$		(slope = -0.297)^a	$3.66 \simeq 4$		(slope = -0.035)^a	$110.15 \simeq 110$

n = number of data points; ^{a}only absolute value considered

Figure 5.4a shows the contact angle(θ) values of 1000ppm CTAC/EG for selected frequencies. Initially when there is no voltage/frequency applied to the drop, the 1000ppm CTAC/EG has a θ of 94° (which is called Young's angle or the contact angle at zero external voltage - θ_0). When 50 $V/200$ Hz voltage is applied to the drop, θ decreases from 94° to 78°. Keeping the voltage constant, if frequency is increased, θ decreases. However after a threshold it starts to increase until it achieves a constant value (see Figure 5.4a). The phenomenon further supports the existence of the RC filter type effect in this experiment, which can be easily visualized by the corresponding *gain* vs. $frequency$ plot (see Figure 5.5b). Chapter 3 discusses this RC filter effect in detail.

5.3.4 Advantages and Potential Future Applications

This detector seems to have number of advantages over existing detecting techniques/devices and variety of future applications as follows,

1) *Low sample volume.* The sample amount needed for this detecter is around 5 μL. Therefore the EWOD detector is ideal for expensive or low volume samples. Also this is suitable for industrial applications due to low sample consumption.

2) *Low Cost.* This device can be fabricated and operated with very low cost.

3) *Low LLD.* For BAC and CTAC the LLD's are ∼13 and ∼4 ppm respectively. Hence this device has low LLD which is suitable for most academic and industrial applications.

4) *Stand Alone Detector.* This device can be used as a stand alone detector to determine or to validate concentration, pH and purity of electrolytes, buffers and other solutions. Thus it may be useful in many ways for an ordinary laboratory.

5) *Portability.* Right now without the signal source, size of the EWOD device is around 75 mm x 25 mm x 50 mm in dimensions. Signal source can easily be

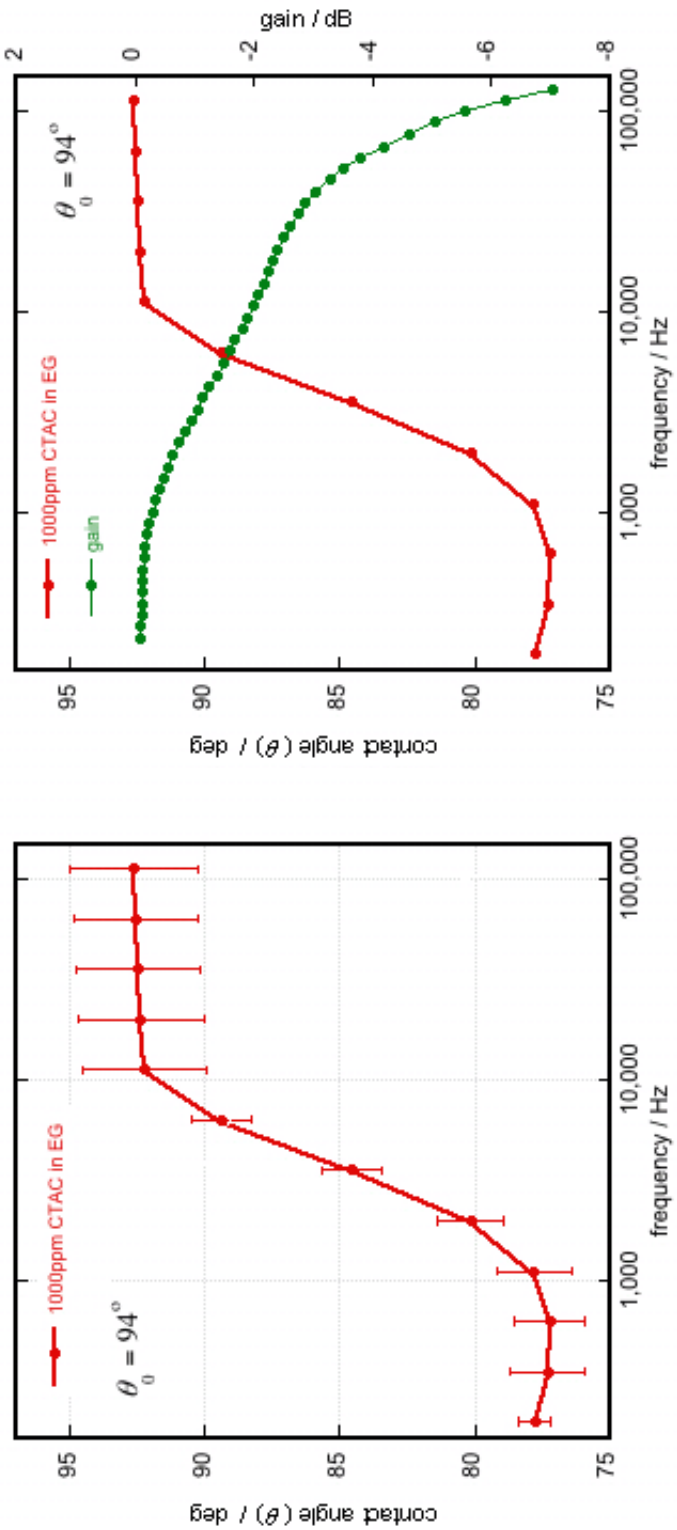

Figure 5.4: Drop shapes during the frequency sweep, a) contact angle vs frequency plot, b) contact angle/gain vs frequency plot

generated by a computer program such as *Labview* and can be supplied through a USB port. Therefore it can be used as a portable device.

6) *Integration with Lab-on-a-Chip Systems.* This detector was developed using an electrowetting experiment setup. Therefore this detector can easily be integrated with electrowetting on dielectric (EWOD) based lab-on-a-chip systems. Since most EWOD based systems operated on AC voltages the same signal source can be used to operate the detector.

7) *Approximate Water Content Determination of Ionic Liquids.* Trace levels of water are present in every liquid even when classified as 'in pure form'. In most applications, determination of trace levels of water in liquids is very important. Karl Fischer (KF) titration and gas chromatography (GC) are the most widely used water determination techniques. However determination of water content in ionic liquids (ILs) with KF and GC is problematic for several reasons: First of all KF is an expensive instrument by itself, second KF reagents are expensive, they always need to used in freshly prepared. Depending on the type, IL can contain 200 *ppm* to 0.29 % water even after drying overnight with a dehydrating agent in a vacuum oven. To determine this amount of water via a KF titrations requires at least 1 - 2 mL sample volume. This is a very large amount of sample volume since synthesis of some ILs at least in 2 mL of volume (such as linear tricationic ILs) can be a lengthy, tedious and expensive process. Since KF is a destructive method, one cannot afford to consume 2 mL of IL just to measure the water content. GC also has several limitations when used to determine water content. Most ILs are viscous, therefore traditional syringes cannot be used in sample injection. ILs tends to clog up and as a consequence routine cleanup is essential. We believe that this EWOD based detector can easily be used to determine approximate water content in ILs. The physical properties (specially σ) of ILs are heavily changing with the content of water present in IL.[107] In fact our

previous studies showed that electrowetting properties also changing with the amount of water in ILs.[2,46] Therefore it is very easy to measure the water content of ILs using this detector.

8) *Alternative Salinometer.* Since this device produces a single f_C value for all dissolved species, including charged species, this can easily be used to measure the salinity or dissolved salt content of a solution.

5.3.5 Other Concerns

The LLD and the performance of the EWOD detector can be improved by altering or controlling any of the following factors: 1) the value of the resistor (R) can be changed by changing the R value, f_C can be shifted either to a lower frequency range or to a higher frequency range. Lower frequency ranges are better to identify more conductive analytes whereas higher frequency ranges are better to identify more dielectric analytes, 2) the C_a, C_T and R_a values can be changed by changing the drop size. It's very difficult to state the effect of drop size to the performance of the detector without a systematic study. In this study, 5 μL analyte drop volume was used. However, in previous reported EWOD experiments different drop volumes were used ($\sim 50\ \mu L$ to $\sim 100\ pL$)[1,43] Hence similar range of sample volumes can be tested in this detector, 3) the C_T value also can be tuned by changing the dielectric layer material. Here in this detector Teflon was used as the dielectric material because of its versatility. However, thin Teflon layers are usually are imperfect and can cause leakage current to flow across the dielectric layer and ultimately reducing the performance of the detector. Another dielectric material such as SiO_2 can be used to minimize the leakage current,[60] 4) in this study ITO pre-coated commercial glass slides were used due to its lower cost. However, due to high resistivity of the ITO coating ($\sim$100 Ω/cm) ITO layer can act as an extra resistor for the system. Also, the resistance caused by

ITO can have different values depending on the position of the analyte drop. That can affect the f_C value. Therefore, the analyte drop always was positioned at a constant length (3 cm) away from Al contact pad for every experiment. This effect can be reduced using gold or silver coated glass slides. However that can elevate the fabrication cost of the device, since gold coated glass slides are approximately 20 times more expensive than ITO coated glass slides, and 7) at higher frequencies impedance generated from the connecting wires can affect f_C value. Therefore it's always better to use minimum amount of connecting wires.

5.4 Conclusion

A novel electrowetting on dielectric (EWOD) based liquid drop detector was successfully fabricated and tested with two biocides. Low LLD's achieved for both biocides tested. The detector has number of advantages such as use of low sample volume and low cost. In addition this device can be used in variety of potential applications.

5.5 Equation 5.1 Derivation

Note that the terms used in this section were defined in Section 3.3.3.1. Figure 5.1 shows the detector setup and equivalent circuit for the EWOD based detector.

Let Z_R, Z_a and Z_T be the impedance of the resistor (82 Ω), ionic liquid and Teflon layer respectively and let V_R, V_a and V_T be the voltages across the resistor (82 Ω), ionic liquid and Teflon layer respectively. Then elementary electric circuit modeling indicates that,

$$Z_R = R; \qquad Z_a = \frac{1}{g_a + j\omega C_a}; \qquad Z_T = \frac{1}{g_T + j\omega C_T}$$

$$V_{in} = V_R + V_a + V_T$$

$$V_{out} = V_a + V_T$$

Therefore, the output voltage (V_{out}) is:

$$V_{out} = \left[\frac{Z_a + Z_T}{Z_R + Z_a + Z_T}\right] V_{in}$$

$$V_{out} = \left[\frac{\frac{1}{g_a + j\omega C_a} + \frac{1}{g_T + j\omega C_T}}{R + \frac{1}{g_a + j\omega C_a} + \frac{1}{g_T + j\omega C_T}}\right] V_{in}$$

$$\frac{V_{out}}{V_{in}} = \left[\frac{g_a + j\omega(C_T + C_a)}{g_a - R\omega^2 C_a C_T + j\omega(g_a R C_T + C_T + C_a)}\right]$$

In order to make the denominator real, the denominator and numerator were multiplied by the complex conjugate of the denominator. Then,

$$\frac{V_{out}}{V_{in}} = \left[\frac{g_a + j\omega(C_T + C_a)}{g_a - R\omega^2 C_a C_T + j\omega(g_a R C_T + C_T + C_a)}\right]$$

In order to make the denominator real, the denominator and numerator were multiplied by the complex conjugate of the denominator. Then,

$$\frac{V_{out}}{V_{in}} = \frac{\begin{array}{c}[g_a(g_a - R\omega^2 C_a C_T) + \omega^2(C_T + C_a)(g_a R C_T + C_T + C_a)] \\ + j\omega[(C_T + C_a)(g_a - R\omega^2 C_a C_T) - g_a(g_a R C_T + C_T + C_a)\end{array}}{1 + \omega^2 R_a^2 (C_a + C_T)^2}$$

$$\left|\frac{V_{out}}{V_{in}}\right| = \left[\left[\frac{V_{in}}{V_{out}}\right] \cdot \left[\frac{V_{in}}{V_{out}}\right]^*\right]^{\frac{1}{2}}$$

Considering only the amplitude,

$$\left|\frac{V_{out}}{V_{in}}\right| = \left[\frac{\left[[g_a(g_a - R\omega^2 C_a C_T) + \omega^2(C_T + C_a)(g_a R C_T + C_T + C_a)]\right]^2 + \omega^2\left[[(C_T + C_a)(g_a - R\omega^2 C_a C_T) - g_a(g_a R C_T + C_T + C_a)\right]^2}{[1 + \omega^2 R_a^2 (C_a + C_T)^2]^2}\right]^{\frac{1}{2}}$$

$R = 82k\Omega$ = constant, $g_a = \frac{1}{R_a}, \omega = 2\pi f$ at cut off frequency (i.e., at $f = f_C$); $\left|\frac{V_{in}}{V_{out}}\right| = \frac{1}{\sqrt{2}}$

Substituting these values to above equation f_C can be written as a function of R_a,C_a and C_T.

$$f_C = F(R_a, C_a, C_T) \qquad (5.1)$$

CHAPTER 6

GENERAL SUMMARY

Ionic liquids (ILs) are a special class of liquids that have negligible vapor pressure and inherently tunable physiochemical properties. Electrowetting properties of ILs were studied in detail in order use them in Electrowetting on Dielectric (EWOD) based devices. In Chapter 2, electrowetting properties of 19 different ILs were examined under DC voltage conditions. All tested ILs showed electrowetting of various magnitudes on an amorphous flouropolymer layer. The study showed that the structure, functionality, and charge density of ILs can affect on the electrowetting behavior. Compared to water and aqueous electrolytes, ILs showed enhanced stability at higher voltages. With DC voltages, the water content of ILs seems to affect the electrowetting properties of water miscible ILs, however water content does not affect the electrowetting properties of water immiscible ILs

In Chapter 3, the electrowetting behavior of ILs under AC voltage conditions were discussed. Nine different ILs with 3 different AC frequencies (60 Hz, 1 kHz, 10 kHz) were investigated experimentally. The electrowetting properties of ILs was found to be directly related to the frequency of the AC voltage. These relationships were further analyzed and explained theoretically. The electrowetting properties of ILs under AC voltages were compared to those under DC voltages. All tested ILs showed greater apparent contact angle changes with AC voltage conditions. The effect of structure and charge density also were examined. Electrowetting reversibility of ILs under AC voltage conditions was studied. Studied ILs showed good reversibility. It was observed that, the effect of water content on electrowetting behavior in AC

voltage conditions was similar to that found for DC voltage conditions. The physical properties of ILs and their electrowetting properties under both DC and AC voltage conditions were tabulated in order to use as references to engineer task-specific electrowetting agents (ILs) for future EWOD based applications. Further, the study showed that in AC voltage experiments, an EWOD device setup acts as a RC filter.

The study revealed that, the cut-off frequency (f_C) of the RC filter is a function of conductivity, dielectric constant, surface tension and double layer thickness of the liquid as well as the applied voltage. That relationship was used to develop a tunable RC filter and an analytical detector based on the RC filter concept. Chapter 4 discusses the development of tunable RC filter. Chapter 5 focuses on the use of a tunable RC filter as an analytical detector. Industrial biocides in different solvents were used to test the performance of this detector. Lower limit of detections achieved for the tested biocides and the detector seems to be a universal detector with very low fabrication costs.

APPENDIX A

PUBLICATION INFORMATION OF CHAPTER 2-4

REFERENCES

[1] Mugele, F.; Baret, J.-C. *J. Phys.: Condens. Matter* **2005,** *17,* R705-R774.

[2] Nanayakkara, Y. S.; Perera, S.; Bindiganavale, S.; Wanigasekara, E.; Moon, H.; Armstrong, D. W. *Anal. Chem.* **2010,** *82,* 3146-3154.

[3] Wheeler, A. R. *Science* **2008,** *322,* 539-540.

[4] Berge, B.; Peseux, J. *Eur. Phys. J. E: Soft Matter* **2000,** *3,* 159-163.

[5] "Varioptic - The Liquid Lens Company", http://www.varioptic.com (accessed 10/09/2010).

[6] Hayes, R. A.; Feenstra, B. J. *Nature* **2003,** *425,* 383-385.

[7] "Liquavista - Electrowetting based low power, always viewable color video displays", http://www.liquavista.com (accessed 10/09/2010).

[8] Nanayakkara, Y. S.; Moon, H.; Armstrong, D. W. *Appl. Mater. Interfaces* **2010,** *2,* 1785-1787.

[9] Nanayakkara, Y. S.; Armstrong, D. W. **2010,** In preparation.

[10] Abdelgawad, M.; Wheeler, A. R. *Advanced Materials* **2009,** *21,* 920-925.

[11] Srinivasan, V.; Pamula, V. K.; Fair, R. B. *Lab Chip* **2004,** *4,* 310-315.

[12] Srinivasan, V.; Pamula, V. K.; Fair, R. B. *Anal.Chim. Acta* **2004,** *507,* 145-150.

[13] Wheeler, A. R.; Moon, H.; Kim, C. J.; Loo, J. A.; Garrell, R. L. *Anal. Chem.* **2004,** *76,* 4833-4838.

[14] Wheeler, A. R.; Moon, H.; Bird, C. A.; Loo, R. R. O.; Kim, C. J.; Loo, J. A.; Garrell, R. L. *Anal. Chem.* **2005,** *77,* 534-540.

[15] Yoon, J. Y.; Garrell, R. L. *Anal. Chem.* **2003,** *75,* 5097-5102.

[16] Moon, H.; Wheeler, A. R.; Garrell, R. L.; Loo, J. A.; Kim, C.-J. *Lab Chip* **2006,** *6,* 1213-1219.

[17] Wijethunga, P.; Nanayakkara, Y. S.; Kunchala, P.; Armstrong, D. W.; Moon, H. **2010,** Submitted.

[18] Kunchala, P.; Moon, H.; Nanayakkara, Y.; Armstrong, D. W. *Proceedings of the ASME 2009 Summer Bioengineering Conference (SBC2009)*; Lake Tahoe, CA, June 17-21, 2009.

[19] Moon, H.; Bindiganavale1, S.; Nanayakkara, Y.; Armstrong, D. W. *Proceedings of the Seventh International ASME Conference on Nanochannels, Microchannels and Minichannels ICNMM2009*; Pohang: South Korea, June 22-24, 2009.

[20] Lee, J.; J., K. *Proceedings of Eleventh Annual International Workshop on MEMS* **1998,** 538-543.

[21] Sen, P.; Kim, C.-J. *IEEE J. Microelectromech. Syst.* **2009,** *18,* 174 -185.

[22] Mukhopadhyay, R. *Anal Chem* **2005,** *77,* 429A-432A.

[23] Anderson, J. L.; Armstrong, D. W.; Wei, G. T. *Anal. Chem.* **2007,** *79,* 4247-4247.

[24] Wilkes, J. S.; Levisky, J. A.; Wilson, R. A.; Hussey, C. L. *Inorg. chem.* **1982,** *21,* 1263-1264.

[25] Sun, P.; Armstrong, D. W. *Anal Chim Acta.* **2010,** *661,* 1-16.

[26] Soukup-Hein, R. J.; Warnke, M. M.; Armstrong, D. W. *Annu. Rev. Anal. Chem.* **2009,** *2,* 145-168.

[27] Liu, R.; Liu, J.-f.; Yin, Y.-g.; Hu, X.-l.; Jiang, G.-b. *Anal. Bioanal. Chem.* **2009,** *393,* 871-883.

[28] Wei, G.-T.; Yang, Z.; Lee, C.-Y.; Yang, H.-Y.; Wang, C. R. C. *J. Am. Chem. Soc.* **2004,** *126,* 5036-5037.

[29] Anderson, J. L.; Armstrong, D. W. *Anal. Chem.* **2005,** *77,* 6453-6462.

[30] Qiu, H.; Jiang, S.; Liu, X. *J. Chromatogr. A* **2006,** *1103,* 265 - 270.

[31] Shetty, P. H.; Youngberg, P. J.; Kersten, B. R.; Poole, C. F. *J. Chromatogr. A* **1987,** *411,* 61 - 79.

[32] Qin, W.; Li, S. F. Y. *Electrophoresis* **2002,** *23,* 4110-4116.

[33] Vaher, M.; Koel, M.; Kaljurand, M. *Chromatographia* **2001,** *53,* S302-S306 10.1007/BF02490346.

[34] Mwongela, S. M.; Numan, A.; Gill, N. L.; Agbaria, R. A.; Warner, I. M. *Anal. Chem.* **2003,** *75,* 6089-6096.

[35] Armstrong, D. W.; Zhang, L.-K.; He, L.; Gross, M. L. *Anal. Chem.* **2001,** *73,* 3679-3686.

[36] Crank, J. A.; Armstrong, D. W. *J. Am. Soc. Mass Spectrom.* **2009,** *20,* 1790 - 1800.

[37] Martinelango, P. K.; Anderson, J. L.; Dasgupta, P. K.; Armstrong, D. W.; Al-Horr, R. S.; Slingsby, R. W. *Anal. Chem.* **2005,** *77,* 4829-4835.

[38] Soukup-Hein, R. J.; Remsburg, J. W.; Dasgupta, P. K.; Armstrong, D. W. *Anal. Chem.* **2007,** *79,* 7346-7352.

[39] Breitbach, Z. S.; Warnke, M. M.; Wanigasekara, E.; Zhang, X.; Armstrong, D. W. *Anal. Chem.* **2008,** *80,* 8828-8834.

[40] Ohno, H., Ed.; *Electrochemical Aspects of Ionic Liquids;* John Wiley and Sons, Inc: New Jersey, 2005.

[41] Buzzeo, M. C.; Hardacre, C.; Compton, R. G. *Analytical Chemistry* **2004,** *76,* 4583-4588.

[42] Chatterjee, D.; Hetayothin, B.; Wheeler, A. R.; King, D. J.; Garrell, R. L. *Lab Chip* **2006,** *6,* 199-206.

[43] Millefiorini, S.; Tkaczyk, A. H.; Sedev, R.; Efthimiadis, J.; Ralston, J. *J. Am. Chem. Soc.* **2006,** *128,* 3098-3101.

[44] Dubois, P.; Marchand, G.; Fouillet, Y.; Berthier, J.; Douki, T.; Hassine, F.; Gmouh, S.; Vaultier, M. *Anal. Chem.* **2006,** *78,* 4909-4917.

[45] Ricks-Laskoski, H. L.; Snow, A. W. *J. Am. Chem. Soc.* **2006,** *128,* 12402-12403.

[46] Nanayakkara, Y. S.; Moon, H.; Payagala, T.; Wijeratne, A. B.; Crank, J. A.; Sharma, P. S.; Armstrong, D. W. *Anal. Chem.* **2008,** *80,* 7690-7698.

[47] Halka, V.; Freyland, W. *Z. Phys. Chem.* **2008),** *222(1),* 117-127.

[48] Wanigasekara, E.; Zhang, X.; Nanayakkara, Y.; Payagala, T.; Moon, H.; Armstrong, D. W. *Appl. Mater. Interfaces* **2009,** *1,* 2126-2133.

[49] Restolho, J.; Mata, J. L.; Saramago, B. *J. Phys. Chem. C* **2009,** *113,* 9321-9327.

[50] Nanayakkara, Y.; Kunchala, P.; Moon, H.; Armstrong, D. W. *Proceedings of the PITTCON 2010*; Orlando, March 1- 5, 2010; The Pittsburgh Conference on Analytical Chemistry and Applied Spectroscopy: Pittsburgh, PA, 2010.

[51] Paneru, M.; Priest, C.; Sedev, R.; Ralston, J. *J. Am. Chem. Soc.* **2010,** *132,* 8301-8308.

[52] Paneru, M.; Priest, C.; Sedev, R.; Ralston, J. *J. Phys. Chem. C* **2010,** *114,* 8383-8388.

[53] Zhang, S.; Hu, X.; Qu, C.; Zhang, Q.; Ma, X.; Lu, L.; Li, X.; Zhang, X.; Deng, Y. *ChemPhysChem* **2010,** *11,* 2327-2331.

[54] Gates, E. D. *Introduction to electronics;* Delmar: Australia ;Albany, [NY], 4th ed.; 2001.

[55] Kumar, A.; Pluntke, M.; Cross, B.; Baret, J.-C.; Mugele, F. *Proceedings of the Materials Research Society Fall Meeting, Boston, November, 2005*; E-N06-01.1.

[56] Jones, T. B. *Langmuir* **2002,** *18,* 4437-4443.

[57] Jones, T. B.; Wang, K. L.; Yao, D. J. *Langmuir* **2004,** *20,* 2813-2818.

[58] Zeng, J.; Korsmeyer, T. *Lab Chip* **2004,** *4,* 265-277.

[59] Chatterjee, D.; Shepherd, H.; Garrell, R. L. *Lab Chip* **2009,** *9,* 1219-1229.

[60] Moon, H.; Cho, S. K.; Garrell, R. L.; Kim, C.-J. *J. App. Phys.* **2002,** *92,* 4080.

[61] Pollack, M. G.; Fair, R. B.; Shenderov, A. D. *Appl. Phys. Lett.* **2000,** *77,*.

[62] Cho, S. K.; Moon, H.; Kim, C. *J. Microelectromech. Syst.* **2003,** *12,* 70-80.

[63] Welters, W. J. J.; Fokkink, L. G. J. *Langmuir* **1998,** *14,* 1535-1538.

[64] Huh, D.; Tkaczyk, A. H.; Bahng, J. H.; Chang, Y.; Wei, H. H.; Grotberg, J. B.; Kim, C. J.; Kurabayashi, K.; Takayama, S. *J. Am. Chem. Soc.* **2003,** *125,* 14678-14679.

[65] Brennecke, J. F.; Maginn, E. J. *AIChE Journal* **2001,** *47,* 2384-2389.

[66] Anderson, J. L.; Ding, R.; Ellern, A.; Armstrong, D. W. *J. Am. Chem. Soc.* **2005,** *127,* 593-604.

[67] Nakagawa, H.; Fujino, Y.; Kozono, S.; Katayama, Y.; Nukuda, T.; Sakaebe, H.; Matsumoto, H.; Tatsumi, K. *J. Power Sources* **2007,** *174,* 1021-1026.

[68] Poole, C. F. *J. Chromatogr. A* **2004,** *1037,* 49-82.

[69] Payagala, T.; Huang, J.; Breitbach, Z. S.; Sharma, P. S.; Armstrong, D. W. *Chem. Mater.* **2007,** *19,* 5848-5850.

[70] Pernak, J.; Skrzypczak, A.; Lota, G.; Frackowiak, E. *Chem. Eur. J.* **2007,** *13,* 3106-3112 ON: 1521-3765.

[71] Sharma, P. S.; Payagala, T.; Wanigasekara, E.; Wijeratne, A. B.; Huang, J.; Armstrong, D. W. *Chem. Mater.* **2008,** *20,* 4182-4184.

[72] Wijeratne, A. B.; Sharma, P. S.; Huang, J.; Schug, K. A.; Armstrong, D. W. *Abstract of Papers 19th International Symposium on Chirality*, San Diego, CA, July 1-7, 2007; P-222.

[73] Mugele, F.; Buehrle, J. *J. Phys.: Condens. Matter* **2007,** *19,* 375112/1-375112/20.

[74] Berthod, A.; Kozak, J.; Anderson, J.; Ding, J.; Armstrong, D. *Theor. Chem. Acc.* **2007,** *117,* 127-135.

[75] Quinn, A.; Sedev, R.; Ralston, J. *J. Phys. Chem. B* **2003,** *107,* 1163-1169.

[76] Freire, M. G.; Carvalho, P. J.; Fernandes, A. M.; Marrucho, I. M.; Queimada, A. J.; Coutinho, J. A. P. *J. Colloid Interface Sci.* **2007,** *314,* 621-630.

[77] Tokuyama, H.; Sasaki, M.; Sakohara, S. *Chem. Eng. Technol.* **2007,** *30,* 139-144.

[78] Saeki, F.; Baum, J.; Moon, H.; Yoon, J.-Y.; Kim, C.-J.; Garrell, R. L. *Abstracts of Papers 222nd ACS National Meeting*, Chicago, IL, August 26-30, 2001; PMSE-008.

[79] Seyrat, E.; Hayes, R. A. *J. Appl. Phys.* **2001,** *90,* 1383-1386.

[80] Kornyshev, A. A. *J. Phys. Chem. B* **2007,** *111,* 5545-5557.

[81] Lazzari, M.; Mastragostino, M.; Soavi, F. *Electrochem. Commun.* **2007,** *9,* 1567-1572.

[82] Baldelli, S. *Acc. Chem. Res.* **2008,** *41,* 421-431.

[83] Daguenet, C.; Dyson, P. J.; Krossing, I.; Oleinikova, A.; Slattery, J.; Wakai, C.; Weingartner, H. *J. Phys. Chem. B* **2006,** *110,* 12682-12688.

[84] Liu, W.; Zhao, T.; Zhang, Y.; Wang, H.; Yu, M. *J. Solution Chem.* **2006,** *35,* 1337-1346.

[85] Uerdingen, M.; Treber, C.; Balser, M.; Schmitt, G.; Werner, C. *Green Chem.* **2005,** *7,* 321-325.

[86] Quilliet, C.; Berge, B. *Curr. Opin. Colloid Interface Sci.* **2001,** *6,* 34-39.

[87] Blake, T. D.; Clarke, A.; Stattersfield, E. H. *Langmuir* **2000,** *16,* 2928-2935.

[88] Ko, S. H.; Lee, H.; Kang, K. H. *Langmuir* **2008,** *24,* 1094-1101.

[89] Hong, J.; Ko, S.; Kang, K.; Kang, I. *Microfluid. Nanofluid.* **2008,** *5,* 263-271.

[90] Carda-Broch, S.; Berthod, A.; Armstrong, D. W. *Anal. Bioanal. Chem.* **2003,** *375,* 191-199.

[91] Wang, W.; Murray, R. W. *Anal. Chem.* **2007,** *79,* 1213-1220.

[92] Oxley, J. D.; Prozorov, T.; Suslick, K. S. *J. Am. Chem. Soc.* **2003,** *125,* 11138-11139.

[93] Oh, J. M.; Ko, S. H.; Kang, K. H. *Langmuir* **2008,** *24,* 8379-8386.

[94] Vallet, M.; Vallade, M.; Berge, B. *Eur. Phys. J. B* **1999,** *11,* 583-591.

[95] Swart, P. L.; Campbell, C. K. *IEEE J Solid-State Circuits* **1972,** *7,* 306-308.

[96] Shapiro, B.; Moon, H.; Garrell, R. L.; Kim, C.-J. *J. Appl. Phys.* **2003,** *93,* 5794.

[97] Raj, B.; Dhindsa, M.; Smith, N. R.; Laughlin, R.; Heikenfeld, J. *Langmuir* **2009,** *25,* 12387-12392.

[98] Jiraseree-amornkun, A.; Worapishet, A.; Klumperink, E.; Nauta, B.; Surakampontorn, W. *IEEE Trans. Circuits Syst. -I* **2008,** *55,* 3641-3654.

[99] Shin, H.; Kim, Y. *IEEE Trans. Circuits Syst. -II* **2010,** *57,* 85-89.

[100] Han, W.; Cho, Y.-H. *J. Microelectromech. Syst.* **2009,** *18,* 773-783.

[101] "Products containing BENZALKONIUM CHLORIDE ", Environmental Working Group, 2010 [online] `http://www.cosmeticsdatabase.com/browse.php?containing=700674(accessed-10/06/10)`.

[102] Prince, S. J.; McLaury, H.-J.; Allen, L. V.; McLaury, P. *J. Pharm. Biomed. Anal.* **1999,** *19,* 877 - 882.

[103] United States Pharmacopeia 23/National Formulary 18, United States Pharmacopeial Convention, Inc., Maryland, 1995, pp. 22182219.

[104] "Products containing CETRIMONIUM CHLORIDE ", Environmental Working Group, 2010 [online] http://www.cosmeticsdatabase.com/browse.php?containing=701258(accessed-10/06/10).

[105] Terol, A.; Gmez-Mingot, M.; Maestre, S. E.; Prats, S.; Todol, J. L.; Paredes, E. *Int. J. Cosmet. Sci.* **2010,** *32,* 65-72.

[106] Anderson, D. *Clin. Chem.* **1989,** *35,* 2152-2153.

[107] Widegren, J. A.; Saurer, E. M.; Marsh, K. N.; Magee, J. W. *J. Chem. Thermodynamics* **2005,** *37,* 569-575.

BIOGRAPHICAL STATEMENT

Yasith S. Nanayakkara obtained his Bachelors of Science degree in Chemistry with Computer Science as a subsidiary from University of Peradeniya, Sri Lanka in 2003. In 2005, he began attending the University of Texas at Arlington as a graduate student. In early 2006, he joined professor Daniel Armstrong′s research group and received his Doctor of Philosophy from the University of Texas at Arlington in December 2010. His research interests include development of electrowetting based analytical devices including detectors and investigations on electrowetting behaviors of ionic liquids for digital microfluidic devices.